

UNIVERSITY OF ZAGREB  
FACULTY OF MECHANICAL ENGINEERING AND NAVAL  
ARCHITECTURE

# **MASTER'S THESIS**

**Martina Šimag**

Zagreb, 2019.

UNIVERSITY OF ZAGREB  
FACULTY OF MECHANICAL ENGINEERING AND NAVAL  
ARCHITECTURE

## **MASTER'S THESIS**

**SIMULATION OF THE VEHICLE INTERIOR NOISE  
GENERATED BY AN EXTERIOR SOUND SOURCE BY  
USING FINITE ELEMENT METHOD (FEM)**

Mentor:

Dr.Sc. Neven Alujević, Docent

Student:

Martina Šimag

Zagreb, 2019.

## **IZJAVA**

*Pod punom moralnom odgovornošću izjavljujem da sam rad izradila samostalno koristeći se znanjem stečenim tijekom studija te navedenom literaturom.*

## **STATEMENT**

*I declare that I have completed this thesis using knowledge and skills gained during my university studies and using specified scientific literature.*

# ACKNOWLEDGMENT

*First and most importantly, I would like to express my sincere gratitude to my thesis supervisor Dr.Sc. Neven Ajuević of the Faculty of Mechanical Engineering and Naval Architecture at University of Zagreb. I am grateful for his helpful comments, suggestions, and constructive criticism throughout the entire thesis. He consistently allowed this paper to be my work, but steered me in the right direction whenever he thought I needed it.*

*Secondly, I would like to thank MSc Mehdi Mehrgou from AVL List GmbH for introducing me to the topic and for the support on the way as well as for the useful comments, remarks and engagement through the learning process of this master thesis.*

*Further, I would like to express my deepest appreciation to MPhil Nikola Naranča for granting me the opportunity of writing this thesis in collaboration with AVL-AST d.o.o. from Zagreb and AVL List GmbH from Graz.*

*I gratefully acknowledge AUDI AG for generously providing all the data needed for the purposes of this thesis.*

*My sincere thanks also go to colleagues in Graz from AVL List GmbH for sharing valuable lessons and providing me with important information during my four-month stay in Graz. I am also grateful to colleagues in Zagreb from AVL-AST d.o.o. for being so supportive and open for discussions.*

*I would like to offer my special thanks to Dr.Sc. Darko Kozarac for introducing me to company AVL-AST d.o.o. and also for showing a great deal of encouragement and support not only during writing of this thesis but also throughout my study.*

*A very special gratitude goes out to my parents Josip and Dubravka and my siblings Lucija, Nikola and Tomislav for providing me with unfailing support and continuous encouragement throughout my years of study and through the process of researching and writing this thesis. I would particularly like to thank all of my friends for constant support and love. This accomplishment would not have been possible without all of you. Thank you.*

*Finally, I would like to express my deepest gratitude to my boyfriend Josip Dvorski. I will be forever grateful for your unconditional love and support.*

*Martina Šimag*

*"If you want to find the secrets of universe, think in terms of energy, frequency and vibration."*

*Nikola Tesla*



SVEUČILIŠTE U ZAGREBU  
FAKULTET STROJARSTVA I BRODOGRADNJE



Središnje povjerenstvo za završne i diplomske ispite  
Povjerenstvo za diplomske ispite studija strojarstva za smjerove:  
procesno-energetski, konstrukcijski, brodstrojarski i inženjersko modeliranje i računalne simulacije

Sveučilište u Zagrebu Fakultet strojarstva i brodogradnje	
Datum	Prilog
Klasa:	
Ur. broj:	

## DIPLOMSKI ZADATAK

Student: **Martina Šimag**

Mat. br.: 0035196391

Naslov rada na hrvatskom jeziku:

**Simulacija buke u unutrašnjosti vozila uzrokovane vanjskim izvorom zvuka koristeći metodu konačnih elemenata (MKE)**

Naslov rada na engleskom jeziku:

**Simulation of the vehicle interior noise generated by an exterior sound source by using finite element method (FEM)**

Opis zadatka:

Reduction of the internal and external noise of the today's cars requires significant effort in the development process. Sometimes critical mistakes are discovered at the very late stage of the development. Significant time and effort is then needed to resolve all issues which consequently increases overall costs. By using simulations, where no hardware components are necessary, and with significantly less effort than in measurements, these problems can be avoided. Main objective of this work is to propose valid methodology for successful vehicle interior and exterior noise simulation in MSC Actran. The focus is the transmission loss from airborne sources out of the car.

Based on everything mentioned above, in this study it is necessary to:

1. Study literature and publications for vehicle interior and exterior acoustics and available simulation models and methodology.
2. Setup of the analytical model of the coupled plate and cavity system, modelling and simulation in MSC Actran.
3. Validation of the numerical results with the analytical results from task 2.
4. Set up the simulation model which describes the vehicle configuration "Body in Blue" run through simulation in MSC Actran.
5. Propose methodology for the vehicle interior and exterior noise simulation for complete examined frequency range.

It is required to make a list of the literature used and to acknowledge help received in preparing the thesis.

Zadatak zadan:

Datum predaje rada:

Predviđeni datum obrane:

7. ožujka 2019.


9. svibnja 2019.

15., 16. i 17. svibnja 2019.

Zadatak zadao:

Predsjednica Povjerenstva:

  
Doc. dr. sc. Neven Alujević

  
Prof. dr. sc. Tanja Jurčević Lulić

# Contents

<b>Contents</b>	<b>III</b>
<b>List of Figures</b>	<b>VIII</b>
<b>List of Tables</b>	<b>IX</b>
<b>List of Nomenclature</b>	<b>XII</b>
<b>List of Abbreviations</b>	<b>XIII</b>
<b>Sažetak</b>	<b>XIV</b>
<b>Abstract</b>	<b>XVI</b>
<b>Prošireni sažetak</b>	<b>XVIII</b>
<b>1 Introduction</b>	<b>1</b>
1.1 Motivation . . . . .	1
1.2 Fundamental aspects . . . . .	2
1.3 Identification of the problem . . . . .	5
1.4 Overview of the thesis structure . . . . .	5
<b>2 Literature review</b>	<b>7</b>
2.1 Statistical Energy Analysis (SEA) . . . . .	8
2.2 Finite element method (FEM) . . . . .	10
2.3 Hybrid SEA/FE analysis . . . . .	13
2.4 Panel acoustic contribution analysis (PACA) . . . . .	14
<b>I Coupled structural-acoustic analysis of the plate and cavity model and validation of the FE solution with the analytical solution</b>	<b>17</b>
<b>3 Model problem</b>	<b>18</b>

<b>4</b>	<b>Analytical modeling of the fluid-structure interaction</b>	<b>22</b>
4.1	Analytical modeling of the plate . . . . .	22
4.1.1	Differential equation of motion for a thin rectangular plate . . . . .	22
4.1.2	Eigenfrequencies and eigenmodes of a simply supported plate . . . . .	24
4.1.3	Forced response of a simply supported plate . . . . .	26
4.2	Analytical modeling of the acoustic cavity . . . . .	29
4.2.1	The acoustic wave equation . . . . .	29
4.2.2	Eigenfrequencies and eigenmodes of a three-dimensional box-shaped acoustic cavity . . . . .	31
4.2.3	Forced response of a three-dimensional box-shaped acoustic cavity . . . . .	34
4.3	Coupled structural-acoustic model . . . . .	36
<b>5</b>	<b>Numerical modeling of the fluid-structure interaction in MSC Actran</b>	<b>41</b>
5.1	Introduction to MSC Actran . . . . .	41
5.2	Computation of the required finite element size . . . . .	45
5.3	Setup of the finite element vibro-acoustic model . . . . .	50
<b>6</b>	<b>Comparison between the analytical and numerical solutions</b>	<b>53</b>
6.1	Comparison of eigenmodes and eigenfrequencies of a simply supported plate . . . . .	54
6.2	Comparison of eigenmodes and eigenfrequencies of a rigid-walled acoustic cavity . . . . .	57
6.3	The FRF between the displacement at the excitation point and the force exciting the plate . . . . .	60
6.4	The FRF between the acoustic pressure at the driver's ear and the force exciting the plate . . . . .	64
6.5	Conclusion . . . . .	69
<b>II</b>	<b>Numerical simulation of the noise transmission from an exterior sound source into a vehicle interior</b>	<b>70</b>
<b>7</b>	<b>Methodology to predict the exterior and interior sound field in ACTRAN</b>	<b>71</b>
7.1	Exterior acoustic model . . . . .	75
7.2	Projection procedure . . . . .	83
7.3	Vibro-acoustic model . . . . .	84
<b>8</b>	<b>Results</b>	<b>92</b>
8.1	Numerical results of the exterior acoustic analysis . . . . .	94
8.2	Numerical results of vibro-acoustic analysis . . . . .	108



<b>9 Conclusions and recommendations for future work</b>	<b>117</b>
<b>Bibliography</b>	<b>121</b>
<b>Appendix</b>	<b>124</b>

# List of Figures

Figure 1.1: Structure-borne and airborne noise sources, [2] . . . . . 4

Figure 2.1: The use of SEA and FEM in relation to frequency range of interest . . . 7

Figure 2.2: The vehicle model in SEA, [5] . . . . . 9

Figure 2.3: Computational steps of the FE method, [6] . . . . . 10

Figure 2.4: Simulation flow of the FE method, [6] . . . . . 11

Figure 2.5: Cutplane of the exterior acoustic model, [6] . . . . . 11

Figure 2.6: Convergence of the infinite element order, [6] . . . . . 12

Figure 2.7: Convergence of the size of the exterior acoustic domain, [6] . . . . . 13

Figure 2.8: Body-in-white vehicle in Hybrid FE/SEA, [8] . . . . . 14

Figure 2.9: The vehicle model of Hybrid FE/SEA, [8] . . . . . 14

Figure 2.10: The PACA work flow, [9] . . . . . 15

Figure 3.1: The plate representing the firewall coupled to a box-shaped acoustic cavity . . . . . 18

Figure 4.1: Bending moments along edges and displacement of a rectangular plate, [12] . . . . . 23

Figure 5.1: Actran work principle, [21] . . . . . 43

Figure 5.2: Actran work flow, [21] . . . . . 43

Figure 5.3: Topology of tetrahedral elements, [22] . . . . . 45

Figure 5.4: Box-shaped acoustic cavity modeled with tetrahedral acoustic elements 46

Figure 5.5: Topology of shell elements, [22] . . . . . 47

Figure 5.6: Rectangular plate modeled with shell elements . . . . . 48

Figure 5.7: Computation of acoustic element size . . . . . 49

Figure 5.8: Computation of structural element size . . . . . 49

Figure 5.9: Simplified numerical vibro-acoustic model . . . . . 50

Figure 5.10: Projection procedure, [22] . . . . . 51

Figure 5.11: Simply supported boundary conditions for thin shell elements, [22] . . . 52

Figure 6.1: Lowest nine natural frequencies and modes of 1.4 m x 1.2m thin simply supported steel plate (analytical solution) . . . . . 55

Figure 6.2:	Lowest nine natural frequencies and modes of 1.4 m x 1.2m thin simply supported steel plate (numerical solution with a mesh of 140x120 shell elements) . . . . .	56
Figure 6.3:	Lowest nine acoustic natural frequencies and modes of a 2.2 m x 1.4 m x 1.2m air-filled cavity with rigid walls (analytical solution) . . . . .	58
Figure 6.4:	Lowest nine acoustic natural frequencies and modes of a 2.2 m x 1.4 m x 1.2m air-filled cavity with rigid walls (numerical solution with mesh of 55x35x30 tetrahedral acoustic elements) . . . . .	59
Figure 6.5:	Driving point receptance for the whole frequency range due to the point force exciting the plate . . . . .	61
Figure 6.6:	Driving point receptance up to 500 Hz due to the point force exciting the plate . . . . .	62
Figure 6.7:	Driving point receptance from 500 Hz up to 1600 Hz due to the point force exciting the plate . . . . .	63
Figure 6.8:	Sound pressure level at driver's ear for the whole frequency range . . . . .	65
Figure 6.9:	Sound pressure level at driver's ear up to 500 Hz . . . . .	66
Figure 6.10:	Sound pressure level at driver's ear from 500 Hz to 1600 Hz . . . . .	67
Figure 6.11:	Sound pressure level at driver's ear up to 300 Hz . . . . .	68
Figure 7.1:	Body-in-blue finite element vehicle model . . . . .	72
Figure 7.2:	Acoustic cavities inside the body-in-blue vehicle . . . . .	72
Figure 7.3:	Computational steps in ACTRAN . . . . .	74
Figure 7.4:	Exterior acoustic model . . . . .	75
Figure 7.5:	The workflow of the creation of the exterior wrap . . . . .	76
Figure 7.6:	Exterior wrap of the body-in-blue vehicle . . . . .	77
Figure 7.7:	Time comparison per frequency, [23] . . . . .	78
Figure 7.8:	Generated exterior acoustic mesh in relation to frequency range . . . . .	79
Figure 7.9:	Rigid baffle in exterior acoustic model . . . . .	80
Figure 7.10:	Exterior sound source positions . . . . .	81
Figure 7.11:	Microphone arrays located around the vehicle . . . . .	82
Figure 7.12:	Projection quality of the interface for the vehicle structure and the passenger compartment cavity with gap and plane tolerance specified as 5 mm and 0.05, respectively . . . . .	86
Figure 7.13:	Projection quality of the interface for the vehicle structure and small front cavity with gap and plane tolerance specified as 5 mm and 0.05, respectively . . . . .	86
Figure 7.14:	Projection quality of the interface for the vehicle structure and B-pillar cavity with gap and plane tolerance specified as 5 mm and 0.05, respectively . . . . .	87

Figure 7.15:	Projection quality of the interface for the vehicle structure and bumper cavity with gap and plane tolerance specified as 5 mm and 0.05, respectively . . . . .	87
Figure 7.16:	Projection quality of the interface for the vehicle structure and small back cavity with gap and plane tolerance specified as 5 mm and 0.05, respectively . . . . .	88
Figure 7.17:	Projection quality of the interface for the vehicle structure and door cavities with gap and plane tolerance specified as 5 mm and 0.05, respectively . . . . .	88
Figure 7.18:	Projection quality of the interface for the vehicle structure and CD-pillar cavities with gap and plane tolerance specified as 5 mm and 0.05, respectively . . . . .	89
Figure 7.19:	Projection quality of the interface for the vehicle structure and trunk cavity with gap and plane tolerance specified as 5 mm and 0.05, respectively . . . . .	89
Figure 7.20:	Projection quality of the interface for the vehicle structure and front feet cavity with gap and plane tolerance specified as 5 mm and 0.05, respectively . . . . .	90
Figure 7.21:	Projection quality of the interface for the vehicle structure and A-pillar cavity with gap and plane tolerance specified as 5 mm and 0.05, respectively . . . . .	90
Figure 7.22:	Projection quality of the interface for the vehicle structure and tailgate cavity with gap and plane tolerance specified as 5 mm and 0.05, respectively . . . . .	91
Figure 7.23:	Position of the interior microphones . . . . .	91
Figure 8.1:	Sound Pressure Level computed on the rigid exterior wrap of the body-in-blue vehicle due to a volume monopole source located at the left rear wheelhouse . . . . .	96
Figure 8.2:	Sound Pressure Level on the rigid exterior wrap of the body-in-blue vehicle due to a volume velocity source located at the left front wheelhouse . . . . .	97
Figure 8.3:	Sound Pressure Level computed on the rigid exterior wrap of the body-in-blue vehicle due to a volume velocity sound source located in the engine compartment . . . . .	98
Figure 8.4:	Sound Pressure Level computed on the rigid exterior wrap of the body-in-blue vehicle due to a volume velocity sound source located at the exhaust . . . . .	99

Figure 8.5:	Sound Pressure Level computed on microphone arrays positioned around the vehicle due to a volume velocity sound source located at the left rear wheelhouse . . . . .	100
Figure 8.6:	Sound Pressure Level computed on microphone arrays positioned around the vehicle due to a volume velocity sound source located at the left front wheelhouse . . . . .	101
Figure 8.7:	Sound Pressure Level computed on microphone arrays positioned around the vehicle due to a volume velocity sound source located in the engine compartment . . . . .	102
Figure 8.8:	Sound Pressure Level computed on microphone arrays positioned around the vehicle due to a volume velocity sound source located at the exhaust . . . . .	103
Figure 8.9:	Frequency Response Function (FRF) calculated between the exterior microphones and volume velocity sound source located at the left rear wheelhouse . . . . .	104
Figure 8.10:	Frequency Response Function (FRF) calculated between the exterior microphones and volume velocity sound source located at the left front wheelhouse . . . . .	105
Figure 8.11:	Frequency Response Function (FRF) calculated between the exterior microphones and volume velocity sound source located in the engine compartment . . . . .	106
Figure 8.12:	Frequency Response Function (FRF) calculated between the exterior microphones and volume velocity sound source located at the exhaust . . . . .	107
Figure 8.13:	Sound Pressure Level computed in the vehicle cavities due to the volume velocity sound source located at the left rear wheelhouse . . . . .	109
Figure 8.14:	Sound Pressure Level computed in the vehicle cavities due to the volume velocity sound source located at the left front wheelhouse . . . . .	110
Figure 8.15:	Sound Pressure Level computed in the vehicle cavities due to the volume velocity sound source located in the engine compartment . . . . .	111
Figure 8.16:	Sound Pressure Level computed in the vehicle cavities due to the volume velocity sound source located at the exhaust . . . . .	112
Figure 8.17:	Frequency Response Function (FRF) calculated between the interior microphones and volume velocity sound source located at the left rear wheelhouse . . . . .	113
Figure 8.18:	Frequency Response Function (FRF) calculated between the interior microphones and volume velocity sound source located at the left front wheelhouse . . . . .	114

Figure 8.19: Frequency Response Function (FRF) calculated between the interior microphones and volume velocity sound source located in the engine compartment . . . . . 115

Figure 8.20: Frequency Response Function (FRF) calculated between the interior microphones and volume velocity sound source located at the exhaust 116

# List of Tables

Table 1.1:	Frequency range of interest for NVH analysis . . . . .	1
Table 1.2:	Decibel scale, [1] . . . . .	3
Table 3.1:	Input dimensions for the flexible plate . . . . .	19
Table 3.2:	Input dimensions for the acoustic cavity . . . . .	19
Table 3.3:	Material properties for the flexible plate . . . . .	20
Table 3.4:	Material properties for the acoustic cavity . . . . .	20
Table 3.5:	Coordinates of the field points of interest . . . . .	20
Table 5.1:	Maximum finite element size of the acoustic cavity . . . . .	46
Table 5.2:	Maximum finite element size of the structural plate . . . . .	48
Table 6.1:	Eigenfrequencies for a 2 mm thick simply supported plate with the dimensions 1.4 m x 1.2 m oriented in <i>yz</i> -plane . . . . .	54
Table 6.2:	Eigenfrequencies for air-filled cavity with rigid walls with dimensions 2.2m x 1.4m x 1.2m . . . . .	57
Table 7.1:	Frequency bands for exterior acoustic component . . . . .	78
Table 7.2:	Gap and plane tolerances specified for projecting the acoustic pressure saved on the wrap onto the structure body . . . . .	83
Table 7.3:	Materials, components and BCs imported from NASTRAN input file	84
Table 8.1:	Coordinates of the microphone positions located outside of the vehicle on the microphone arrays . . . . .	93
Table 8.2:	Coordinates of the microphone positions located in the vehicle interior	93

# List of Nomenclature

## Latin symbols

$A$	Pa	Amplitude of the acoustic plane wave
$A$	N	Amplitude of the dynamic force
$a_{n_x n_y n_z}$	-	Modal participation factor vector for acoustic model
$c$	m/s	Sound speed
$\tilde{c}$	m/s	Complex sound speed
$c_b$	m/s	Phase velocity
$c_g$	m/s	Group velocity
$C_{m n n_x n_y n_z}$	-	Modal coupling matrix
$D_0$	Nmm	Bending stiffness of the plate
$D$	Nmm	Complex bending stiffness
$D_{n_x n_y n_z m n}$	-	Modal coupling matrix
$E_0$	N/mm <sup>2</sup>	Young's modulus
$E$	N/mm <sup>2</sup>	Complex Young's modulus
$f$	Hz	Frequency
$F$	N	Dynamic force
$f_{mn}$	Hz	Natural frequency
$F_{mn}$	N	Modal force matrix
$g$	-	Time dependent function
$g_{mn}$	-	Modal participation factor vector for structural model
$h$	mm	Plate thickness
$H_{p,F}$	1/mm <sup>2</sup>	Frequency Response Function
$H_{p,V}$	Pa/(m <sup>3</sup> /s)	Frequency Response Function
$k$	1/m	Acoustic wave number
$\tilde{k}$	1/m	Complex acoustic wave number
$k_m$	1/m	Bending wave number in the direction of $y$ -axis
$k_n$	1/m	Bending wave number in the direction of $z$ -axis
$k_x$	1/m	Acoustic wave number in the direction of $x$ -axis
$k_y$	1/m	Acoustic wave number in the direction of $y$ -axis
$k_z$	1/m	Acoustic wave number in the direction of $z$ -axis



$K_{mn}$	N/mm	Structural modal stiffness matrix
$K_{n_x n_y n_z}$	mm	Acoustic modal stiffness matrix
$L_{S_{max}}$	mm	Maximum structural finite element size
$L_{F_{max}}$	mm	Maximum acoustic finite element size
$L_x$	mm	Dimension of the cavity
$L_y$	mm	Dimension of the cavity and plate
$L_z$	mm	Dimension of the cavity and plate
$L_p$	dB	Sound Pressure Level (SPL)
$m$	-	Modal number along $y$ -axis
$M$	-	Modal order along $y$ -axis
$M_y$	Nm	Bending moment about $y$ -axis
$M_z$	Nm	Bending moment about $z$ -axis
$M_{mn}$	kg	Structural modal mass matrix
$M_{n_x n_y n_z}$	ms <sup>2</sup>	Acoustic modal mass matrix
$n$	-	Modal number along $z$ -axis
$N$	-	Modal order along $z$ -axis
$n_F$	-	Number of elements per acoustic wavelength
$n_S$	-	Number of elements per structural wavelength
$n_x$	-	Modal number along $x$ -axis
$N_x$	-	Modal order along $x$ -axis
$n_y$	-	Modal number along $y$ -axis
$N_y$	-	Modal order along $y$ -axis
$n_z$	-	Modal number along $z$ -axis
$N_z$	-	Modal order along $z$ -axis
$p$	N/mm <sup>2</sup>	Acoustic pressure
$\hat{p}$	N/mm <sup>2</sup>	Amplitude of the acoustic plane wave
$p_{ac}$	N/mm <sup>2</sup>	Acoustic pressure
$p_{atm}$	N/mm <sup>2</sup>	Atmospheric pressure
$p_{ext}$	N/mm <sup>2</sup>	Acoustic pressure
$p_{int}$	N/mm <sup>2</sup>	Acoustic pressure
$(p_g)_i$	N/mm <sup>2</sup>	Panel contributed sound pressure
$p_{ref}$	N/mm <sup>2</sup>	Reference pressure
$p_{tot}$	N/mm <sup>2</sup>	Total pressure
$Q$	kg/s	Mass flow
$(r_c)_i$	-	Panel acoustic contribution ratio

$u_x$	mm	Finite element displacement in the direction of $x$ -axis
$u_y$	mm	Finite element displacement in the direction of $y$ -axis
$u_z$	mm	Finite element displacement in the direction of $z$ -axis
$\vec{u}$	m/s	Particle velocity vector
$u_x$	m/s	Particle velocity along $x$ -axis
$u_y$	m/s	Particle velocity along $y$ -axis
$u_z$	m/s	Particle velocity along $z$ -axis
$V$	m <sup>3</sup> /s	Volume velocity
$w$	mm	Displacement of plate
$x_F$	mm	Force position coordinate
$X_{w,F}$	mm/N	Driving Point Receptance
$Y$	-	Spatially dependent function
$y_F$	mm	Force position coordinate
$Z$	-	Spatially dependent function

### Greek symbols

$\alpha$	-	Acoustic attenuation coefficient
$\beta$	-	Adiabatic bulk modulus
$\delta$	-	Viscous damping
$\eta$	-	Structural damping
$\theta_x$	-	Finite element rotation about $x$ -axis
$\theta_y$	-	Finite element rotation about $y$ -axis
$\theta_z$	-	Finite element rotation about $z$ -axis
$\kappa$	1/m	Bending wave number
$\nu$	-	Poisson's ratio
$\rho$	kg/m <sup>3</sup>	Air density
$\rho$	kg/m <sup>3</sup>	Density disturbance in the medium
$\rho_0$	kg/m <sup>3</sup>	Density in the undisturbed medium
$\rho_s$	kg/m <sup>3</sup>	Steel density
$\rho_t$	kg/m <sup>3</sup>	Total density
$\varphi_{mn}$	-	Eigenfunction of a simply supported plate
$\varphi_{n_x n_y n_z}$	-	Eigenfunction of the rigid wall acoustic cavity
$\omega$	rad/s	Circular frequency

# List of Abbreviations

## Abbreviations

BC	Boundary Condition
BEM	Boundary Element Method
CAE	Computer Aided Engineering
CPU	Central Processing Unit
FEM	Finite Element Method
FRF	Frequency Response Function
IEM	Infinite Element Method
NVH	Noise, Vibration, Harshness
PACA	Panel Acoustic Contribution Analysis
RAM	Random Access Memory
SEA	Statistical Energy Analysis
SPL	Sound Pressure Level

# Sažetak

Proizvođači automobila postaju sve svjesniji da razina buke u unutrašnjosti vozila uvelike utječe na odluku kupca o kupnji. To se osobito odnosi na osobna vozila visoke klase. Stoga, poboljšanje vibroakustičke kvalitete osobnih vozila postaje važan i neizbježan predmet razvoja i istraživanja u automobilskoj industriji. Za inženjere koji se bave bukom i vibracijama vrlo je važno moći točno predvidjeti zvuk u unutrašnjosti vozila u ranoj fazi konstruiranja. Na taj način izbjegavaju se znatno veći troškovi u kasnijim fazama razvoja novih modela vozila.

U ovom radu, razvijena je metoda za proračun buke u unutrašnjosti osobnog vozila u programskom paketu ACTRAN. Programski paket se temelji na metodi konačnih elemenata (MKE). Ovaj programski paket jedan je od zastupljenijih numeričkih alata za vibroakustičke analize u suvremenoj europskoj automobilskoj industriji.

U prvom dijelu rada, razvijen je model koji uključuje slobodno oslonjenu deformabilnu pravokutnu ploču, kojom se modelira vatronepropusni zid između prostora motora s unutrašnjim izgaranjem i putničkog prostora, potpuno spregnutu s pravokutnom akustičkom šupljinom kojom se modelira putnički prostor automobila. Preostalih 5 zidova akustičke šupljine pretpostavljeni su krutima. Dimenzije modela izabrane su tako da približno odgovaraju dimenzijama stvarnog vozila. Počevši s diferencijalnim jednadžbama gibanja posebno za ploču i akustičku šupljinu, metodom modalne dekompozicije izvedena je matrična jednadžba za potpuno spregnuti vibro-akustički model. Također, izrađen je i analogni numerički model pomoću programskog paketa ACTRAN. Uspoređujući karakteristične rezultate dobivene analitičkom i numeričkom metodom, određene su prikladne veličine konačnih elementa i maksimalna frekvencija kod koje se razina buke u unutrašnjosti vozila daje odrediti s dovoljnom točnošću.

U drugom dijelu rada razvijena je numerička metoda za proračun zvuka u unutrašnjosti stvarnog vozila koristeći ACTRAN. Proučavaju se tri najvažnija izvora buke kod vozila: buka koju proizvodi motor s unutrašnjim izgaranjem, buka koja nastaje kotrljanjem kotača po podlozi te buka koju proizvodi ispušni sustav. Geometrija primjera vozila odgovara geometriji jedne luksuzne limuzine. Razvijena metoda temelji se na pristupu koji se sastoji od tri koraka, a primijenjena je u frekvencijskom rasponu od 100 Hz do 1600 Hz. U prvom koraku kreira se numerički simulacijski model koji opisuje radijaciju

zvuka iz izvora smještenih izvan vozila. Navedeni model služi za računanje raspodjele zvučnog tlaka na krutoj ovojnici karoserije vozila. Zvučno polje nastaje uslijed zvuka narinutog iz akustičkih izvora karakteristične volumne brzine (engl. "volume velocity source"). Izvori zvuka smješteni su na četiri karakteristična mjesta: kod lijevog stražnjeg kotača, kod lijevog prednjeg kotača, u prostoru motora te kod ispušnog lonca. U drugom koraku, polje kompleksnog akustičkog tlaka izračunato po površini krute ovojnice vozila projicira se na pojedine dijelove karoserije. U trećem koraku, izračunato polje akustičkog tlaka se koristi kao uzbuda za deformabilne dijelove karoserije (tzv. konfiguracija "body-in-blue"). Na kraju, izračunate su funkcije frekvencijskog odziva između akustičkog tlaka u šest karakterističnih točaka unutrašnjosti vozila i volumne brzine izvora sa četiri navedene lokacije. Također, izračunata je, prikazana i diskutirana raspodjela akustičkog tlaka u cijelom putničkom prostoru.

**Ključne riječi: zvuk, vibracije, vibro-akustika, buka u unutrašnjosti vozila, vibroakustička kvaliteta vozila, metoda konačnih elemenata**

# Abstract

Vehicle manufacturers are becoming more and more aware that the interior sound quality of a vehicle greatly affects the customer's decision to make a purchase. This is especially true with passenger cars in the upper market segment. Therefore, improving noise, vibration and harshness (NVH) quality of passenger vehicles has become an increasingly important topic in the automotive industry. As such, it is of great interest for noise and vibration engineers to be able to accurately predict the interior sound of a car in the early stage of the vehicle design. This is necessary to avoid substantially increased costs in the later vehicle development stages.

In this thesis, a methodology to predict the interior sound field in a passenger road vehicle is developed using a commercial Finite Element (FE) software ACTRAN. This piece of software is a current state-of-the-use in the European car manufacturing industry.

In the first part of the thesis, a simply supported flexible rectangular plate, which represents the firewall between the engine compartment and the passenger space, is fully coupled to a box-shaped acoustic cavity having the other five walls rigid. The model geometry is chosen such that it roughly approximates a real car. Starting from separate differential equations of motions for the plate and the acoustic cavity, a fully coupled vibro-acoustic model is developed using the modal decomposition technique. An equivalent numerical model is also built in ACTRAN. By comparing some characteristic results obtained using the analytical model and the numerical model, the FE size and the maximum frequency where the interior sound pressure levels can still be accurately predicted are determined.

In the second part of the thesis a numerical, FE-based methodology to predict the interior noise due to three principal sound sources in an example road vehicle is developed using ACTRAN. The three noise sources are: the engine noise, the tyre-rolling noise, and the exhaust noise. The geometry of the example vehicle corresponds to a real luxury sedan. The methodology developed is based on a three-step procedure applied in the frequency range of interest from 100 Hz to 1600 Hz. In the first step, the finite element exterior acoustic model is built in order to calculate the surface pressure distribution on the rigid exterior wrap of the vehicle. The acoustic medium is

excited by exterior volume velocity sound sources at four characteristic locations. The four locations are chosen at the left rear wheelhouse, at the left front wheelhouse, in the engine compartment and at the exhaust. In the second step, the complex acoustic pressure distribution on the rigid exterior wrap of the structural parts of the vehicle is calculated. It is used in the third step to excite the flexible "body-in-blue" vehicle. Frequency Response Functions (FRFs) between the volume velocities of the four characteristic exterior sound sources and the acoustic pressures at six characteristic interior locations are calculated. Also the whole distribution of the sound pressure in the vehicle interior is computed, presented and discussed.

**Keywords: Sound, Vibration, Vibroacoustics, Vehicle interior noise, Automotive NVH, FEM**

# Prošireni sažetak

Cilj ovog diplomskog rada jest predložiti metodologiju za predviđanje buke u unutrašnjosti i izvan automobalnog vozila. Nadalje, zadatak je primijeniti predloženu metodologiju za proračun buke stvarnog automobila. Rad je izrađen na Fakultetu strojarstva i brodogradnje Sveučilišta u Zagrebu u suradnji s tvrtkama AVL-AST d.o.o. iz Zagreba i AVL List GmbH iz Graza.

U posljednjih dvadesetak godina vibroakustička kvaliteta tehničkih proizvoda postaje iznimno važna za kompetitivnost gospodarstava zemalja EU kao i za blagostanje njihovih građana. Primjerice, zagađenje bukom u prometu drugi je po redu uzrok povećanja smrtnosti građana EU. Njegovanje relevantnih inženjerskih disciplina i ciljana izobrazba novih stručnjaka u tom području jednako je važna i za razvoj hrvatskog gospodarstva i društva. Kao rezultat napora automobilske industrije da zadovolji sve strože standarde u pogledu zagađenja bukom, jedan od bitnih tehničkih zahtjeva kod razvoja novih modela automobila su niske emisije buke u okoliš, a kod modela više klase također i postizanje vrlo visoke akustičke udobnosti u putničkom prostoru. U takvim situacijama je potrebno u ranim fazama konstruiranja vozila moći predvidjeti zvuk u putničkom prostoru kako bi se izbjegli znatno veći troškovi u kasnijim fazama razvoja. U tu svrhu razvijene su razne metode za predviđanje zvuka u unutrašnjosti vozila. U području visokih frekvencija primjenjuje se SEA (engl. Statistical Energy Analysis) metoda za analizu vibro-akustičkih sustava. Ova metoda spada u skupinu energijskih metoda gdje se dinamički sustav promatra kao sustav sastavljen od više podsustava, a analiza buke u unutrašnjosti vozila vrši se računanjem protoka akustičke energije između tih podsustava. U području niskih frekvencija, jedna od najprimjenjivanijih metoda za predviđanje zvuka u unutrašnjosti vozila je metoda konačnih elemenata (MKE) gdje se vibro-akustički sustav diskretizira pomoću konačnih elemenata, a pristup se temelji na transformaciji spregnutih diferencijalnih jednadžbi gibanja u sustav algebarskih jednadžbi. Posljednjih godina razvijaju se i hibridne metode kojima je cilj povećati točnost proračuna buke u području srednjih frekvencija gdje niti SEA metoda niti MKE za sada ne postižu zadovoljavajuću točnost. Očekivana prednost hibridnih metoda je mogućnost točnijeg proračuna i analize vibro-akustičkog ponašanja sustava u cijelom



frekvencijskom području.

U ovom radu, razvijena je metoda za proračun buke u unutrašnjosti osobnog vozila u programskom paketu ACTRAN. Programski paket se temelji na metodi konačnih elemenata, a glavna primjena paketa je opisivanje akustičkog ponašanja dinamičkih i vibro-akustičkih sustava.

U prvom dijelu rada, razvijen je pojednostavljeni matematički vibro-akustički model osobnog vozila. Model uključuje slobodno oslonjenu deformabilnu pravokutnu ploču potpuno spregnutu s pravokutnom akustičkom šupljinom. Preostalih 5 zidova akustičke šupljine pretpostavljeni su krutima. Pločom se modelira vatronepropusni zid između prostora motora s unutrašnjim izgaranjem i putničkog prostora, dok se akustičkom šupljinom modelira putnički prostor automobila. Dimenzije modela izabrane su tako da približno odgovaraju dimenzijama stvarnog vozila. Najprije su izvedene diferencijalne jednadžbe gibanja posebno za ploču i za akustičku šupljinu, a potom je metodom modalne dekompozicije izvedena matična jednadžba za potpuno spregnuti vibro-akustički model. Diferencijalne jednadžbe gibanja kod slobodnih vibracija izvedene su bez prigušenja, dok su kod analize prisilnih vibracija uzeta u obzir strukturalna i akustička prigušenja. Strukturalno prigušenje izvedeno je uzimajući u obzir kompleksni dio modula elastičnosti, a akustičko prigušenje, koje nastaje zbog viskoznosti zraka, opisano je kao kompleksni dio valnog broja. Također, izrađen je i analogni numerički model pomoću programskog paketa Actran. Pomoću njega je prikazan i način modeliranja vibro-akustičke sprege te su navedeni i objašnjeni parametri kojima se kontrolira kvaliteta sprezanja strukturalnog i akustičkog modela. Izračunate su vlastite frekvencije za ploču i akustičku šupljinu te su prikazane forme vibriranja. Također, izračunate su funkcije frekvencijskog odziva između pomaka ploče na mjestu uzbude i dinamičke uzbudne sile, kao i funkcije frekvencijskog odziva između tlaka u putničkom prostoru i dinamičke uzbudne sile. Uspoređujući rezultate dobivene analitičkom i numeričkom metodom, određene su prikladne veličine konačnih elemenata i maksimalna frekvencija kod koje se razina buke u unutrašnjosti vozila daje odrediti s dovoljnom točnošću.

U drugom dijelu rada razvijena je metoda za proračun zvuka u unutrašnjosti stvarnog vozila koristeći ACTRAN. Geometrija primjera vozila odgovara geometriji jedne luksuzne limuzine. Proučavaju se tri najvažnija izvora buke kod vozila: buka koju proizvodi motor s unutarnjim izgaranjem, buka koja nastaje kotrljanjem kotača po podlozi te buka koju proizvodi ispušni sustav. Razvijena metoda temelji se na pristupu koji se sastoji od tri koraka, a primijenjena je u frekvencijskom rasponu od 100 Hz do 1600 Hz. U prvom koraku kreira se numerički simulacijski model koji opisuje radijaciju

zvuka iz izvora smještenih izvan vozila. Navedeni model služi za računanje raspodjele zvučnog tlaka na krutoj ovojnici karoserije vozila. Zvučno polje nastaje uslijed zvuka narinutog iz akustičkih izvora karakteristične volumne brzine. Izvori zvuka smješteni su na četiri karakteristična mjesta: kod lijevog stražnjeg kotača, kod lijevog prednjeg kotača, u prostoru motora te kod ispušnog lonca. Zbog približno simetrične geometrije vozila dovoljno je uzeti u obzir samo jedan par kotača na jednoj strani vozila. Kako bi se smanjilo računalno vrijeme trajanja simulacije, u ovom koraku korištena je metoda adaptivnog generiranja mreže konačnih elemenata koja uključuje automatsko generiranje mreže akustičke domene izvan vozila za svaki frekvencijski pojas. Stoga, metodom adaptivnog generiranja mreže cjelokupno frekvencijsko područje podijeljeno je u više frekvencijskih pojasa, a veličina konačnih elemenata određena je prema maksimalnoj frekvenciji svakog od frekvencijskih pojasa. Drugim riječima, u svakom frekvencijskom pojasu postoji mreža konačnih elemenata s prikladnom veličinom konačnog elementa. Ovom tehnologijom zamijenjena je dosad korištena metoda u kojoj je veličina konačnih elemenata određena prema maksimalnoj frekvenciji cjelokupnog frekvencijskog područja. Time se postižu značajne uštede procesorskog vremena. U drugom koraku, polje kompleksnog akustičkog tlaka izračunato po površini krute ovojnice vozila projicira se na pojedine dijelove karoserije. Postupak projiciranja se vrši u pomoćnom programu "Export load" koji je dio programskog paketa ACTRAN. U trećem koraku, polje akustičkog tlaka izračunatog na pojedinim dijelovima karoserije vozila koristi se kao uzbuda za deformabilne dijelove karoserije (tzv. konfiguracija "body-in-blue"). Nakon pretvorbe NASTRAN ulazne datoteke u ACTRAN i sprezanja strukturalnog modela sa akustičkim, izrađen je numerički vibro-akustički simulacijski model. U ovom radu data su objašnjenja vezana uz sprezanje strukturalnog modela koji se sastoji od modela karoserije vozila i akustičkog modela koji se sastoji od modela šupljina ispunjenih zrakom u unutrašnjosti vozila. Na kraju, izračunate su funkcije frekvencijskog odziva između akustičkog tlaka u šest karakterističnih točaka unutrašnjosti vozila i volumne brzine izvora sa četiri navedene lokacije izvan vozila. Nadalje, izračunate su i funkcije frekvencijskog odziva između akustičkog tlaka u šest točaka izvan vozila i volumne brzine akustičkih izvora sa četiri navedene lokacije. Također, izračunata je, prikazana i diskutirana raspodjela akustičkog tlaka u cijelom putničkom prostoru. Dodatno je izračunato i prikazano polje akustičkog tlaka na povišini krute ovojnice karoserije vozila i polje akustičkog tlaka na plohama na kojima se inače smještaju mikrofoni izvan vozila kod eksperimentalne analize buke vozila u gluhoj komori.

# Chapter 1

## Introduction

### 1.1 Motivation

The sound quality of the vehicle interior noise has become a very important aspect in perceiving the overall quality of a vehicle. For this reason the acoustical comfort, which is influenced by sound and vibration, is becoming a very important topic among acoustic engineers. Often, acoustic engineers are encountering opposing situations where no disturbing noises should be heard, but on the other hand the sound from, e.g. engine should fulfill the expectations of the driver. Therefore, achieving a good quality sound is often in conflict with other NVH targets. NVH stands for Noise (audible response), Vibration (tactile response) and Harshness (rough or granting to the senses). Noise is a generic term for measuring sound levels. Further more, vibration refers to mechanical oscillations about an equilibrium point, whereas harshness is a transient event, e.g. caused by road irregularities. Table 1.1 shows the frequency range of interest of noise, vibration and harshness analysis.

**Table 1.1: Frequency range of interest for NVH analysis**

Noise	30 Hz - 10000 Hz
Vibration	up to 200 Hz
Harshness	30 Hz - 400 Hz

The main objective of the NVH analysis of a vehicle is to achieve:

- low vibration at comfort points, e.g. steering wheel, and
- low Sound Pressure Level (SPL) at driver's and passenger's ear.

Moreover, it is cost efficient to reduce vehicle interior noise at the early design stage. Therefore, at this stage it is helpful to employ analytical and numerical methods to predict vehicle interior sound. Analytical methods could work for simplified models of vehicles and cavities, whereas numerical methods such as FEM, have been the most successful tool for modeling the complex geometry of the vehicle body structure and interior space *in the low frequency range*. Method for modeling a complex vibro-acoustic system *at high frequencies* is the Statistical Energy Analysis (SEA), which is nowadays being widely used. Moreover, method for predicting the interior noise *in the mid-frequency range*, the hybrid FE/SEA method, is emerging.

## 1.2 Fundamental aspects

Acoustics is the science of sound and noise. Sound (lat. *sonum* meaning sound, noise) is a small variation of pressure  $p_{ac}$  around a mean reference value  $p_{atm}$ , e.g. atmospheric pressure in the air:

$$p_{tot}(t) = p_{atm} + p_{ac}(t), \quad (1.1)$$

where

$$p_{atm} \gg p_{ac}(t).$$

To simplify notation in future nomenclature, acoustic sound pressure will be written  $p(t)$  instead of  $p_{ac}(t)$ .

On the other hand, noise is an acoustic phenomenon with audible response considered unpleasant or annoying. [1].

Our field of interest is focused on general linear acoustics and vibro-acoustics. The latter studies noise generation by vibrating structures or the vibration of structures induced by acoustic fields, whereas linear acoustics deals with the basic acoustic phenomena such as e.g. reflection and absorption, resonance, sound radiation, diffraction, refraction, etc.

Furthermore, a question opens up: how can sound or sound levels be measured

objectively? The ear mechanism is able to handle both very small and very large values of acoustic pressure, but by the virtue of non-linearity of ear, it responds more efficiently to sounds of very small amplitude than to those of very large amplitude. In order to present the entire spectrum simultaneously, a logarithmic scale is used, which compresses the high amplitudes and expands the low ones. The correlation between the absolute sound pressure and its decibel level is shown in Table 1.2.

**Table 1.2: Decibel scale, [1]**

Decibel	Example	Scale
0 dB = 0.00002 Pa	Threshold of hearing	1x
20 dB = 0.0002 Pa	Anechoic Chamber	10x
40 dB = 0.002 Pa	Quiet Office Room	100x
60 dB = 0.02 Pa	Car interior idling	1000x
80 dB = 0.2 Pa	Loud radio	10000x
100 dB = 2 Pa	Emergency Vehicle Siren	100000x
120 dB = 20 Pa	Rock concert (pain)	1000000x
140 dB = 200 Pa	Jet engine (damage)	10000000x

Sound Pressure Level (SPL) represents the acoustic pressure relative to a reference pressure in a logarithmic scale. It is measured in decibels. Sound Pressure Level is expressed as

$$L_p = 20 \log_{10} \left( \frac{p}{p_{ref}} \right) \quad (1.2)$$

where  $p$  is the acoustic pressure and  $p_{ref}$  is the reference sound pressure. The reference sound pressure is usually the threshold of human hearing, i.e.  $2 \cdot 10^{-5}$  Pa.

Moreover, in order to be able to predict the vehicle interior noise, transfer functions have to be calculated. To analyze the transfer function from source to receiver, a Source-Transmitter-Receiver Model is introduced. In this case, the receiver can be a human occupant, i.e. a driver or a passenger in the vehicle. Furthermore, the source can be structure-borne or airborne. Figure 1.1 shows typical sources that are of great importance when analyzing the vehicle interior noise. Structure-borne sources inject energy directly into the body structure causing them to vibrate, whereas airborne sources inject energy into the acoustic medium that is surrounding the vehicle. The most dominant airborne sources are the engine, the tires and the exhaust, and these sources are considered in the vibro-acoustic analysis in this thesis.

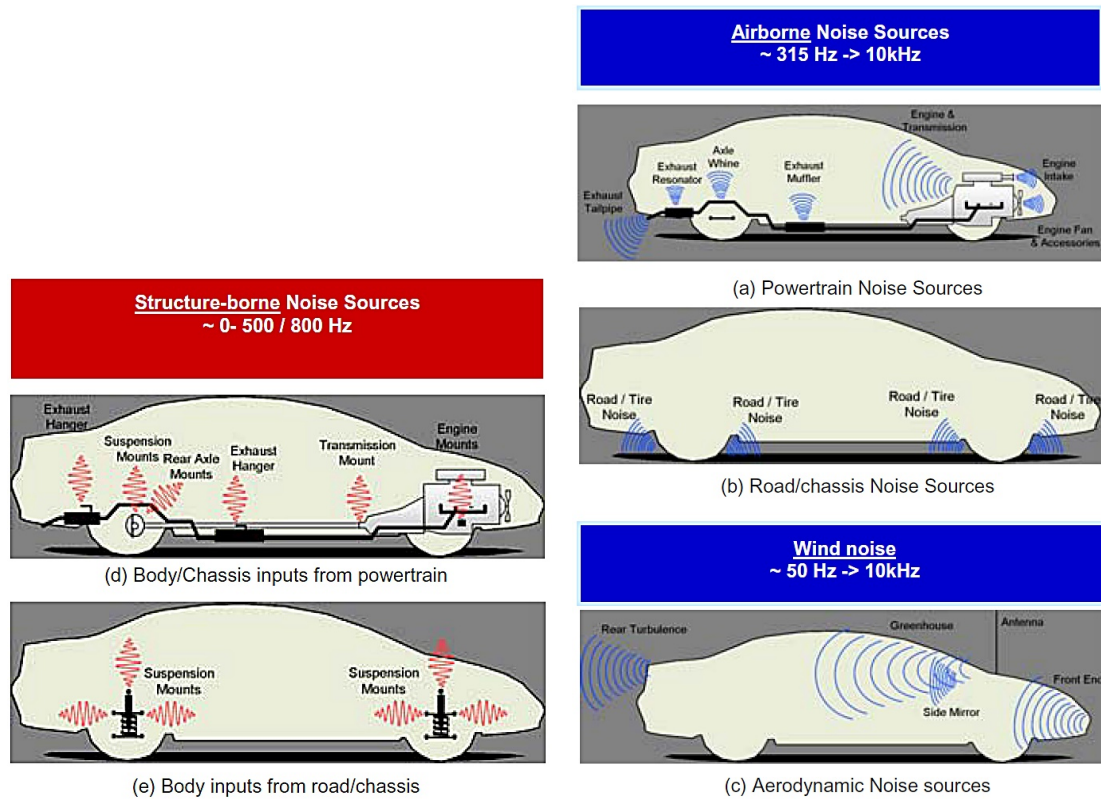


Figure 1.1: Structure-borne and airborne noise sources, [2]

Finally, everything that is between the source and the receiver is the transmission system. This transmission can be purely airborne, e.g. the airborne path between the loudspeaker outside of the vehicle and driver's ear in the vehicle's cavity. This airborne path can only be attenuated by acoustic isolation such as e.g. firewall, acoustical sealing, sound absorber assembly for rear floor, etc. By adding the trim or 'sound package' to a vehicle, the effect is trifold. First, it adds resistive and reactive impedance to the internal cavities of the vehicle, i.e. it adds acoustic absorption to the cavity and modifies natural frequencies of the cavity. Second, it adds resistive and reactive impedance to the body structure, i.e. it adds mass, stiffness and damping to the body structure. Third, it isolates and decouples the structure and the cavity.

Alternately, the transmission path can be structure-borne, e.g. structure-borne path between the engine mounts and the vehicle interior panels. This vibration at the vehicle interior panels is causing small disturbances in the acoustic medium, again, creating airborne transmission path to the human occupant.

## 1.3 Identification of the problem

Following problems are identified as the main tasks of this thesis:

- In order to understand the physics of the linear acoustics and the vibro-acoustics, the first task is to study literature, and also publications for the vehicle interior and exterior acoustics and available simulation models and methodologies.
- The second task is to find the analytical formulation of the coupled equations of the structural-acoustic system for a model which represents the simplified vehicle and cavity model. Also, this task considers the creation of a finite element model that corresponds to the created analytical model.
- The third task is to validate the numerical results with the analytical of the coupled structural-acoustic system.
- The fourth task is to simulate the transmission of noise through the vehicle model which describes the vehicle configuration body-in-blue into the vehicle interior due to the exterior sound source.
- The final task is to propose a valid methodology to predict the vehicle interior and exterior sound field for the complete examined frequency range.

## 1.4 Overview of the thesis structure

The aim of this thesis is to propose a methodology to predict the exterior and interior sound field due to the exterior sound source. The first, introductory chapter briefly addresses the fundamental aspects of NVH.

Chapter 2 gives a review of literature study on interior and exterior acoustics and available simulation models and methodologies.

At this point, the thesis is divided in two parts. The first part considers the analytical and numerical modeling of the coupled structural-acoustic system and the validation of the numerical vibro-acoustic model with the analytical. The second part considers the numerical simulation of the noise transmission into a vehicle interior due to the exterior sound source. Moreover, this part also holds the results obtained from the numerical

simulation in Actran.

Chapter 3 gives a brief introduction to a coupled structural-acoustic model problem.

Chapter 4 covers the analytical formulation of the coupled equations of the structural-acoustic system, whereas the setup of the numerical simulation of the equivalent coupled structural-acoustic system is presented in Chapter 5.

Chapter 6 covers the validation of the numerical vibro-acoustic model with the analytical model. Moreover, numerical results obtained in Actran and analytical results solved using Matlab are presented and discussed.

Chapter 7 deals with the setup of the numerical simulation on a real body-in-blue vehicle to simulate the transmission of noise into the vehicle interior due to the exterior sound source. This chapter also outlines the methodology to predict the exterior and interior sound field. Numerical results of the established methodology are presented and discussed in Chapter 8.

Chapter 9 briefly outlines the conclusions drawn from the performed research and recommendations for the future work.



# Chapter 2

## Literature review

It is of great interest among sound engineers to predict the interior sound of a cabin, whether it is a cabin of an airplane, helicopter cabin or vehicle cabin. Finite Element (FE) Analysis, Statistical Energy Analysis (SEA) or Hybrid FE-SEA analysis are the most used methods to predict the vehicle interior sound. Their application depends on the frequency range of interest. Figure 2.1 shows the adjustable use of SEA and FEM in relation to frequency and complexity. Finite element method (FEM) is used to predict vehicle interior noise in the low-frequency range. Statistical energy analysis (SEA) method is used by many automobile industries to model automotive vibro-acoustic systems at high frequencies. SEA has been confirmed as a good tool in models with a very large number of structural parts.

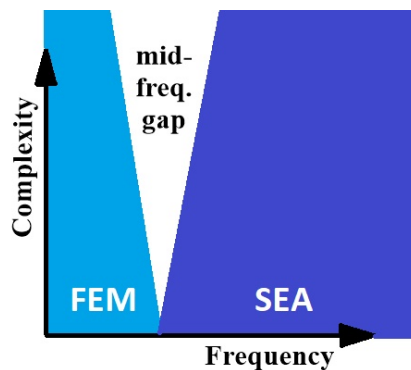


Figure 2.1: The use of SEA and FEM in relation to frequency range of interest

Furthermore, in the recent years, the need to describe the response of a dynamic system at mid-frequencies has risen. In this event, a hybrid FE-SEA approach is developed, which

objective is to combine the low frequency performance of the FE method with the high frequency performance of SEA to produce a single technique to compute the response of the dynamic system across a wide frequency range. The coupling of the FE and SEA method is not easy because the methods differ in two ways:

- FE is based on a dynamic balance, whereas SEA is based on the conservation of the energy flow.
- FE is a deterministic method, whereas SEA is a statistical method.

In following sections, each of methods are described. In addition, a method for improving the NVH of the vehicle interior, Panel Acoustic Contribution Analysis (PACA), is presented.

## 2.1 Statistical Energy Analysis (SEA)

Statistical Energy Analysis (SEA) is a standard energy method to predict vehicle vibration and interior noise. It was developed by R. H. Lyon [3]. SEA has been successfully used in room acoustics and in aerospace structures. The development of SEA arose from the need of engineers to predict vibrational response of large vehicles in high frequency range. Although in that period (1960) computational methods for predicting vibrational modes of structures were available, the size of the models and the speed of the computation were such that engineers could only predict a few of the lowest vibration modes. Since then, SEA has been applied to dynamic systems with many modes where the modes are grouped into subsystems and evaluated statistically. This gives reasonable good results for a reasonable cost. Since SEA is a statistical average approach, at low frequency a lack of modal density (meaning few modes in low frequency range) can lead to poor representation of actual results. With this in mind, SEA can be used to predict the response of a system with small number of modes, but the statistics of the results must be understood carefully.

According to [4], *"a system was divided up into subsystems, the subsystem parameters were expressed probabilistically, and the vibrational state of the system was expressed in terms of time-average total vibrational energy of each of the subsystems, i.e. a global, rather than a local, measure. Vibratory inputs were expressed in terms of time-average*

*input powers, rather than in terms of external forces or displacements.*” Moreover, each subsystem can be idealized to represent a beam, plate, rod, pipe, or acoustic space. In other words, the multi-degree-of-freedom finite element model is replaced by a single-degree-of-freedom finite element model and frequency response function is replaced by a energy response function. The flow of the acoustic energy through various structure body parts is calculated in order to determine the dominant paths of noise transmission to the passenger compartment.

Figure 2.2 shows an example of division of a dynamic system, where total of 36 subsystems were made to be used in SEA [5].

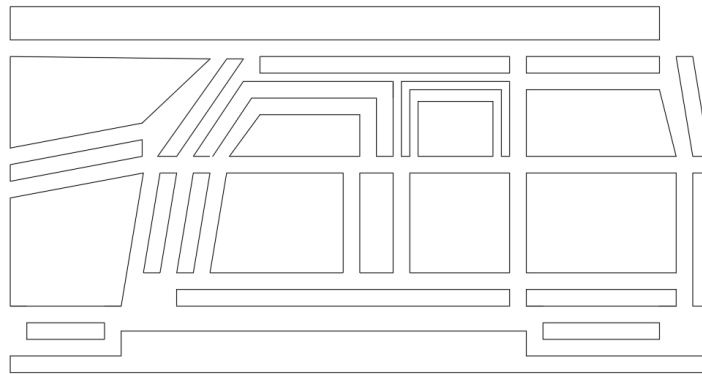


**Figure 2.2: The vehicle model in SEA, [5]**

To conclude:

1. SEA is based on the energy of the vibrating systems and the response results are given in frequency and space averaged values.
2. SEA divides a complex structure into appropriate substructures. This task can be considered difficult because there is not a clear and simple rule on how to divide such a complex system.
3. SEA groups resonant modes together and treat their response statistically. This significantly reduces the number of degree of freedom of the model. Consequently, the computational cost and memory consumption are also reduced. However, it is necessary that the modal overlap is large so that that the modal response of the structure analyses is insignificant. It is for this reason that the SEA-based methods are used in the high frequency range where the modal overlap is typically high.

4. An important problem in SEA's theory is how to enter parameters such as damping, coupling loss factor, absorption coefficients, wave types, etc.

## 2.2 Finite element method (FEM)

A finite element methodology to predict the airborne noise transmission between the source and the sound pressure level at the passenger's ears is presented in [6].

This methodology is divided into two steps. First step involves the exterior acoustic field all around the vehicle. The acoustic pressure field on the exterior surface of the vehicle is computed where exhaust system is considered as acoustic source. The second step consists in computing the interior vibro-acoustic response of the vehicle by using the surface pressure field from step one as excitation applied to the trimmed body of the vehicle. The computational steps and simulation flow are illustrated in Figure 2.3 and Figure 2.4.

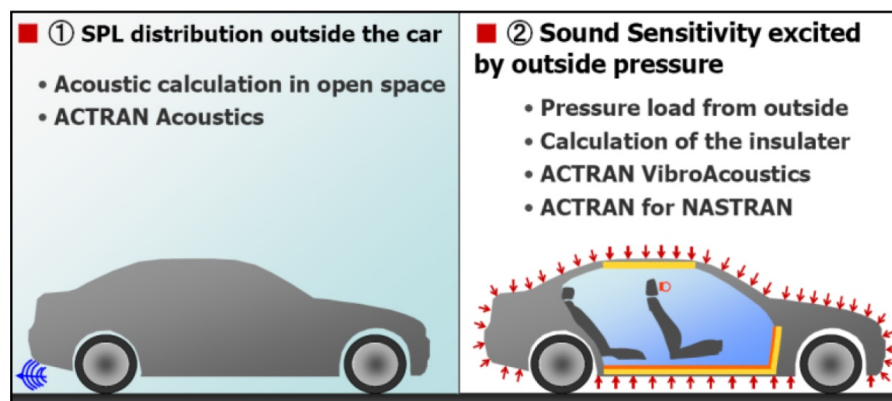


Figure 2.3: Computational steps of the FE method, [6]

The impedance matrices of the various trim components in the vehicle and the exterior sound field are computed in Actran. These results are then the input for the Nastran Trimmed Body Analysis. The modal extraction of the cavity and structure is performed in Nastran.

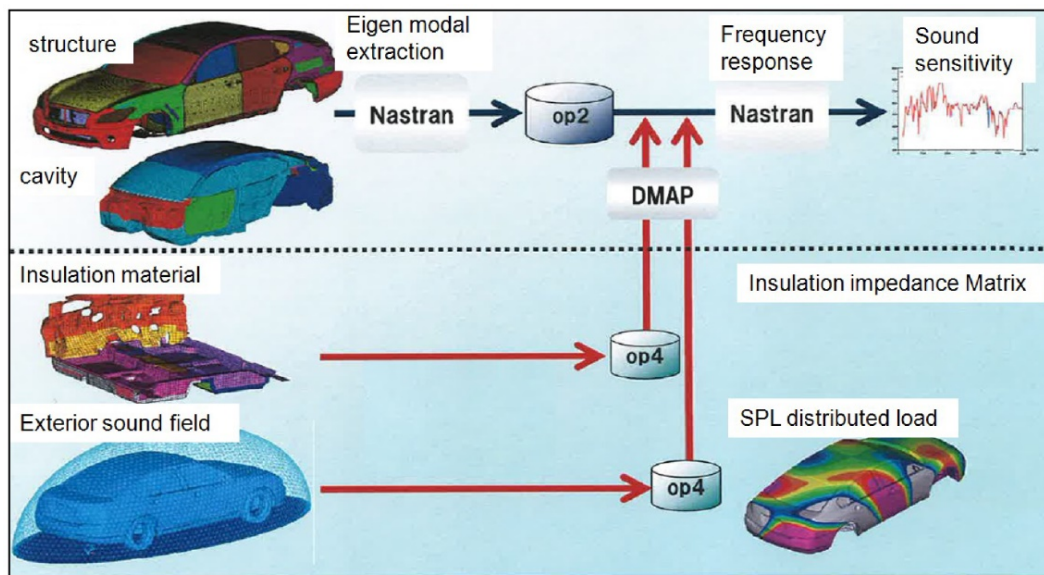


Figure 2.4: Simulation flow of the FE method, [6]

The exterior acoustic medium is modeled using finite and infinite elements. Acoustic finite elements are used to predict the near field propagation, whereas infinite elements are used for the far field propagation. The infinite elements represent the non-reflecting boundary condition, while ground is considered as a perfect reflecting surface. It is a half-free field space. The acoustic source is a spherical pulsating source located at the exhaust pipe. This model is shown in Figure 2.5.

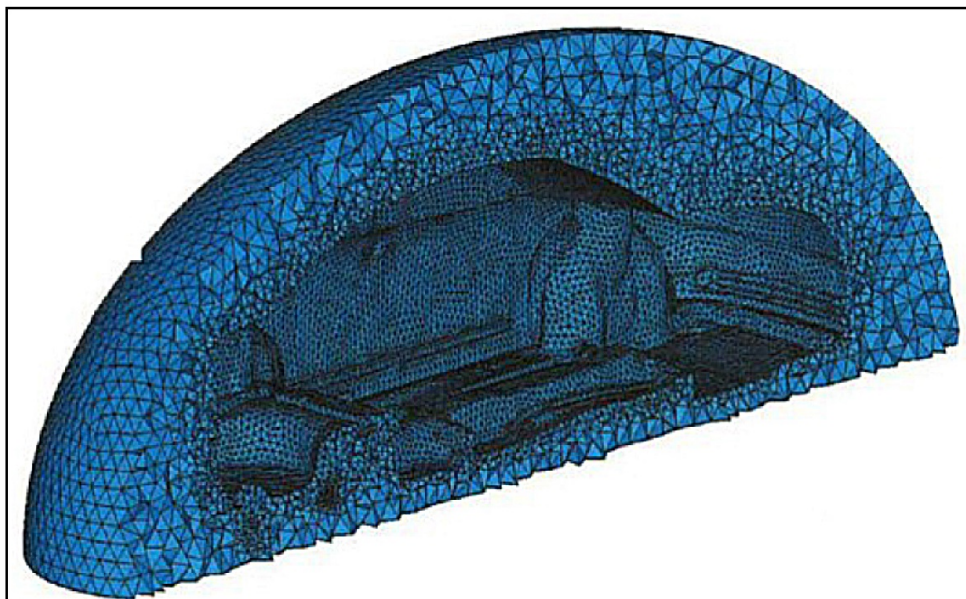


Figure 2.5: Cutplane of the exterior acoustic model, [6]

Two parameters that are important in finding the balance between the accuracy of the results and the computational cost (RAM, CPU) are

- infinite element order, and
- the size of the exterior acoustic domain.

Infinite element order is the "polynomial order used in the expansion of the pressure value in far field". While increasing the infinite element order, the accuracy of the computed values is improved, but the size of the model (number of degrees of freedom) also increases. A simulation has been computed with three infinite element orders (5, 10 and 20, respectively). The results are presented in Figure 2.6. It can be concluded that the convergence is achieved when the infinite element order was 10, where computed results of the sound pressure level are the same when the infinite element order is 20.

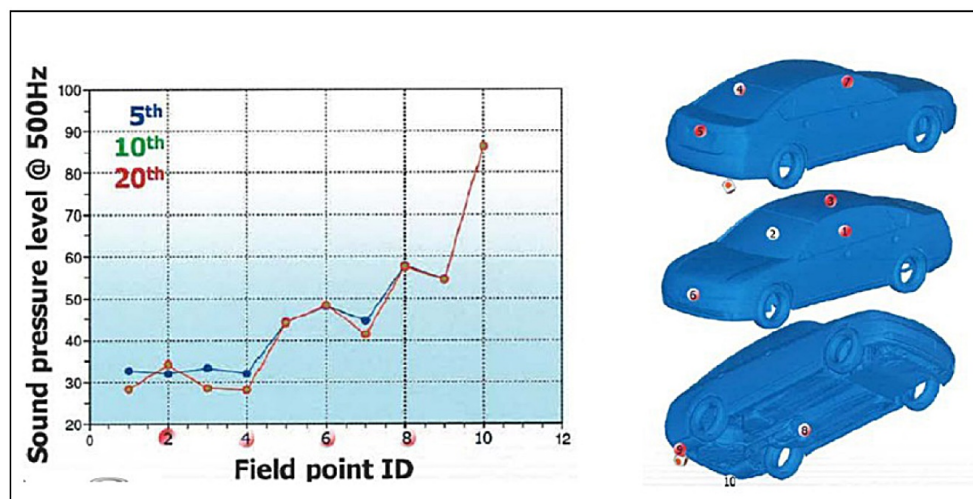


Figure 2.6: Convergence of the infinite element order, [6]

Another parameter driving the computational performance and the results accuracy is the size of the exterior acoustic domain, i.e., the distance between the vehicle surface and the interface of the finite and infinite elements. Figure 2.5 shows the convergence of the exterior acoustic domain for the baseline model and the model with the 1.5 times increased distance.

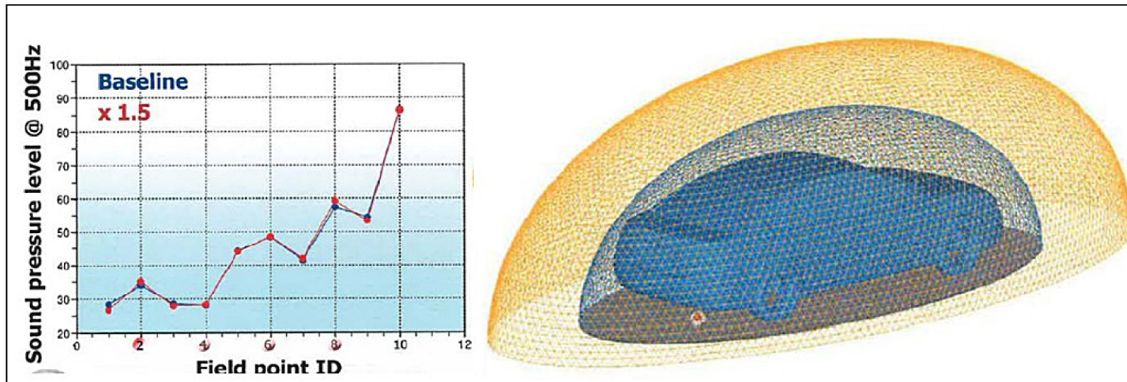


Figure 2.7: Convergence of the size of the exterior acoustic domain, [6]

## 2.3 Hybrid SEA/FE analysis

A hybrid SEA/FE analysis combines the Finite Element Method with the Statistical Energy Analysis in the mid-frequency range. The first step in using hybrid SEA/FE analysis is to divide a complex system into deterministic and statistical subsystems. The division of the system can be applied in sense of the wavelength i.e. components with the long wavelength behavior (meaning low modal density) are described using FE method and components with the short wavelength behaviour (meaning high modal density) are described with SEA. Therefore, deterministic components are modelled using Finite Element method, whereas other components are modelled as SEA subsystems. In other words, the components with large number of degrees of freedom are described statistically with the SEA method, while other components are described with FE method. The mix of the FE and SEA makes this method computationally efficient [7].

An example of the body-in-white vehicle is shown in Figure 2.8. The Figure shows the division of the complex vehicle system in the FE and the SEA subsystems [8]. The large plate subsystems due to the short wavelength behavior (or subsystems with high modal density) are assigned into SEA subsystems. The large plate systems are e.g. roof, front and rear windshields, window glasses and floor. On the other hand, the beam-type subsystems due to the long wavelength behavior (or subsystems with the low modal density) are assigned into FE subsystems. The beam-type components are e.g. A-pillar, B-pillar, C-pillar and subframe. The hybrid FE-SEA model is shown in Figure 2.9.

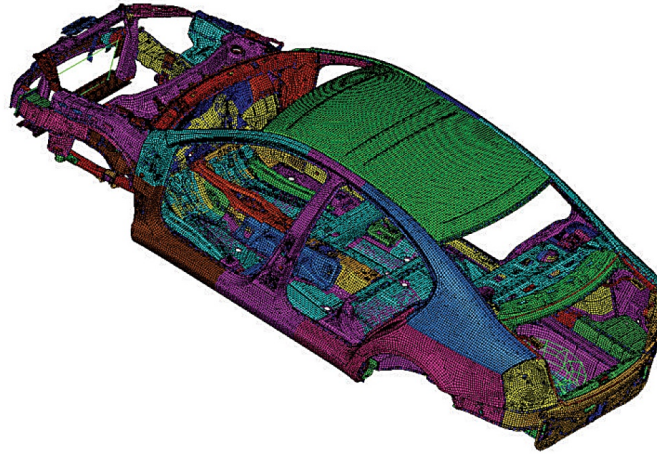


Figure 2.8: Body-in-white vehicle in Hybrid FE/SEA, [8]

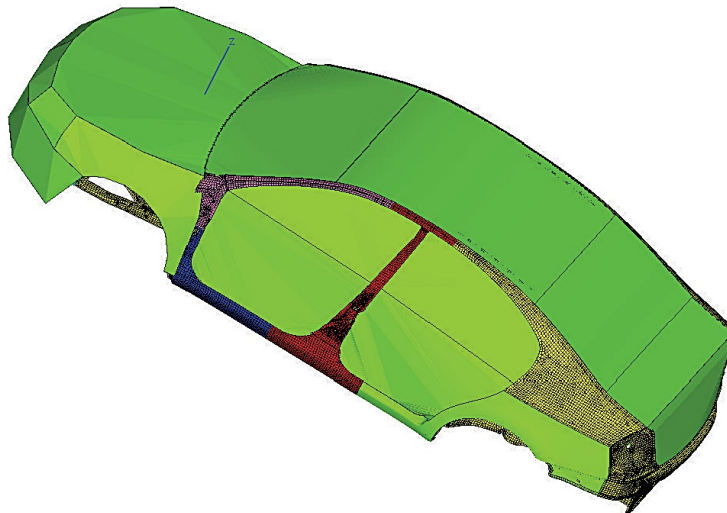


Figure 2.9: The vehicle model of Hybrid FE/SEA, [8]

The finite element model of the vehicle includes 249481 nodes, whereas the hybrid FE-SEA model contains only 89605 nodes. It is 159876 nodes less which will lead to the reduction in computation time and memory consumption.

## 2.4 Panel acoustic contribution analysis (PACA)

Panel acoustic contribution analysis (PACA) is an advanced engineering tool used to improve the NVH behaviour of the vehicle. This approach is based on the fact that the vehicle interior sound is the superposition of the acoustic pressures generated by an



individual panel. For that reason, PACA categorizes the vehicle body panels according to their contribution to the total sound pressure. There are 3 categories according to PACA [9]:

- positive contribution areas,
- negative contribution areas, and
- neutral areas.

In positive contribution areas the Sound Pressure Level is increased as the vibration amplitude increases, whereas in negative contribution areas the Sound Pressure Level is reduced as the vibration amplitude increases. Neutral areas have no significant effect on the Sound Pressure Level. PACA is able to determine the contribution of the vehicle panels to the total interior sound and pinpoint the areas of the panel that need modifications in order to achieve better NVH quality.

Figure 2.10 shows the work flow of the PACA.

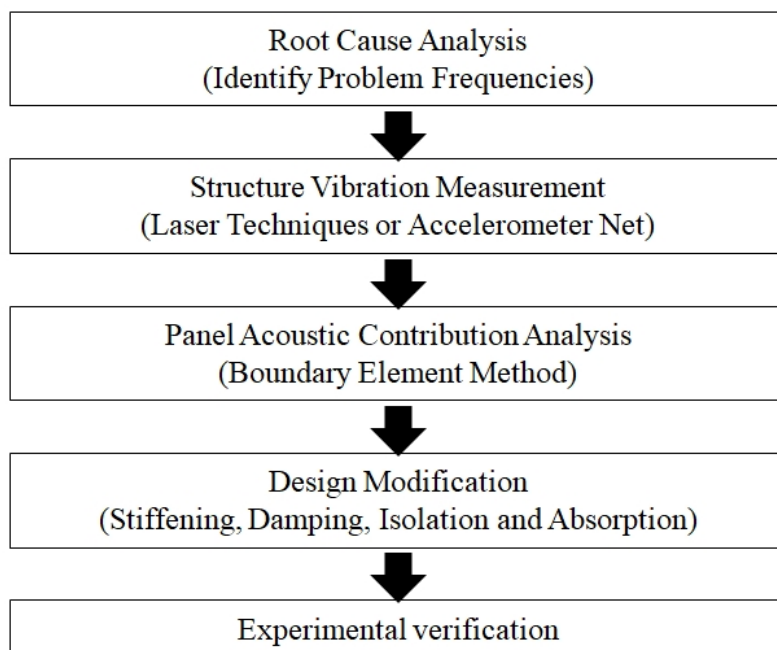


**Figure 2.10: The PACA work flow, [9]**

The first step considers the identification of noise sources. Next, structure vibration are measured with the help of laser technology or accelerometer nets. These measured result are then mapped onto the Boundary Element Model (BEM) of the vehicle. The third step

considers the analysis after which the contribution results are produced. Finally, structural modification are made with respect to PACA results. In addition, experimental results are run to confirm the predictions. The panel acoustic contribution ratio is [9]:

$$(r_c)_i = \frac{(p_g)_i}{|p|} \quad (2.1)$$

where  $(p_g)_i$  is the sound pressure contributed by an individual panel and  $|p|$  is the absolute total interior sound pressure. The current PACA method is not completely suitable for refinement of the complete interior sound field. The reason lies in the fact that current PACA is performed for only one sound pressure peak at one field point in the interior sound field. Thus, the acoustic performance of the entire interior sound field cannot be expressed only with the sound pressure response in one field point. Moreover, if the sound pressure response in one field point is reduced, it does not mean that the sound pressure response of the complete vehicle interior is reduced. In order to improve the present PACA method two parameters were introduced: acoustic contribution sum and total sound field contribution. The definition of these two parameters can be found in [10].

## Part I

**Coupled structural-acoustic analysis  
of the plate and cavity model and  
validation of the FE solution with  
the analytical solution**

# Chapter 3

## Model problem

The analytical and numerical models described in this chapter are used to predict the sound transmission through a plate acoustically coupled with a rectangular cavity. This model serves to validate the vibro-acoustic model that will be of great interest in the second part of the thesis. A single rectangular flexible plate is coupled with acoustic cavity that has 5 rigid walls, as shown in Figure 3.1.

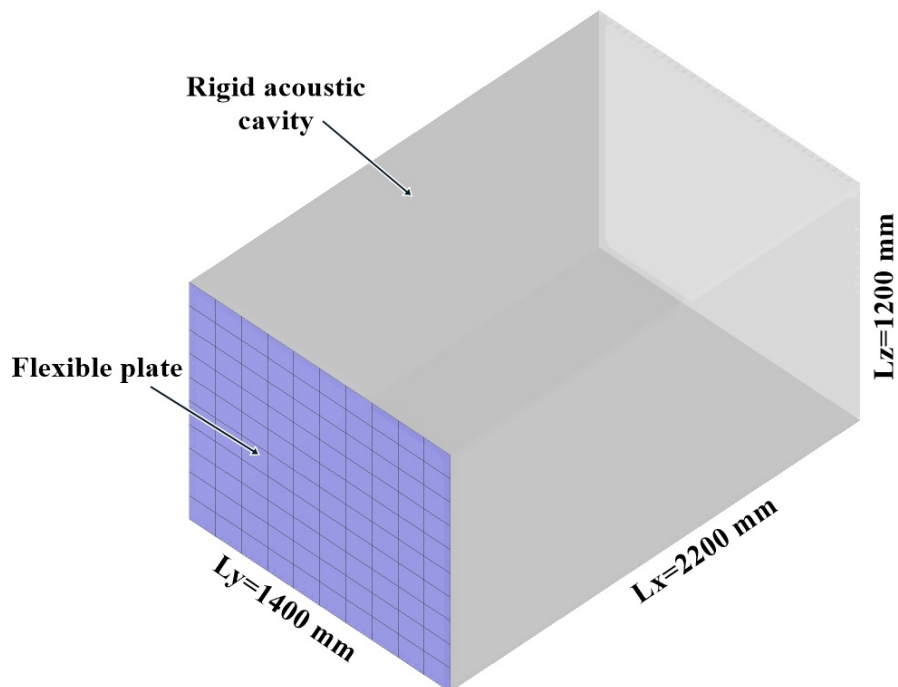


Figure 3.1: The plate representing the firewall coupled to a box-shaped acoustic cavity

This example of the rectangular plate and box-shaped cavity is a considerable simplification of the complicated vehicle structure and enclosed cavity. A simply supported plate represents the firewall between the engine compartment and the passenger space, whereas the rectangular acoustic cavity represents the passenger compartment. The interior pressure field will be affected by the dynamic properties of the cavity, by the dynamic properties of the plate and by the nature of coupling of these two dynamic systems.

A frequency-dependent dynamic point load is applied to the flexible plate:

$$F = A(\omega) \cdot \cos(\omega t) \quad (3.1)$$

where  $A(\omega)$  is the amplitude of the force depending on the frequency. In this case, the amplitude is constant through the whole frequency range, i.e.  $A(\omega) = 1$ .

Tables 3.1 and 3.2 show the dimensions of the flexible plate and cavity, as well as the number and length of structural and acoustic finite elements.

**Table 3.1: Input dimensions for the flexible plate**

Plate	Unit	x	y	z
Center position	mm	0	0	0
Rotation angle	-	0	0	0
Dimension	mm	0	1400	1200
No. of elements	-	0	140	120
Length of the element	mm	0	10	10

**Table 3.2: Input dimensions for the acoustic cavity**

Cavity	Unit	x	y	z
Center position	mm	0	0	0
Rotation angle	-	0	0	0
Dimension	mm	2200	1400	1200
No. of elements	-	110	70	60
Length of the element	mm	20	20	20

Steel and air material properties that are used for modeling the flexible plate and the acoustic cavity are listed in Tables 3.3 and 3.4.

**Table 3.3: Material properties for the flexible plate**

Plate	Symbol	Unit	Value
Thickness	$h$	mm	2
Density	$\rho_s$	kg/m <sup>3</sup>	7850
Young modulus	$E_0$	MPa	210000
Poisson's ratio	$\nu$	-	0.25
Structural damping	$\eta$	-	0.01

**Table 3.4: Material properties for the acoustic cavity**

Cavity	Symbol	Unit	Value
Speed of sound	$c_0$	m/s	340
Viscous damping	$\delta$	-	0.02

Two frequency response functions (FRF) are calculated. First the FRF is calculated between the force applied to the plate and the displacement of the plate at the excitation point. Frequency Response Function calculated between the force and displacement at the same point is also called driving point receptance. The second FRF is the one calculated between the force applied to the plate and the sound pressure level in the cavity at the position of the driver's ear. The coordinates of the field points of interest are listed in Table 3.5.

**Table 3.5: Coordinates of the field points of interest**

Field point	Unit	x	y	z
Excitation point	mm	0	960	400
Driver's ear	mm	550	1050	400

The analytical model is presented in three steps. First, differential equations governing plate and acoustic cavity dynamic behaviour are given. Second, the natural frequencies and vibration modes of the plate and acoustic cavity are calculated. Finally, the frequency response of the coupled structural-acoustic system is shown and discussed. The free vibration problem of the coupled system is solved by entirely neglecting damping, however, in the analysis of the forced response of the system the structural damping is taken into account by assuming a complex Young's modulus, whereas acoustic damping is taken into account by assuming a complex acoustic wave number.

The vibro-acoustic FE model is created in MSC Actran. A brief introduction to MSC Actran is presented. Moreover, the process of determining the finite element size of the acoustic and structural components is shown, as well as the setup of the FE model.

The comparison between the analytical and numerical results is presented and discussed. The comparison is made for the calculated eigenfrequencies and eigenmodes of a simply supported plate and acoustic cavity with rigid walls. Furthermore, comparison of FRF calculated analytically and numerically is shown and discussed.

# Chapter 4

## Analytical modeling of the fluid-structure interaction

### 4.1 Analytical modeling of the plate

#### 4.1.1 Differential equation of motion for a thin rectangular plate

The model used in this thesis is known as the Kirchhoff model, and according to [11] the differential equation of motion of a thin, homogeneous plate placed in  $yz$ -plane is given by

$$\frac{\partial^4 w}{\partial y^4} + 2\frac{\partial^4 w}{\partial y^2 \partial z^2} + \frac{\partial^4 w}{\partial z^4} + \frac{\rho_s h}{D_0} \frac{\partial^2 w}{\partial t^2} = 0 \quad (4.1)$$

where  $w(x, y)$  is the out-of-plane displacement of the plate,  $\rho_s$  is the material density of the plate,  $h$  is the thickness of the plate and  $D_0$  is the bending stiffness of the plate. Bending stiffness is given by

$$D_0 = \frac{E_0 h^3}{12(1 - \nu^2)} \quad (4.2)$$

where  $E_0$  is Young's modulus and  $\nu$  is Poisson's ratio. Equation (4.1) can be written in a more compact form:

$$\nabla^2 (\nabla^2 w) + \frac{\rho_s h}{D_0} \frac{\partial^2 w}{\partial t^2} = 0 \quad (4.3)$$

where  $\nabla^2$  is the two-dimensional Laplace operator

$$\nabla^2 = \frac{\partial^2}{\partial y^2} + \frac{\partial^2}{\partial z^2}.$$



If there is a pressure  $p(x, y, z)$  exciting the plate in the positive  $x$ - direction, the motion of the plate is governed by a nonhomogeneous equation

$$\nabla^2 (\nabla^2 w) + \frac{\rho_s h}{D_0} \frac{\partial^2 w}{\partial t^2} = \frac{p}{D_0}. \quad (4.4)$$

A plane flexural wave propagating along the positive  $y$ -axis of the plate with the displacement  $w(y, z)$  can be described as

$$w(y, z) = A e^{i(\omega t - \kappa y)} \quad (4.5)$$

where  $A$  is the amplitude of the flexural wave and  $\kappa$  is the bending wave number.

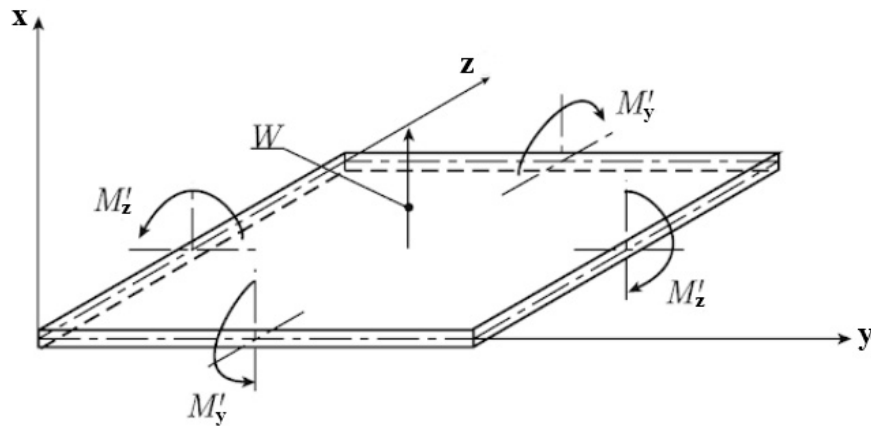


**Figure 4.1: Bending moments along edges and displacement of a rectangular plate, [12]**

The displacement  $w(y, z)$  expressed in equation (4.5) is the solution to the wave equation (4.1) if the wave number is

$$\kappa = \left[ \frac{\rho_s h \omega^2}{D_0} \right]^{\frac{1}{4}} = \left[ \frac{12(1 - \nu^2) \omega^2}{E_0 h^2} \right]^{\frac{1}{4}}. \quad (4.6)$$

The bending wave number (4.6) has a different frequency dependence in comparison to acoustic wave number. In equation (4.6) the bending wave number depends on the square root of the frequency, whereas acoustic wave number (4.50) has a linear frequency dependency. The phase velocity  $c_b$  and group velocity  $c_g$  for dispersive

bending waves are defined as

$$\begin{aligned} c_b &= \frac{\omega}{\kappa}, \\ c_g &= \frac{\partial \omega}{\partial \kappa} = 2c_b. \end{aligned} \quad (4.7)$$

Group speed is the speed at which energy is transported by a wave, whereas phase speed is the speed of the wave propagation.

Next, the differential equation governing transverse vibration of the simply supported plate is considered. Boundary conditions for a simply supported plate located in  $yz$ -plane (see Figure 4.1) are

$$\begin{aligned} w = 0; \quad M_y = 0; \quad \text{for } z = 0 \quad \text{and } z = L_z, \\ w = 0; \quad M_z = 0; \quad \text{for } y = 0 \quad \text{and } y = L_y. \end{aligned} \quad (4.8)$$

### 4.1.2 Eigenfrequencies and eigenmodes of a simply supported plate

The solution to the differential equation (4.1) can be expressed in the form:

$$w(y, z, t) = Y(y)Z(z)g(t) \quad (4.9)$$

where  $Y(y)$  and  $Z(z)$  are spatially dependent functions and  $g(t)$  is a time dependent function. Boundary conditions described in (4.8) are satisfied if

$$Y(y)Z(z) = \varphi_{mn}(y, z) = \sin(k_m y) \sin(k_n z), \quad (4.10)$$

where wave numbers  $k_m$  and  $k_n$  are given in the positive  $y$ - and  $z$ -direction, respectively by

$$\begin{aligned} k_m &= \frac{m\pi}{L_y}, \\ k_n &= \frac{n\pi}{L_z}. \end{aligned} \quad (4.11)$$

where  $m$  is the modal number in the  $y$ -axis and  $n$  is the modal number in the  $z$ -axis, and  $L_y$  and  $L_z$  are the dimensions of the rectangular plate. The function  $\varphi_{mn}$  is an

eigenfunction of a simply supported rectangular plate. Furthermore, these eigenfunctions are orthogonal or

$$\int \int dydz \varphi_{mn} \varphi_{rs} = \langle \varphi_{mn} | \varphi_{rs} \rangle = \frac{L_y L_z}{4}, \quad (4.12)$$

if  $m = r$  and  $n = s$ , otherwise zero.

Finally, the displacement  $w(y, z)$  can be expressed as an infinite sum of the eigenfunctions:

$$w(y, z, t) = \sum_{m \ n} g_{mn}(t) \sin(k_m y) \sin(k_n z). \quad (4.13)$$

Equation (4.13) is the solution to the differential equation (4.1).

In the case of the free vibrations, i.e. when no external force is applied to the plate, the plate can only oscillate at certain eigen- or natural frequencies  $f_{mn}$ . Using equation (4.13) the fourth order spatial derivatives are given as

$$\begin{aligned} \frac{d^4 w}{dy^4} &= g_{mn} \sin(k_m y) \sin(k_n z) k_m^4, \\ \frac{d^4 w}{dy^2 dz^2} &= g_{mn} \sin(k_m y) \sin(k_n z) k_m^2 k_n^2, \\ \frac{d^4 w}{dz^4} &= g_{mn} \sin(k_m y) \sin(k_n z) k_n^4. \end{aligned} \quad (4.14)$$

Substituting equation (4.14) in equation (4.1) one obtains homogeneous differential equation of free vibrations with the solution for a simply supported plate:

$$\begin{aligned} D_0 (k_m^4 + 2k_m^2 k_n^2 + k_n^4) g_{mn} \sin(k_m y) \sin(k_n z) - \\ - \rho_s h \omega_0 g_{mn} \sin(k_m y) \sin(k_n z) = 0. \end{aligned} \quad (4.15)$$

Equation (4.15) can be simplified to

$$D_0 (k_m^4 + 2k_m^2 k_n^2 + k_n^4) - \rho_s h \omega_0 = 0. \quad (4.16)$$

With the definition of wave numbers in equation (4.11), eigenfrequencies are obtained from equation (4.16) and given by

$$\omega_0 = \sqrt{\frac{D_0}{\rho_s h} \left[ \left( \frac{m\pi}{L_y} \right)^4 + 2 \left( \frac{m\pi}{L_y} \right)^2 \left( \frac{n\pi}{L_z} \right)^2 + \left( \frac{n\pi}{L_z} \right)^4 \right]}. \quad (4.17)$$

Thus, the eigenfrequency  $f_{mn}$  for mode  $m, n$  is given by:

$$f_{mn} = \frac{\omega_{0mn}}{2\pi} = \frac{\pi}{2} \sqrt{\frac{D_0}{\rho_s h}} \left[ \left( \frac{m}{L_y} \right)^2 + \left( \frac{n}{L_z} \right)^2 \right], \quad (4.18)$$

where  $m$  is the modal number along the  $y$ -axis and  $n$  is the modal number along the  $z$ -axis.

### 4.1.3 Forced response of a simply supported plate

The forced response of the plate located in  $yz$ -plane can be determined by means of the mode summation technique. The differential equation governing the forced response of the plate is

$$D_0 \nabla^4 w(y, z) + \rho_s h \frac{\partial^2 w(y, z)}{\partial t^2} = q(y, z, t) \quad (4.19)$$

The solution  $w(y, z, t)$  of the differential equation (4.19) is introduced in equation (4.13). In order to obtain the function  $g_{mn}(t)$ , the differential equation of motion (4.19) is multiplied by  $\varphi_{mn}$ . The results is thereafter integrated over the plate area giving

$$\begin{aligned} \int_0^{L_z} \int_0^{L_y} D_0 \nabla^4 w(y, z) \varphi_{mn}(y, z) dy dz + \\ + \rho_s h \frac{\partial^2 g_{mn}}{\partial t^2} \langle \varphi_{mn}(y, z) | \varphi_{mn}(y, z) \rangle = \\ = \langle q(y, z, t) | \varphi_{mn}(y, z) \rangle \end{aligned} \quad (4.20)$$

where  $\langle \varphi_{mn}(y, z) | \varphi_{mn}(y, z) \rangle$  and  $\langle q(y, z, t) | \varphi_{mn}(y, z) \rangle$  are defined as

$$\begin{aligned} \langle \varphi_{mn}(y, z) | \varphi_{mn}(y, z) \rangle &= \int_0^{L_z} \int_0^{L_y} \varphi_{mn}(y, z) \varphi_{mn}(y, z) dy dz, \\ \langle q(y, z, t) | \varphi_{mn}(y, z) \rangle &= \int_0^{L_z} \int_0^{L_y} q(y, z, t) \varphi_{mn}(y, z) dy dz. \end{aligned} \quad (4.21)$$

The eigenfunctions  $\varphi_{mn}(y, z)$  and the displacement  $w(y, z)$  satisfy the same boundary conditions. The first expression on the left hand side in equation (4.20) is integrated by

parts

$$\begin{aligned}
& \int_0^{L_z} \int_0^{L_y} D_0 \nabla^4 w(y, z) \varphi_{mn}(y, z) dy dz = \\
& = \int_0^{L_z} \int_0^{L_y} D_0 w(y, z) \nabla^4 \varphi_{mn}(y, z) dy dz = \\
& = D_0 (k_m^2 + k_n^2)^2 \int_0^{L_z} \int_0^{L_y} w(y, z) \varphi_{mn}(y, z) dy dz = \\
& = D_0 (k_m^2 + k_n^2)^2 g_{mn} \int_0^{L_z} \int_0^{L_y} \varphi_{mn}(y, z) \varphi_{mn}(y, z) dy dz = \\
& = D_0 (k_m^2 + k_n^2)^2 g_{mn} \langle \varphi_{mn}(y, z) | \varphi_{mn}(y, z) \rangle .
\end{aligned} \tag{4.22}$$

The differential equation of motion is now reduced to

$$D_0 (k_m^2 + k_n^2)^2 g_{mn} \langle \varphi_{mn} | \varphi_{mn} \rangle + \rho_s h \frac{\partial^2 g_{mn}}{\partial t^2} \langle \varphi_{mn} | \varphi_{mn} \rangle = \langle q | \varphi_{mn} \rangle . \tag{4.23}$$

This can be written as

$$K_{mn} g_{mn} + M_{mn} \frac{\partial^2 g_{mn}}{\partial t^2} = F_{mn} \tag{4.24}$$

where  $K_{mn}$ ,  $M_{mn}$  and  $F_{mn}$  are modal stiffness, modal mass and modal force matrices, respectively. This is equivalent to the equation of motion for a 1-DOF system. The generalized or modal parameters are

$$\begin{aligned}
M_{mn} &= \rho_s h \int_0^{L_z} \int_0^{L_y} \varphi_{mn}^2(y, z) dy dz, \\
K_{mn} &= D_0 (k_m^2 + k_n^2)^2 \int_0^{L_z} \int_0^{L_y} \varphi_{mn}^2(y, z) dy dz, \\
F_{mn} &= \int_0^{L_z} \int_0^{L_y} q(y, z, t) \varphi_{mn}(y, z) dy dz.
\end{aligned} \tag{4.25}$$

If time dependence is assumed through  $e^{-i\omega t}$ , equation (4.24) becomes

$$(K_{mn} - \omega^2 M_{mn}) g_{mn} = F_{mn} \tag{4.26}$$

where

$$\begin{aligned}M_{mn} &= \rho_s h \frac{L_y L_z}{4}, \\K_{mn} &= D_0 \frac{L_y L_z}{4} \left[ \left( \frac{m\pi}{L_y} \right)^2 + \left( \frac{n\pi}{L_z} \right)^2 \right]^2, \\F_{mn} &= A(\omega) \varphi_{mn}(y_F, z_F) = A(\omega) \sin(k_m y_F) \sin(k_n z_F).\end{aligned}\tag{4.27}$$

where  $x_F$  and  $y_F$  are the coordinates where the force is applied (see Table 3.5) and  $m$  and  $n$  can take values  $1, 2, \dots$

## 4.2 Analytical modeling of the acoustic cavity

### 4.2.1 The acoustic wave equation

In order to derive a linearized acoustic wave equation, the equation of continuity, equation of motion and thermodynamic equation of state need to be introduced. The derivation of these equations can be found in any book on acoustics, see for example [13], [14].

The equation of continuity gives a relation between the density and the particle velocity. The linearized equation of continuity is given by

$$\frac{\partial \rho}{\partial t} + \rho_0 \Delta \cdot \vec{u} = 0, \quad (4.28)$$

and in one dimension

$$\frac{\partial \rho}{\partial t} + \rho_0 \frac{\partial u_x}{\partial x} = 0. \quad (4.29)$$

The equation of motion gives a relation between the pressure and the particle velocity in a sound field. The linear equation of motion is

$$\rho_0 \frac{\partial \vec{u}}{\partial t} + \Delta p = 0, \quad (4.30)$$

and in one dimension,

$$\rho_0 \frac{\partial u_x}{\partial t} + \frac{\partial p}{\partial x} = 0. \quad (4.31)$$

The thermodynamic equation of state relates the inner forces, i.e., the pressure, to the deformations, i.e., density changes. For small pressure disturbances, a linear relation is obtained:

$$p = \rho \left. \frac{\partial p_t}{\partial \rho_t} \right|_{\rho_t = \rho_0}, \quad (4.32)$$

or

$$p = \beta \rho / \rho_0, \quad (4.33)$$

where adiabatic bulk modulus is defined as

$$\beta = \rho_0 \frac{\partial p_t}{\partial \rho_t}.$$

With the use of the linearized continuity equation (4.29) and (4.28), the linearized equation of motion (4.31) and (4.30) and the thermodynamic equation of state 4.32, a linearized wave equation is derived. By differentiating the equation of continuity (4.29) one obtains

$$\frac{\partial^2 \rho}{\partial t^2} + \rho_0 \frac{\partial^2 u_x}{\partial x \partial t} = 0. \quad (4.34)$$

The spatial derivative of the equation of motion (4.31) is

$$\rho_0 \frac{\partial^2 u_x}{\partial x \partial t} + \frac{\partial^2 p}{\partial x^2} = 0. \quad (4.35)$$

Subtraction of equation (4.34) from equation (4.35) gives

$$\frac{\partial^2 p}{\partial x^2} - \frac{\partial^2 \rho}{\partial t^2} = 0. \quad (4.36)$$

Equation of state (4.33) eliminates  $\rho$  giving

$$\frac{\partial^2 p}{\partial x^2} - \frac{\rho_0}{\beta} \frac{\partial^2 p}{\partial t^2} = 0. \quad (4.37)$$

The wave equation governing the propagation of small acoustic disturbances through a homogeneous, inviscid, isotropic, compressible fluid written in rectangular Cartesian coordinates  $(x, y, z)$  in terms of acoustic pressure  $p$  is given by

$$\frac{\partial^2 p}{\partial x^2} - \frac{1}{c^2} \frac{\partial^2 p}{\partial t^2} = 0. \quad (4.38)$$

The constant  $c$  is defined as

$$c = \sqrt{\frac{\beta}{\rho_0}}. \quad (4.39)$$

It is the speed of propagation of a small acoustic disturbance in the medium i.e. the speed of sound. In the same fashion, a linearized wave equation can be derived for three dimensions. The linearized wave equation for three dimensions is given by

$$\nabla^2 p - \frac{1}{c^2} \frac{\partial^2 p}{\partial t^2} = 0. \quad (4.40)$$



The general solution of the wave equation (4.38) for a plane wave propagating in the  $x$ -direction is of the form

$$p(x, t) = f\left(t - \frac{x}{c}\right) + g\left(t + \frac{x}{c}\right). \quad (4.41)$$

The solution  $f(t - \frac{x}{c})$  implies that there is wave traveling in the positive direction along the  $x$ -axis with the propagation speed  $c$ , whereas the solution  $g(t + \frac{x}{c})$  implies that there is a wave traveling in the negative direction along the  $x$ -axis with the same speed  $c$ .

With the help of Fourier series, complex harmonic pressure for one-dimensional plane wave is obtained

$$\mathbf{p}(x, t) = \hat{p}_+ e^{i(\omega t - kx)} + \hat{p}_- e^{i(\omega t + kx)} \quad (4.42)$$

where  $k$  is the acoustic wave number and is given by

$$k = \omega/c. \quad (4.43)$$

The first term on the right-hand of equation (4.42) side refers to propagation in the positive  $x$ -direction, and the second term to propagation in the negative  $x$ -direction.

## 4.2.2 Eigenfrequencies and eigenmodes of a three-dimensional box-shaped acoustic cavity

As previously introduced by equation (4.42) the general harmonic solution for one-dimensional plane wave is of the form

$$\mathbf{p}(x, t) = \hat{p} e^{\pm k_x x} e^{i\omega t} \quad (4.44)$$

where the time dependence is a harmonic function of circular frequency  $\omega$ .

Substituting expression (4.44) into the wave equation (4.40), we can see that the latter is satisfied, if  $p(x, t)$  is a solution of the Helmholtz equation

$$\frac{\partial^2 p}{\partial x^2} + k_x^2 p = 0. \quad (4.45)$$

By analogy with the one-dimensional Helmholtz equation, the three-dimensional Helmholtz equation is obtained

$$\nabla^2 p + k^2 p = 0 \quad (4.46)$$

where  $\nabla^2$  is equal to

$$\nabla^2 = \frac{\partial^2}{\partial x^2} + \frac{\partial^2}{\partial y^2} + \frac{\partial^2}{\partial z^2}. \quad (4.47)$$

Let us now consider acoustic wave motion in a room with dimensions  $L_x$ ,  $L_y$  and  $L_z$ . The medium is loss free and the walls are infinitely rigid. The boundary condition at all bounding surfaces is that the particle velocity normal to the surface must be zero (*hard boundary condition* or *zero-velocity condition*). For a plane wave propagating in three-dimensional space the sound field is given as

$$p(\vec{r}, t) = \hat{p}e^{i(\omega t \pm k_x x \pm k_y y \pm k_z z)} \quad (4.48)$$

where the minus sign stands for propagation in the respective coordinate axis' positive direction (*forward travelling wave*), and the plus sign in the negative direction of the coordinate axis (*backward travelling wave*). Because of all possible combinations of propagation direction in equation (4.48), the sound field in a room will consist of eight waves:

$$\begin{aligned} p(\vec{r}, t) = & (\hat{p}_1 e^{-i(k_x x + k_y y + k_z z)} + \hat{p}_2 e^{i(k_x x + k_y y + k_z z)} + \\ & + \hat{p}_3 e^{-i(k_x x + k_y y - k_z z)} + \hat{p}_4 e^{i(k_x x + k_y y - k_z z)} + \hat{p}_5 e^{-i(k_x x - k_y y + k_z z)} + \\ & + \hat{p}_6 e^{i(k_x x - k_y y + k_z z)} + \hat{p}_7 e^{i(k_x x - k_y y - k_z z)} + \hat{p}_8 e^{-i(k_x x - k_y y - k_z z)}) e^{i\omega t}. \end{aligned} \quad (4.49)$$

Substituting [4.49] in the Helmholtz wave equation [4.45] yields the condition that the components  $k_x$ ,  $k_y$  and  $k_z$  of the wave number must satisfy

$$|\vec{k}| = k = \frac{\omega}{c} = \sqrt{k_x^2 + k_y^2 + k_z^2}. \quad (4.50)$$

The particle velocity perpendicular to the surface must be zero. Thus, the boundary conditions are

$$\begin{aligned} u_x &= 0 \quad \text{at} \quad x = 0 \quad \text{and} \quad x = L_x, \\ u_y &= 0 \quad \text{at} \quad y = 0 \quad \text{and} \quad y = L_y, \\ u_z &= 0 \quad \text{at} \quad z = 0 \quad \text{and} \quad z = L_z. \end{aligned} \quad (4.51)$$

Reflection at an infinite rigid surface occurs without change in amplitude or phase, and

from that follows that

$$\hat{p}_1 = \hat{p}_2 = \hat{p}_3 = \hat{p}_4 = \hat{p}_5 = \hat{p}_6 = \hat{p}_7 = \hat{p}_8. \quad (4.52)$$

Setting  $\hat{p}_1, \hat{p}_2, \dots, \hat{p}_8$  to  $\hat{p}/8$  and developing the exponential terms into the form  $e^{i\theta} = \cos \theta + i \sin \theta$ , yields

$$p(\vec{r}, t) = \hat{p} \cos(k_x x) \cos(k_y y) \cos(k_z z) e^{i\omega t}. \quad (4.53)$$

The particle velocity can be determined with the help of equation of motion

$$\rho_0 \frac{\partial \vec{u}}{\partial t} + \nabla p = 0. \quad (4.54)$$

In the vector component form  $u_x(\vec{r}, t)$  is obtained as

$$u_x(\vec{r}, t) = -\frac{1}{\rho_0} \int \frac{\partial p}{\partial x} dt = -\frac{1}{\rho_0 i \omega} \frac{\partial p}{\partial x}. \quad (4.55)$$

The velocity vector components are therefore

$$\begin{aligned} u_x(\vec{r}, t) &= \hat{p} \frac{k_x}{i\omega\rho_0} \sin(k_x x) \cos(k_y y) \cos(k_z z) e^{i\omega t}, \\ u_y(\vec{r}, t) &= \hat{p} \frac{k_y}{i\omega\rho_0} \sin(k_y y) \cos(k_x x) \cos(k_z z) e^{i\omega t}, \\ u_z(\vec{r}, t) &= \hat{p} \frac{k_z}{i\omega\rho_0} \sin(k_z z) \cos(k_x x) \cos(k_y y) e^{i\omega t}. \end{aligned} \quad (4.56)$$

It can be seen that the boundary conditions at  $x = 0$ ,  $y = 0$  and  $z = 0$  are satisfied. In order to satisfy the boundary conditions at  $x = L_x$ ,  $y = L_y$  and  $z = L_z$ , the conditions  $\sin(k_x L_x) = 0$ ,  $\sin(k_y L_y) = 0$  and  $\sin(k_z L_z) = 0$  are required so that the components of the wave number vector become

$$k_x = \frac{n_x \pi}{L_x}; \quad k_y = \frac{n_y \pi}{L_y}; \quad k_z = \frac{n_z \pi}{L_z}; \quad (4.57)$$

where  $n_x$ ,  $n_y$  and  $n_z$  can take on values 0,1,2, ... .

With the help of equations (4.57) and (4.50) and using the relation  $2\pi f = \omega = kc$  the

eigenfrequencies or eigenvalues of the cavity are found to be

$$f(n_x, n_y, n_z) = \frac{c}{2} \sqrt{\left(\frac{n_x}{L_x}\right)^2 + \left(\frac{n_y}{L_y}\right)^2 + \left(\frac{n_z}{L_z}\right)^2}. \quad (4.58)$$

Thus, the room has an eigenfrequency and a corresponding eigenmode for every combination of  $n_x$ ,  $n_y$  and  $n_z$ .

### 4.2.3 Forced response of a three-dimensional box-shaped acoustic cavity

The solution  $p(x, y, z, t)$  to the Helmholtz equation (4.46) can be expressed as an infinite sum over the orthogonal eigenfunctions satisfying the boundary conditions for a cavity with rigid walls. Consequently, the sound field can be written as

$$p(x, y, z, t) = \sum_{n_x \ n_y \ n_z} a_{n_x, n_y, n_z}(t) \varphi_{n_x n_y n_z}(x, y, z) \quad (4.59)$$

where the eigenfunction is given by

$$\begin{aligned} \varphi_{n_x n_y n_z}(x, y, z) &= \cos(k_x x) \cos(k_y y) \cos(k_z z); \\ k_x &= n_x \pi / L_x; \quad k_y = n_y \pi / L_y; \quad k_z = n_z \pi / L_z. \end{aligned} \quad (4.60)$$

The sound pressure can be written as

$$p(x, y, z, t) = \sum_{n_x \ n_y \ n_z} a_{n_x, n_y, n_z}(t) \cos(k_x x) \cos(k_y y) \cos(k_z z). \quad (4.61)$$

The function  $a_{n_x, n_y, n_z}$  can be obtained by multiplying the Helmholtz wave equation (4.46) by  $\varphi_{n_x n_y n_z}$ . The results is thereafter integrated over the volume of the cavity giving

$$\begin{aligned} &\int_0^{L_z} \int_0^{L_y} \int_0^{L_x} \nabla^2 p(x, y, z, t) \varphi_{n_x n_y n_z}(x, y, z) dx dy dz - \\ &- \int_0^{L_z} \int_0^{L_y} \int_0^{L_x} \frac{1}{c^2} \frac{\partial^2 p(x, y, z, t)}{\partial t^2} \varphi_{n_x n_y n_z}(x, y, z) dx dy dz = 0. \end{aligned} \quad (4.62)$$

The first expression on the left hand side in equation (4.62) is integrated by parts

$$\begin{aligned}
& \int_0^{L_z} \int_0^{L_y} \int_0^{L_x} \nabla^2 p(x, y, z, t) \varphi_{n_x n_y n_z}(x, y, z) dx dy dz = \\
& = \int_0^{L_z} \int_0^{L_y} \int_0^{L_x} \nabla^2 \varphi_{n_x n_y n_z}(x, y, z) p(x, y, z, t) dx dy dz = \\
& = (k_x^2 + k_y^2 + k_z^2) \int_0^{L_z} \int_0^{L_y} \int_0^{L_x} p(x, y, z, t) \varphi_{n_x n_y n_z}(x, y, z) dx dy dz = \tag{4.63} \\
& = (k_x^2 + k_y^2 + k_z^2) a_{n_x n_y n_z} \int_0^{L_z} \int_0^{L_y} \int_0^{L_x} \varphi_{n_x n_y n_z}(x, y, z) \varphi_{n_x n_y n_z}(x, y, z) dx dy dz = \\
& = (k_x^2 + k_y^2 + k_z^2) a_{n_x n_y n_z} < \varphi_{n_x n_y n_z}(x, y, z) | \varphi_{n_x n_y n_z}(x, y, z) > .
\end{aligned}$$

The wave equation for the cavity is now reduced to

$$(k_x^2 + k_y^2 + k_z^2) a_{n_x n_y n_z} < \varphi_{n_x n_y n_z} | \varphi_{n_x n_y n_z} > - \frac{1}{c^2} \frac{\partial^2 a_{n_x n_y n_z}}{\partial t^2} < \varphi_{n_x n_y n_z} | \varphi_{n_x n_y n_z} > = 0. \tag{4.64}$$

This can be written as

$$K_{n_x n_y n_z} a_{n_x n_y n_z} - M_{n_x n_y n_z} \frac{\partial^2 a_{n_x n_y n_z}}{\partial t^2} = 0 \tag{4.65}$$

where  $K_{n_x n_y n_z}$ ,  $M_{n_x n_y n_z}$  are modal stiffness and modal mass matrices, respectively. The modal parameters are

$$\begin{aligned}
M_{n_x n_y n_z} &= \frac{1}{c^2} \int_0^{L_z} \int_0^{L_y} \int_0^{L_x} \varphi_{n_x n_y n_z}^2(x, y, z) dx dy dz, \\
K_{n_x n_y n_z} &= (k_x^2 + k_y^2 + k_z^2) \int_0^{L_z} \int_0^{L_y} \int_0^{L_x} \varphi_{n_x n_y n_z}^2(x, y, z) dx dy dz.
\end{aligned} \tag{4.66}$$

If the time dependence is assumed through  $e^{-i\omega t}$ , equation (4.65) transforms into

$$(K_{n_x n_y n_z} a_{n_x n_y n_z} - \omega^2 M_{n_x n_y n_z}) a_{n_x n_y n_z} = 0 \tag{4.67}$$

where

$$\begin{aligned}
M_{n_x n_y n_z} &= \frac{1}{c^2} \frac{L_x L_y L_z}{8} \\
K_{n_x n_y n_z} &= \frac{L_x L_y L_z}{8} \left[ \left( \frac{n_x \pi}{L_x} \right)^2 + \left( \frac{n_y \pi}{L_y} \right)^2 + \left( \frac{n_z \pi}{L_z} \right)^2 \right]
\end{aligned} \tag{4.68}$$

### 4.3 Coupled structural-acoustic model

The coupled structural-acoustic model represents a fusion of the structural model of the simply supported plate and the acoustic model of the enclosed cavity described in the previous chapters. The coupled equations of motion for a simply supported plate (4.26) interacting with the enclosed box-shaped cavity (4.67) can be expressed in the modal matrix form:

$$\left[ \begin{pmatrix} K_{mn} & C_{mnn_xn_yn_z} \\ 0 & K_{n_xn_yn_z} \end{pmatrix} - \omega^2 \begin{pmatrix} M_{mn} & 0 \\ D_{n_xn_yn_zmn} & M_{n_xn_yn_z} \end{pmatrix} \right] \begin{bmatrix} g_{mn} \\ a_{n_xn_yn_z} \end{bmatrix} = \begin{bmatrix} F_{mn} \\ 0 \end{bmatrix} \quad (4.69)$$

where the upper equation refers to structural system and lower equation refers to acoustic system. In these equations  $g_{mn}$  is a vector representing modal participation factors of the structural system, whereas  $a_{n_xn_yn_z}$  is a vector representing modal participation factors of the acoustic system.  $[K_{mn}]$  and  $[K_{n_xn_yn_z}]$  represent diagonal modal stiffness matrices for structural and acoustic system, respectively.  $[M_{mn}]$  and  $[M_{n_xn_yn_z}]$  represent diagonal modal mass matrices for structural and acoustic system, respectively.  $[F_{mn}]$  represents modal force vectors. The structural and acoustic coupling of the plate and the cavity are represented through matrix  $D_{n_xn_yn_zmn}$  which transforms the structural accelerations to acoustic excitations of the cavity, and also a coupling matrix  $C_{mnn_xn_yn_z}$  which transforms the acoustic pressures to loads acting on the structure [15]. The coupling surface is in the  $yz$ -plane. Therefore at  $x = 0$ , the eigenfunctions for structural and acoustic model are

$$\begin{aligned} \varphi_{mn}(y, z) &= \sin(k_m y) \sin(k_n z) \\ \varphi_{n_xn_yn_z}(0, y, z) &= \cos(k_x \cdot 0) \cos(k_y y) \cos(k_z z) = \\ &= \cos(k_y y) \cos(k_z z) \end{aligned}$$

where  $\varphi_{mn}$  is the eigenfunction defining the structural displacement normal to the coupling surface and  $\varphi_{n_xn_yn_z}$  is the eigenfunction defining the acoustic pressure on the coupling surface. Modal coupling matrix represents a product of the structural modes with the acoustic cavity modes, i.e., a product of eigenfunctions  $\varphi_{mn}$  and  $\varphi_{n_xn_yn_z}$ . This is then

integrated over the area of the coupling surface:

$$\begin{aligned}
C_{mnn_xn_yn_z} &= \langle \varphi_{mn}(y, z) \mid \varphi_{n_xn_yn_z}(0, y, z) \rangle = \\
&= \int_0^{L_z} \int_0^{L_y} \varphi_{mn}(y, z) \varphi_{n_xn_yn_z}(0, y, z) > dydz = \\
&= \int_0^{L_z} \int_0^{L_y} \sin(k_m y) \sin(k_n z) \cos(k_y y) \cos(k_z z) dydz
\end{aligned} \tag{4.70}$$

$$\begin{aligned}
D_{n_xn_yn_zmn} &= -\rho_0 \langle \varphi_{mn}(y, z) \mid \varphi_{n_xn_yn_z}(0, y, z) \rangle = \\
&= -\rho_0 \int_0^{L_z} \int_0^{L_y} \varphi_{mn}(y, z) \varphi_{n_xn_yn_z}(0, y, z) > dydz = \\
&= -\rho_0 \int_0^{L_y} \int_0^{L_z} \sin(k_m y) \sin(k_n z) \cos(k_y y) \cos(k_z z) dydz
\end{aligned} \tag{4.71}$$

The coupling matrix  $C_{mnn_xn_yn_z}$  is for  $m \neq n_y$  and  $n \neq n_z$  equal to

$$\frac{L_y L_z}{\pi^2} \frac{(-1)^n (-1)^{n_z} mn (-1)^m (-1)^{n_y} - (-1)^n (-1)^{n_z} mn - mn (-1)^m (-1)^{n_y} + mn}{m^2 n^2 - m^2 n_z^2 - n_y^2 n^2 + n_y^2 n_z^2}$$

and for  $m = n_y$  and  $n = n_z$

$$C_{mnn_xn_yn_z} = 0.$$

The coupling matrix  $D_{n_xn_yn_zmn}$  is for  $m \neq n_y$  and  $n \neq n_z$  equal to

$$-\rho_0 \frac{L_y L_z}{\pi^2} \frac{(-1)^n (-1)^{n_z} mn (-1)^m (-1)^{n_y} - (-1)^n (-1)^{n_z} mn - mn (-1)^m (-1)^{n_y} + mn}{m^2 n^2 - m^2 n_z^2 - n_y^2 n^2 + n_y^2 n_z^2}$$

and for  $m = n_y$  and  $n = n_z$

$$D_{n_xn_yn_zmn} = 0.$$

Finally, equation (4.69) can be solved to calculate natural frequencies and mode shapes of the coupled vibro-acoustic system.

It should be noted that acoustic eigenfunction  $\varphi_{n_xn_yn_z}$  implies that at the interface of the coupled plate and cavity model, the normal velocity of the particle is zero, see equation (4.51). Because of the vibration of the plate, the latter is not true, i.e. normal velocity of the particle at the interface is not zero. However, at a small distance from the interface the normal velocity of the acoustic particle converges to the correct value, i.e. the normal velocity of the plate vibration. As the number of acoustic modes used in the modal summation for the acoustic domain increases, this small distance tends to decrease. This

is in fact a manifestation of the Gibbs' phenomenon. Although the summation of rigid wall acoustic modes does not converge to the correct boundary normal velocity, it does converge correctly to the surface pressure, which is all that is needed for a correct formulation of the coupled equations [16],[17].

The losses in the structural plate and acoustic cavity will influence the response of the coupled structural-acoustic system. By adding damping, vibrations can be reduced, in particular at resonance frequencies which will also have impact on the noise radiated from the structure. The structural losses for flexural waves can be incorporated into the wave equation by defining the Young's modulus  $E$  as a complex parameter:

$$E = E_0(1 + i\eta) \quad (4.72)$$

where  $\eta$  is the loss factor. Loss factor is defined as the ratio between imaginary part and real part of the Young's modulus:

$$\eta = \frac{\text{Im}(E)}{\text{Re}(E)}. \quad (4.73)$$

The bending stiffness is therefore

$$D = \frac{Eh^3}{12(1 - \nu^2)} = \frac{h^3}{12(1 - \nu^2)} E_0(1 + i\eta) = D_0(1 + i\eta). \quad (4.74)$$

Both  $E_0$  and  $\eta$  are real quantities.

The internal losses in fluids, i.e. air, occur due to the air viscosity. Air viscosity induces an exponential decrease of a plane wave's amplitude with increasing the distance. The sound field with the effect of the attenuation of plane waves can be expressed as follows:

$$p = e^{-ikx} e^{-\alpha x} = e^{-\tilde{k}x} \quad (4.75)$$

where  $\alpha$  is the attenuation coefficient. The attenuation effect can be analyzed as addition of an imaginary part of the wave number. In this case, acoustic wave number becomes complex:

$$\tilde{k} = k - i\alpha = \frac{\omega - i\alpha c}{c} = \frac{\omega}{c} \left( 1 - \frac{i\alpha c}{\omega} \right). \quad (4.76)$$

Assuming  $1 - \epsilon \approx \frac{1}{1+\epsilon}$  for  $\epsilon \ll 1$  and applying this to equation (4.76) the complex wave



number is given by

$$\tilde{k} \approx \frac{\omega}{c \left(1 + i \frac{\alpha c}{\omega}\right)}. \quad (4.77)$$

This attenuation effect can be carried by the speed of sound

$$\tilde{k} \approx \frac{\omega}{\tilde{c}} \quad (4.78)$$

where  $\tilde{c}$  is

$$\tilde{c} = c \left(1 + i \frac{\alpha c}{\omega}\right) = c \left(1 + i \frac{\alpha}{k}\right) = c(1 + i\delta). \quad (4.79)$$

The acoustic loss factor  $\delta$  is the ratio between the imaginary part and the real part of the speed of sound

$$\delta = \frac{Im(c)}{Re(c)}. \quad (4.80)$$

These viscous losses are often regarded for acoustic radiation in closed cavities, but for exterior acoustic problem they have very little impact on the results and are often neglected [18].

In case when structural and acoustic damping are considered, the modal matrices in equation (4.69) change. The modal stiffness matrices are therefore

$$\begin{aligned} K_{mn} &= D_0(1 + i\eta) \frac{L_y L_z}{4} \left[ \left(\frac{m\pi}{L_y}\right)^2 + \left(\frac{n\pi}{L_z}\right)^2 \right]^2, \\ K_{n_x n_y n_z} &= \frac{L_x L_y L_z}{8} \left[ \left(\frac{n_x \pi}{L_x}\right)^2 + \left(\frac{n_y \pi}{L_y}\right)^2 + \left(\frac{n_z \pi}{L_z}\right)^2 \right], \end{aligned} \quad (4.81)$$

and modal mass matrices are

$$\begin{aligned} M_{n_x n_y n_z} &= \frac{1}{c_0^2 (1 + i\delta)^2} \frac{L_x L_y L_z}{8}, \\ M_{mn} &= \rho_s h \frac{L_y L_z}{4}. \end{aligned} \quad (4.82)$$

In obtaining the modal solution, only a selected portion of structural modes  $\varphi_{mn}$  and cavity modes  $\varphi_{n_x n_y n_z}$  are considered in the structural-acoustic model, i.e. finite numbers of modal numbers  $m$  and  $n$  for structural models, as well as modal numbers  $n_x, n_y$  and  $n_z$  for acoustic model are selected. This is done to keep the calculation time and computational

cost under control. The model truncation orders are selected as follows

$$M = 24, N = 24, N_x = 20, N_y = 15, N_z = 15.$$

These values are selected on the basis of a frequency range of interest. This means that we are introducing an approximation. It also means that the number of degrees of freedom in the system is limited to

$$\begin{aligned} M \cdot N + (N_x + 1) \cdot (N_y + 1) \cdot (N_z + 1) &= \\ = 24 \cdot 24 + (20 + 1) \cdot (15 + 1) \cdot (15 + 1) &= 5952 \end{aligned}$$

In modal modeling the degrees of freedom are the eigenmodes, which means, when the equation (4.69) is solved for eigenvalues, we obtain 5952 eigenvalues, one per degree of freedom.

After obtaining modal participation factors for structural and acoustic models ( $g_{mn}$  and  $a_{n_x n_y n_z}$ , respectively) from equation (4.69)), the structural displacement and sound pressure at points of interest are evaluated from equations (4.13) and (4.61).

# Chapter 5

## Numerical modeling of the fluid-structure interaction in MSC Actran

### 5.1 Introduction to MSC Actran

ACTRAN (acronym of *ACoustic TRANsmission*, also known as the Acoustic NASTRAN) is a finite element-based computer aided engineering software to solve acoustics, vibro-acoustics, and aero-acoustics problems. Actran is being developed by Free Field Technologies, a Belgian software company which is wholly owned by the MSC Software Corporation. As an alternative to BEM (*Boundary Element Method*), Actran uses IE (*Infinite Elements*) for modelling non-reflecting boundary conditions and calculating far field. [19], [20].

The Actran software is currently divided and licensed into different modules:

- **Actran Acoustics** is the foundation module of the Actran Suite for acoustic radiation problems and weakly coupled-acoustic simulations. Some of the robust capabilities of this module include extraction of acoustic modes, sound field computation in cavities with either modal or physical approaches, sound radiation analysis of vibrating structures, sound propagation analysis in ducts and enclosed cavities, etc.
- **Actran Vibroacoustics** is a module dedicated to strongly coupled vibro-acoustic

simulations;

- **Actran AeroAcoustics** is a module designed for computational aeroacoustics. It is a module that can predict the noise generated by complex flows;
- **Actran for Trimmed bodies** is a module dedicated to trimmed body analyses, where typical applications are car cabins;
- **Actran SEA** is a module created for SEA (*Statistical Energy Analysis*);
- **Actran TM** is a module for turbo-machinery noise prediction;
- **Actran DGM** solves the linearized Euler equations using discontinuous finite elements and is used for predicting the noise propagation in complex physical conditions;
- **Actran VI** is user interface designed for pre-processing of all advanced Actran modules including importing, creating, editing and exporting of Actran analyses, generating and modifying acoustic meshes. Actran VI is also designed for post-processing of the results, including visualization and animation of the results. Actran VI supports several mesh formats (Nastran BDF, ANSYS RST and CBD, Actran DAT and NFF, I-DEAS UNV, Patran Neutral Format) as input for creating Actran input files. The post-processing tool supports different results formats (OP2, UNV, NFF, RST, HDF and punch files).

Actran provides a large library of material models, a complete element library that includes infinite elements, rich set of boundary conditions, operating conditions and sources, high performance solvers to solve large size problems.

Figure 5.1 shows Actran work principle. The input is a file (or several files) containing all the model setup, i.e. mesh, material models with material properties, components depending on the physics involved, boundary conditions, output requests, etc. Actran acts as a solver. The output are result files (FRF (*Frequency Response Functions*), Output Maps) and report files (log, resources, time, ...).

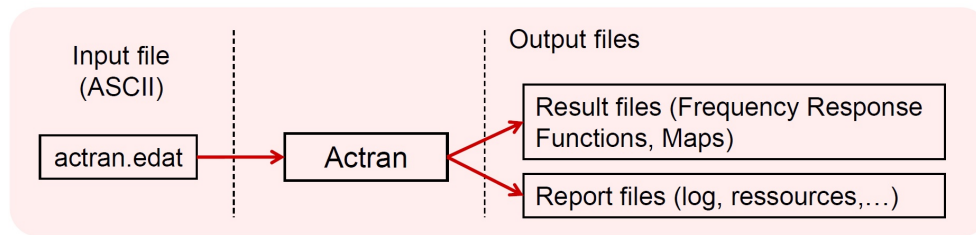


Figure 5.1: Actran work principle, [21]

Figure 5.2 shows Actran work flow. The mesh can be created in Actran VI or any other meshing software (Patran, SimExpert, ANSA, ...). The Actran model is created in Actran VI. The computation of the Actran model is done in Actran with a specified solver (MUMPS, ...). Post-processing of the results can be done in ActranVI where visualization and animation of results is done and PLTViewer (FRF) where plotting of the FRF is done.

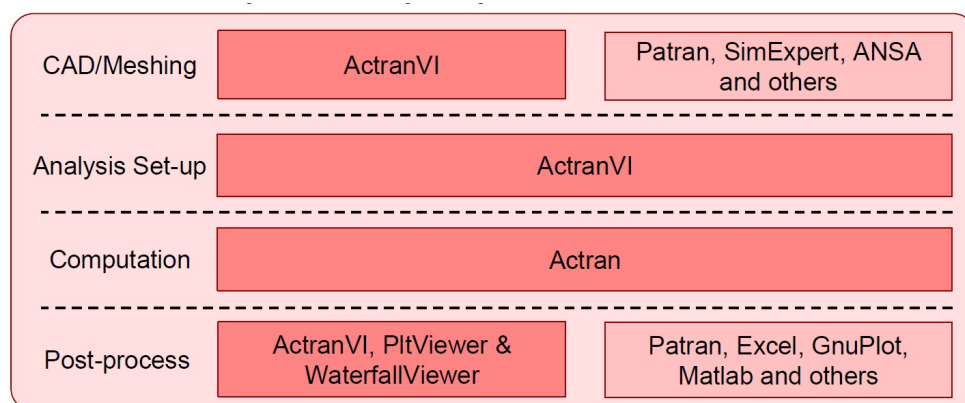


Figure 5.2: Actran work flow, [21]

Eigenvalue extraction, frequency response computation and compressible flow analysis can be done in Actran.

Direct frequency response is used to compute the response of an acoustic, vibro-acoustic or aero-acoustic system to a excitation in physical coordinates, whereas modal coordinates are used in modal frequency response. The following system of equations is set-up and solved for various frequencies  $\omega = 2\pi f$  in direct frequency response:

$$(\mathbf{K} + i\omega\mathbf{C} - \omega^2\mathbf{K})x(\omega) = F(\omega) \quad (5.1)$$

yielding values of the unknown vector  $x(\omega)$  for every frequency  $\omega$ . In modal frequency response, system of equations is set-up and solved

$$\begin{pmatrix} Z_{SS} & Z_{SF} \\ Z_{SF}^T & Z_{FF} \end{pmatrix} \cdot \begin{pmatrix} \alpha_S(\omega) \\ \alpha_F(\omega) \end{pmatrix} = \begin{pmatrix} \Phi_S^T \cdot F_S(\omega) \\ \Phi_F^T \cdot \frac{F_F(\omega)}{\omega^2} \end{pmatrix} \quad (5.2)$$

yielding values of the unknown vector  $\begin{pmatrix} \alpha_S(\omega) \\ \alpha_F(\omega) \end{pmatrix}$  for every frequency  $\omega$ . To compute the modes of a closed acoustic cavity or an undamped structure the modal extraction is used. The modal extraction solves the following eigenvalue problem:

$$\mathbf{Kp} = \omega^2 \mathbf{Mp} \quad (5.3)$$

with  $\mathbf{K}$  the stiffness matrix and  $\mathbf{M}$  the mass matrix. [22]

## 5.2 Computation of the required finite element size

The enclosed acoustic cavity is modelled with linear tetrahedral linear acoustic elements. Figure 5.3 shows tetrahedral elements with 4 and 10 nodes, i.e., linear and quadratic tetrahedral elements. Each node carries a single degree of freedom, i.e., the acoustic pressure.

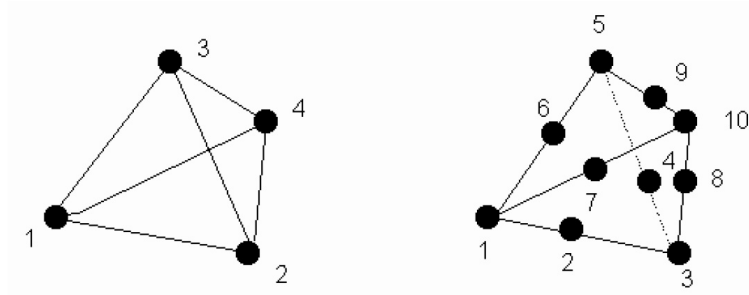


Figure 5.3: Topology of tetrahedral elements, [22]

The maximum finite element mesh size of the acoustic cavity is directly related to minimum wavelength:

$$k = \frac{c}{f_{max}} \quad (5.4)$$

where  $k$  is the acoustic wavelength,  $c$  is the speed of sound and  $f_{max}$  is the maximum value of the frequency of interest.

For linear elements, a rule of thumb is to use 8 to 10 linear elements per wavelength to capture the acoustic fluctuation, whereas for quadratic elements, it is recommended to use 4 to 6 quadratic elements. Therefore, the maximum acoustic element size can be calculated as

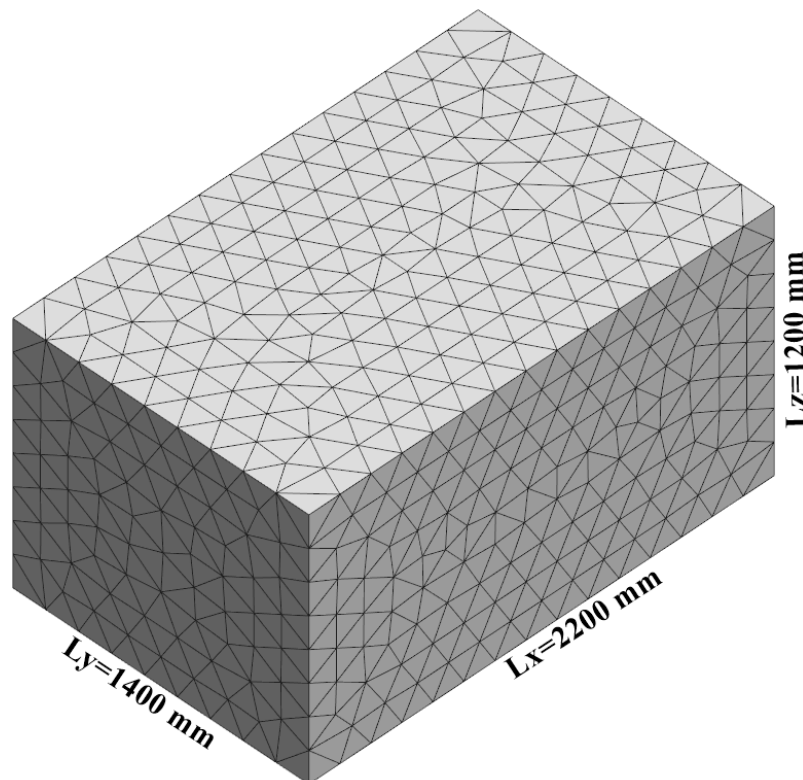
$$L_{F_{max}} = \frac{k}{10} = \frac{c}{10 \cdot f_{max}} \quad (5.5)$$

Table 5.1 gives all parameters used to calculate the maximum size of the acoustic finite element.

**Table 5.1: Maximum finite element size of the acoustic cavity**

Property	Symbol	Unit	Value
Frequency	$f_{max}$	Hz	1600
Speed of sound	$c$	m/s	340
Acoustic wavelength	$k$	m	0.2125
No. of elm per wavelength	$n_F$	-	10
Maximum acoustic element size	$L_{F_{max}}$	m	0.02125

The chosen element size of the acoustic finite element is 20 mm. Figure 5.4 shows the created acoustic mesh of the enclosed rectangular cavity. The acoustic mesh contains 4568794 tetrahedral linear acoustic elements.

**Figure 5.4: Box-shaped acoustic cavity modeled with tetrahedral acoustic elements**

Next, the thin plate is modeled with finite elements for visco-elastic thin shells. These elements are in future reference called shell elements. Shell element represents a component with one very small dimension and two larger dimensions. In order to use these elements, a condition has to be satisfied - to have roughly a factor 1/15 between



thickness and next higher dimension. Each node has six degrees of freedom, i.e. the displacement components  $u_x$ ,  $u_y$  and  $u_z$  in the  $x$ ,  $y$  and  $z$  direction and the rotation components  $\theta_x$ ,  $\theta_y$  and  $\theta_z$ . Figure 5.5 shows the shell elements with 4 and 8 nodes i.e. linear and quadratic element.

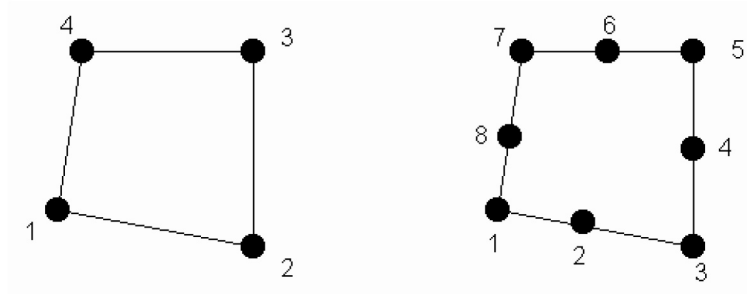


Figure 5.5: Topology of shell elements, [22]

The steel plate is meshed according to the criterion based on the bending wavelength:

$$\kappa = \frac{c_b}{f_{max}}, \quad (5.6)$$

where  $c_b$  is the phase velocity and  $f_{max}$  is the maximum frequency that is going to be considered. The phase velocity  $c_b$  is given by

$$c_b = \sqrt{\omega h \sqrt{\frac{E_0}{12\rho_s(1-\nu^2)}}} \quad (5.7)$$

where  $\omega$  is the frequency and  $h$  is the thickness.

With linear shell elements, the maximum shell element size can be calculated by

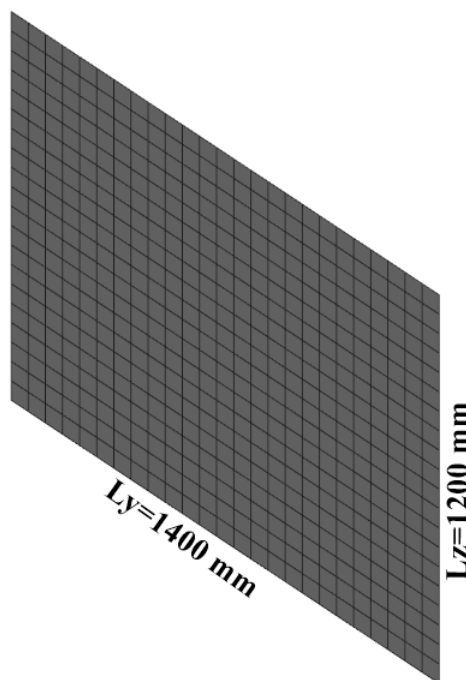
$$L_{S_{max}} = \frac{\kappa}{10} = \frac{c_b}{10 \cdot f_{max}} \quad (5.8)$$

Table 5.2 gives all parameters for the calculation of the maximum size of the shell element.

**Table 5.2: Maximum finite element size of the structural plate**

Property	Symbol	Unit	Value
Frequency	$f_{max}$	Hz	1600
Young modulus	$E_0$	GPa	210
Poisson ratio	$\nu$	-	0.25
Thickness	$h$	mm	2
Density	$\rho_s$	kg/m <sup>3</sup>	7850
Structural wavelength	$\kappa$	m	0.11
No. of elm per wavelength	$n_S$	-	10
Maximum structural element size	$L_{Smax}$	m	0.011

The chosen element size of the structural finite element is 10 mm. Figure 5.6 shows the created structural mesh of the plate. The structural mesh contains 16800 linear shell elements.

**Figure 5.6: Rectangular plate modeled with shell elements**

The acoustic and bending wavelengths and their required finite element size for particular frequency can be computed within ActranVI. This is shown in Figures 5.7 and 5.8 which show the parameters used for computation of the acoustic element size and structural element size.

Wavelength computation

Acoustics Structural Porous Viscothermal

Results:

Wavelength: 0.2125

Static Speed of sound: 340.0

Element size: 0.02125

Input:

Frequency: 1600 Specific heat (constant volume): 716

Total Speed of sound: 340 Number of elms/wavelength: 10

Flow: 0

Specific heat (constant pressure): 1004

Close

Figure 5.7: Computation of acoustic element size

Wavelength computation

Acoustics Structural Porous Viscothermal

Results:

Bending lambda: 0.11005105736

Element size: 0.011005105736

Shear lambda: 2.04448925302

Input:

Frequency: 1600 Density: 7850

Young modulus:  $2.1 \times 10^{11}$  Number of elms/wavelength: 10

Poisson ratio: 0.25

Thickness: 0.002

Close

Figure 5.8: Computation of structural element size

### 5.3 Setup of the finite element vibro-acoustic model

Vibro-acoustic model consists of the component that represents acoustic cavity which is coupled to a component that represents elastic plate located in  $yz$ -plane. Other 5 sides of the rectangular cavity are considered rigid.

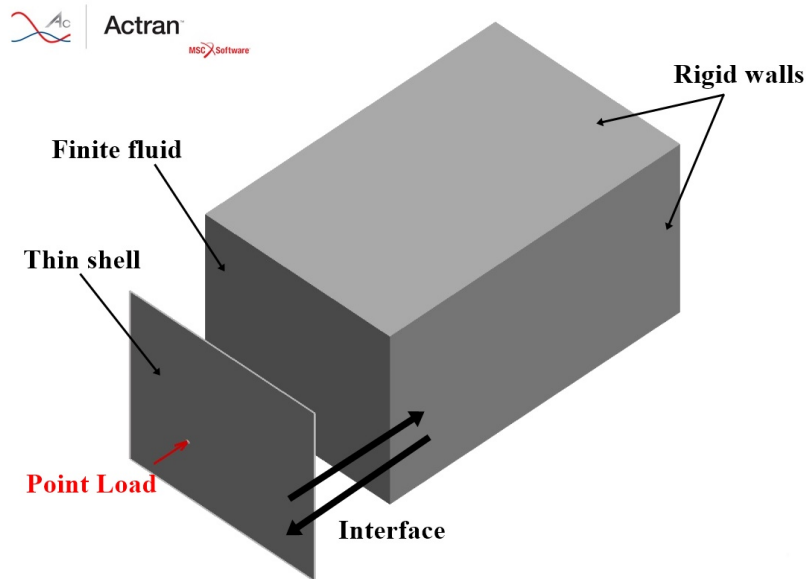


Figure 5.9: Simplified numerical vibro-acoustic model

Acoustic cavity is modeled with the help of the "finite fluid" component which is an Actran standard component for modeling finite acoustic media. The finite fluid material is specified. The properties of the finite fluid material are given in Table 3.4.

The plate is modeled with "thin shell" component which is also an Actran standard component to model transverse thin elements. The thickness of the plate and material are specified. The properties of the isotropic solid material are given in Table 3.3.

Vibro-acoustic model contains both acoustic and structural meshes. On one hand the creation of the structure mesh is guided by the bending wavelength. On the other hand the acoustic mesh is created in accordance with the acoustic wavelength. For the same frequency, these two meshes can have different element sizes. To couple the acoustic and structural components in an Actran analysis, an elastic-acoustic interface is created. The interface connector is used to handle mesh incompatibilities, e.g. different mesh size, element type, interpolation order - linear or quadratic. Additionally, interface connector

is used for modelling trim components in the analysis of a trimmed vehicle.

The interface links two coupling surfaces, where the first coupling surface is selected to be the mesh of the structure and the second coupling surface is the skin of the acoustic cavity mesh. It is necessary to specify the surface having the finest mesh as the first coupling surface in order to get the good mapping quality. Figure 5.10 shows the projection of nodes of the first coupling surface onto the second coupling surface. The procedure deals with the extrusion of the first coupling surface along the local normal direction to the surface onto second coupling surface. This projection procedure is controlled by two parameters - gap- and plane tolerance:

- gap tolerance is the absolute value of the extrusion of the pseudo-mesh along the normal direction to the surface, and
- plane tolerance is a relative value which extends the size of the extruded pseudo-mesh along its face plane.

Two surfaces will not be coupled when the gap between them is larger than the gap tolerance. In this case, gap tolerance is set to be 1 mm, while plane tolerance is set to be 0.01. Nodes that are located outside of the pseudo-mesh will not be mapped - see Figure 5.10 the node that is "Not found" .

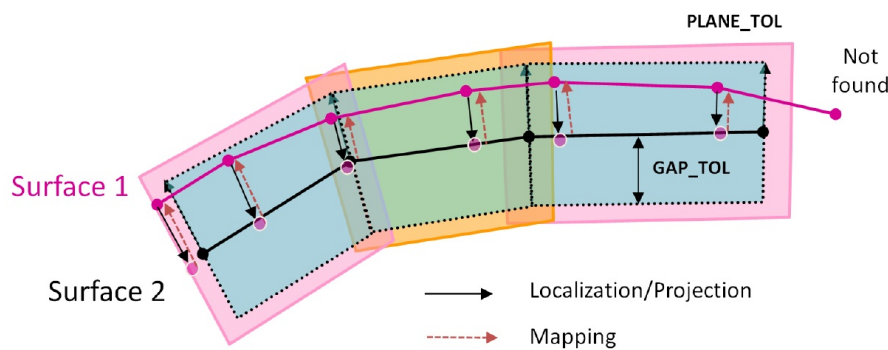


**Figure 5.10: Projection procedure, [22]**

Two boundary conditions need to be specified. First, the plate is simply supported along its edges. Thus, a simple support is modelled by restraining only the translational degrees of freedom, i.e.  $u_x$ ,  $u_y$  and  $u_z$  in the  $x$ ,  $y$  and  $z$  direction. In Actran this is done by defining the displacement boundary conditions and specifying the zero field boundary

condition on the edges of the plate. The definition of the simply supported boundary condition is shown in Figure 5.11.

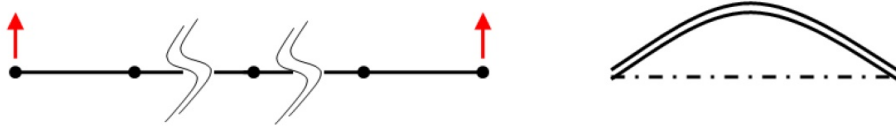


Figure 5.11: Simply supported boundary conditions for thin shell elements, [22]

Second, the plate is excited by an external harmonic force. A point load boundary condition is specified. The amplitude of the point load is set to 1 N and the force is oriented in the direction of the positive  $x$ -axis. The coordinates of the grid point on which point load is applied are given in Table 3.5.

In order to calculate Frequency Response Function (FRF) at the points of interests, e.g. excitation point and driver's ear, an output of Frequency Response Function is specified. The coordinates of the points of interest are given in Table 3.5.

# Chapter 6

## Comparison between the analytical and numerical solutions

This chapter shows the comparison between the analytical and numerical solution of the models discussed in previous chapters. Analytical solution is computed using Matlab, while numerical solution is obtained from ACTRAN.

Analytical solutions of eigenfrequencies are computed for a simply supported plate and a rigid-wall acoustic cavity and compared with the numerical solution. Also, a visual comparison between the eigenmodes of the same models is made.

Two Frequency Response Functions (FRFs) are calculated both analytically and numerically, as discussed in previous chapters. This chapter also shows the comparison between the calculated FRFs for analytical and numerical model. Moreover, discrepancies between the analytical and numerical solution are discussed.

## 6.1 Comparison of eigenmodes and eigenfrequencies of a simply supported plate

The analytical solution of eigenfrequencies of a simply supported plate is calculated with the help of equation (4.18), while numerical solution is obtained from the model set up in ActranVI for the modal extraction of a plate simply supported along the edges.

The first 10 eigenfrequencies and the corresponding mode numbers are listed in Table 6.1, given for a 2 mm thick simply supported plate located in  $yz$ -plane with dimensions 1.4 m x 1.2 m. It is evident from the Table 6.1 that the plate has an eigenfrequency and a corresponding eigenmode for every combination of  $m$  and  $n$  mode counts. Table 6.1 shows a good agreement of the numerical solution with the analytical (analytical) solution.

**Table 6.1: Eigenfrequencies for a 2 mm thick simply supported plate with the dimensions 1.4 m x 1.2 m oriented in  $yz$ -plane**

Mode no.	m	n	Analytical solution	Numerical solution
1	1	1	5.8359	5.83072
2	2	1	13.251	13.24282
3	1	2	15.9286	15.92345
4	2	2	23.3437	23.32455
5	3	1	25.6094	25.6059
6	1	3	32.7498	32.75615
7	3	2	35.7021	35.67656
8	2	3	40.1648	40.14886
9	4	1	42.9111	42.9249
10	3	3	52.5292	52.48653

Figure 6.1 shows the lowest nine natural frequencies and mode shapes of the steel plate. numerical solution of the same plate model is shown in Figure 6.2.

The excellent agreement of the analytical and numerical results verifies the numerical plate model.



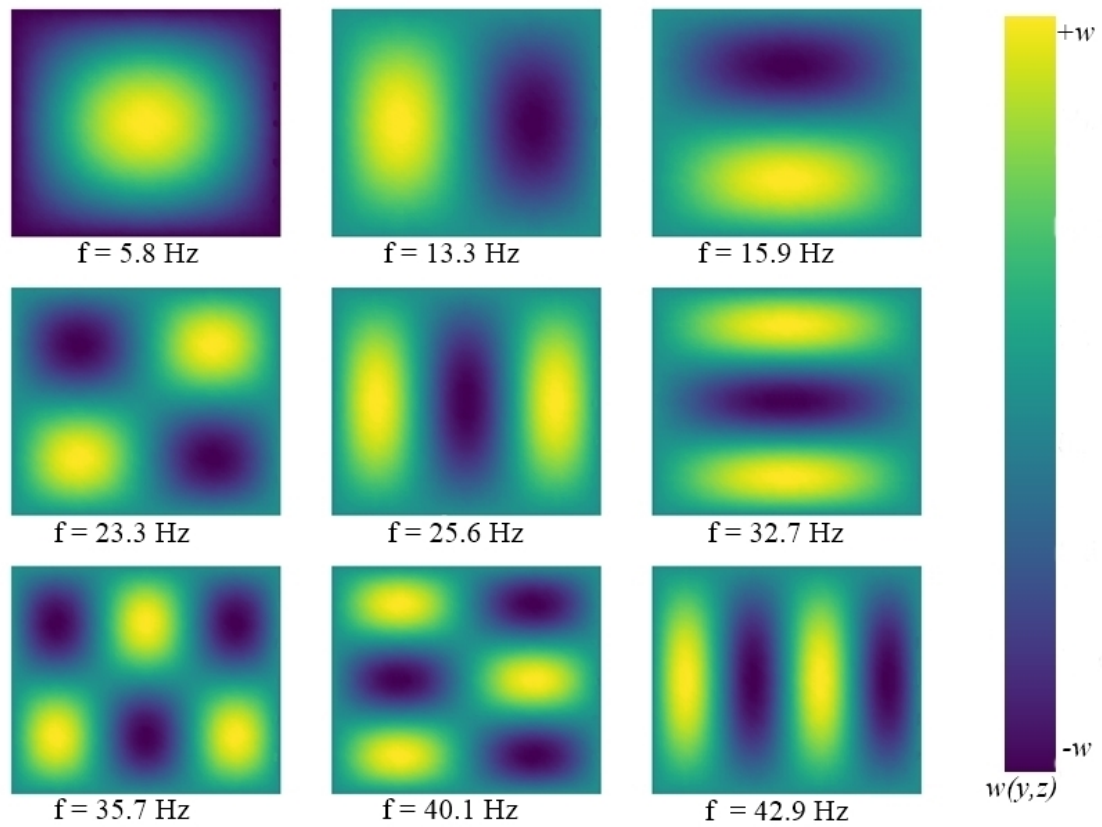


Figure 6.1: Lowest nine natural frequencies and modes of 1.4 m x 1.2m thin simply supported steel plate (analytical solution)

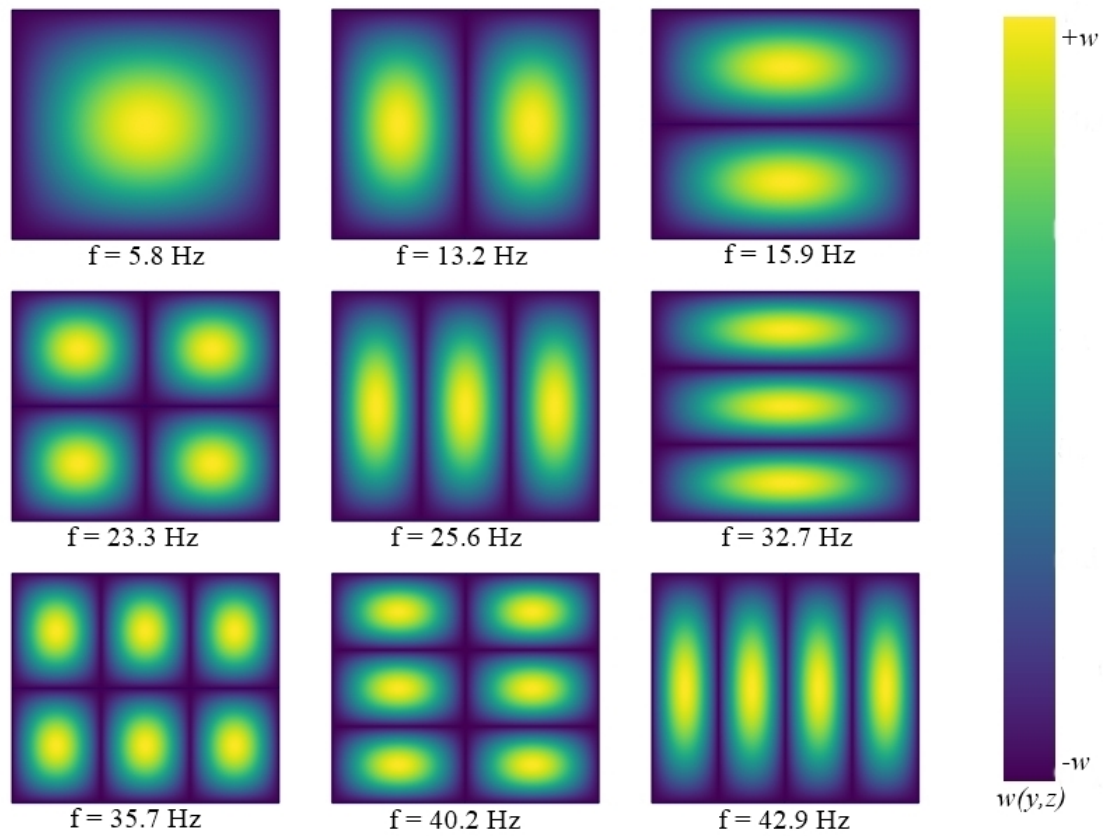


Figure 6.2: Lowest nine natural frequencies and modes of 1.4 m x 1.2m thin simply supported steel plate (numerical solution with a mesh of 140x120 shell elements)

## 6.2 Comparison of eigenmodes and eigenfrequencies of a rigid-walled acoustic cavity

The analytical solution of eigenfrequencies of a rigid-wall acoustic cavity is calculated with the help of equation (4.58), whereas numerical solution is obtained from the model set up in ActranVI for modal extraction of a rigid-wall acoustic cavity.

The first 10 eigenfrequencies and the corresponding mode numbers are listed in Table 6.2, given for a rigid-wall acoustic cavity with dimensions 2.2 m x 1.4 m x 1.2 m. It is evident from the Table 6.2 that the acoustic cavity has an eigenfrequency and a corresponding eigenmode for every combination of  $n_x$ ,  $n_y$  and  $n_z$  mode counts.

Table 6.2 shows comparison between the analytical and the numerical solution of a rigid-walled acoustic cavity model.

**Table 6.2: Eigenfrequencies for air-filled cavity with rigid walls with dimensions 2.2m x 1.4m x 1.2m**

Mode no.	$n_x$	$n_y$	$n_z$	Analytical solution	Numerical solution
1	0	0	0	0	0
2	1	0	0	77.2727	77.2816
3	0	1	0	121.4286	121.4655
4	0	0	1	141.6667	141.7266
5	1	1	0	143.9304	143.9868
6	2	0	0	154.5455	154.6153
7	1	0	1	161.3707	161.4525
8	0	1	1	186.586	186.7119
9	2	1	0	196.5431	196.6826
10	1	1	1	201.954	202.1066

Figure 6.3 shows the lowest nine acoustic natural frequencies and mode shapes of acoustic cavity with rigid walls. The numerical solution of the same rigid wall acoustic cavity is shown in the Figure 6.4. The good agreement of the analytical and numerical results verifies the numerical acoustic model of the acoustic cavity with rigid walls.

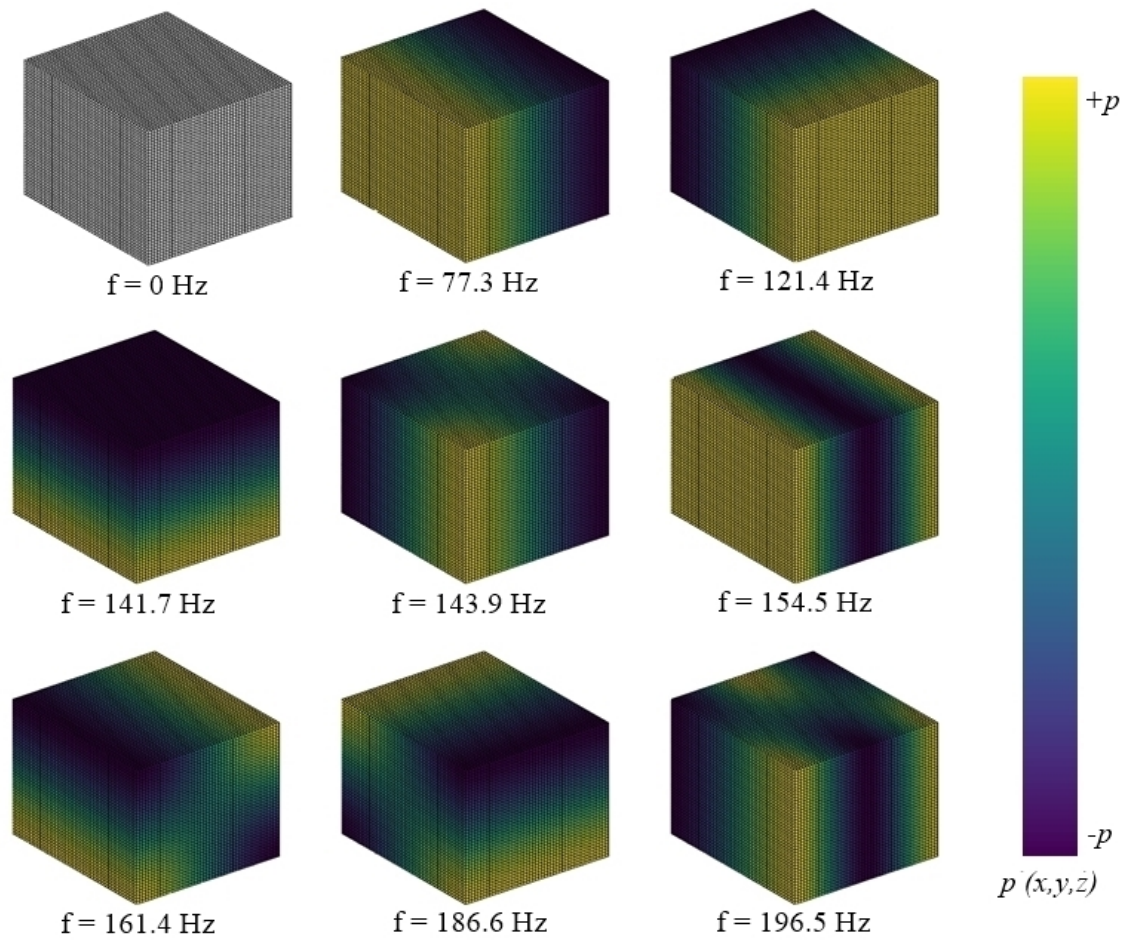


Figure 6.3: Lowest nine acoustic natural frequencies and modes of a 2.2 m x 1.4 m x 1.2m air-filled cavity with rigid walls (analytical solution)

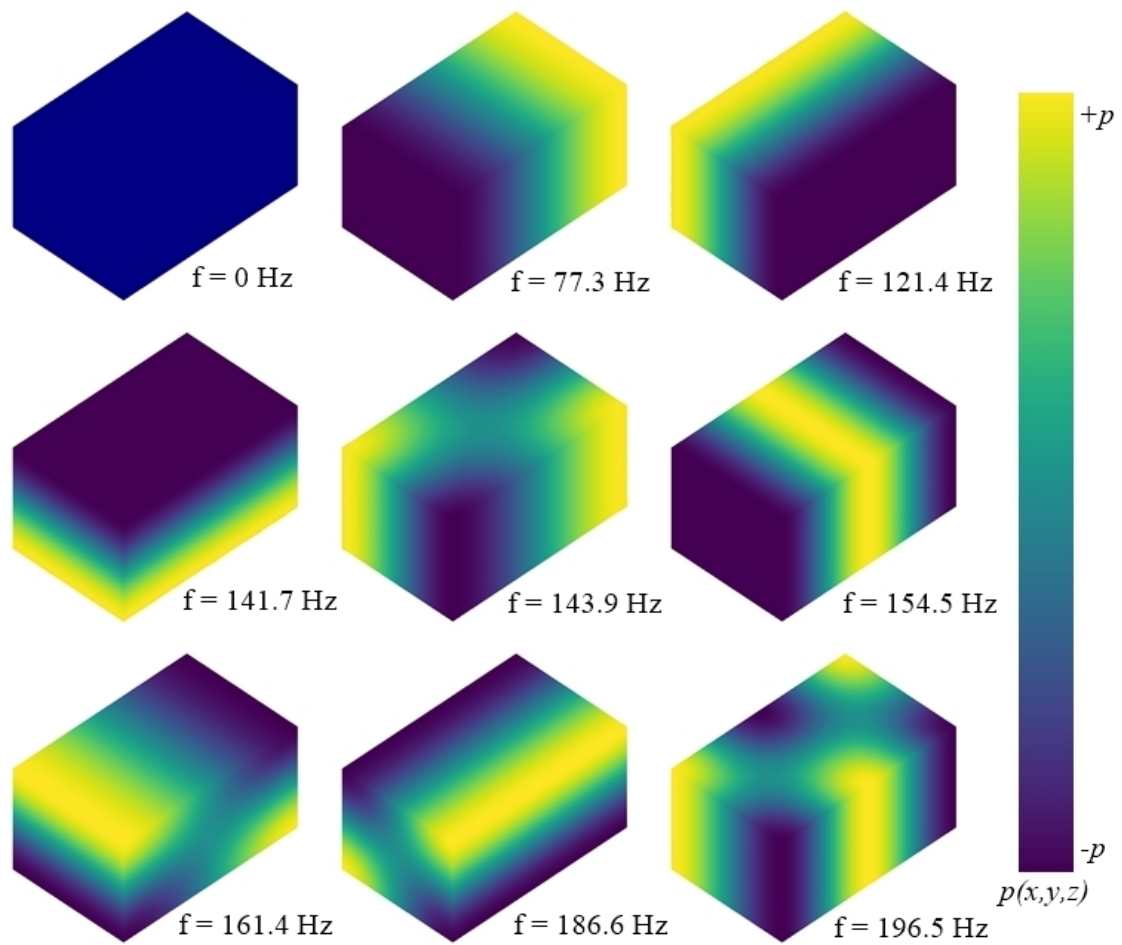


Figure 6.4: Lowest nine acoustic natural frequencies and modes of a 2.2 m x 1.4 m x 1.2m air-filled cavity with rigid walls (numerical solution with mesh of 55x35x30 tetrahedral acoustic elements)

### 6.3 The FRF between the displacement at the excitation point and the force exciting the plate

Frequency Response Function (FRF) at the excitation point (or driving point receptance) is computed as:

$$X_{w,F}(\omega) = \frac{w(\omega)}{F(\omega)} \quad (6.1)$$

where  $w(\omega)$  is the output (displacement), and  $F(\omega)$  is the input (force). The units for the displacement and force are [mm] and [N], respectively.

Figure 6.5 shows the comparison of the numerical solution and analytical solution of the displacement at the excitation point for the whole frequency range. If we take a better look at Figure 6.6, one can notice that up to 500 Hz the curve of the numerical solution follows the curve of the analytical solution in a very good manner.

Furthermore, if we take a look at Figure 6.7, one can notice that there are some discrepancies between the numerical solution and the analytical solution. It can be concluded that the numerical results become less accurate when the frequency increases. At higher frequency, the plate mesh captures plate modes less accurately as the bending wavelength decreases. Moreover, acoustic mesh also captures acoustic modes less accurately as the acoustic wavelength decreases, but this effect is minor compared to the plate model. Numerical accuracy can be improved by further refining the mesh, i.e. by increasing the number of elements per wavelength. This will result in the increase of the computational time and the memory consumption by the software in numerical calculation.

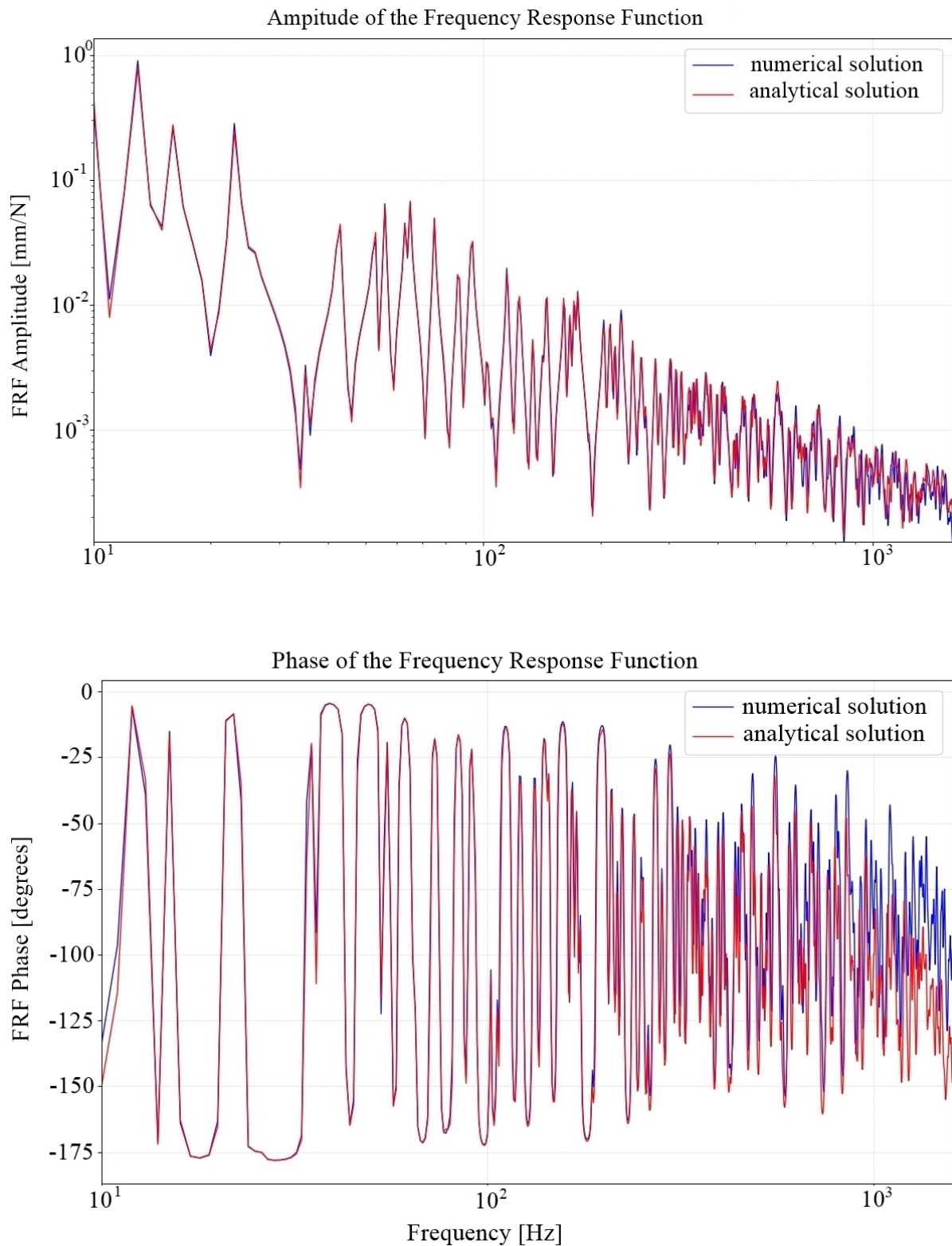


Figure 6.5: Driving point receptance for the whole frequency range due to the point force exciting the plate

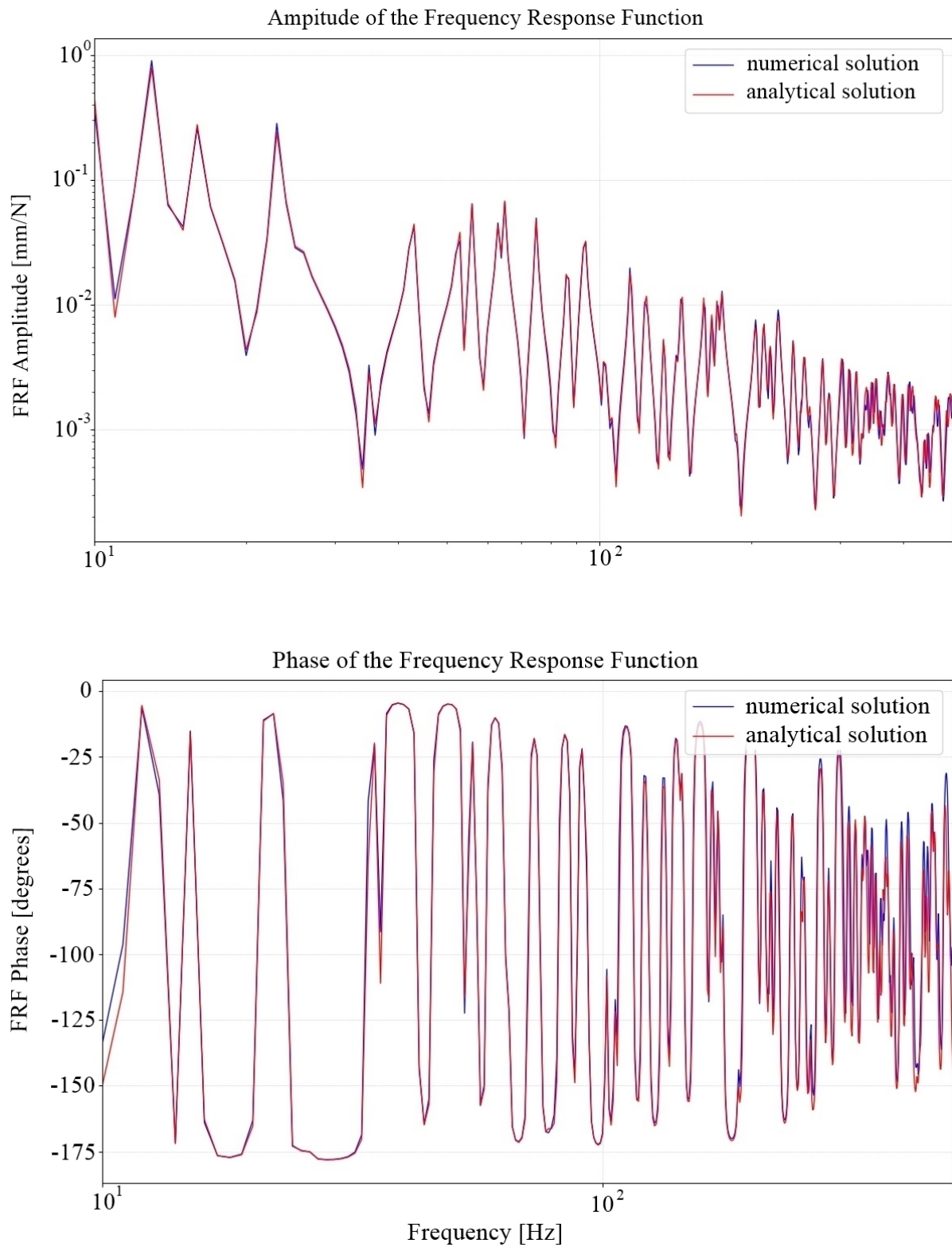


Figure 6.6: Driving point receptance up to 500 Hz due to the point force exciting the plate



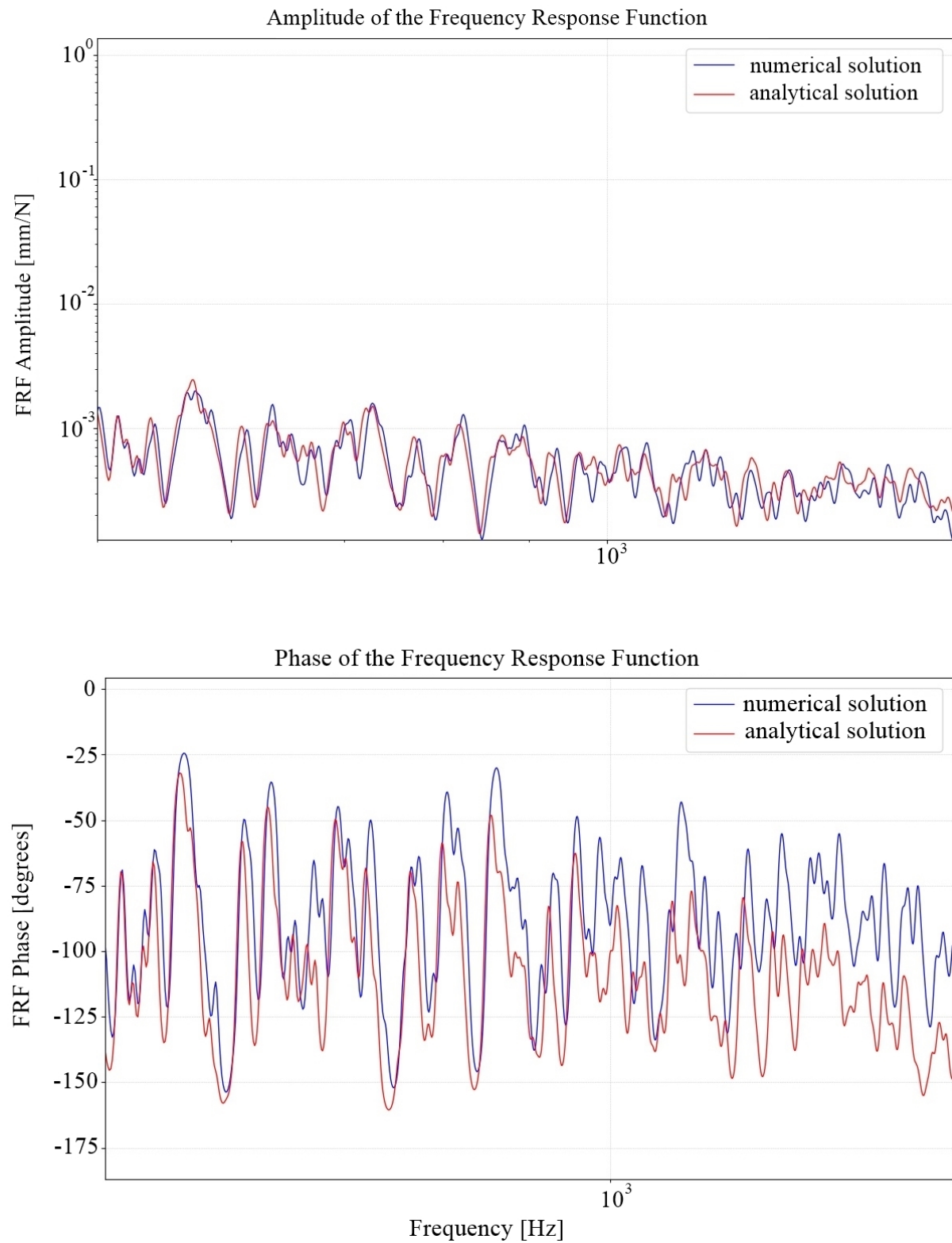


Figure 6.7: Driving point receptance from 500 Hz up to 1600 Hz due to the point force exciting the plate

## 6.4 The FRF between the acoustic pressure at the driver's ear and the force exciting the plate

Frequency Response Function (FRF) at driver's ear can be expressed as

$$H_{p,F}(\omega) = \frac{p(\omega)}{F(\omega)} \quad (6.2)$$

where  $p(\omega)$  is the output (acoustic pressure), and  $F(\omega)$  is the input (force). The units of the acoustic pressure and force are [Pa] and [N], respectively.

The FRF between the acoustic pressure at the driver's ear and force at the excitation point is expressed in decibel and can be computed as

$$H_{p,F}(dB) = 20 \cdot \log_{10} \frac{p}{F} \quad (6.3)$$

where  $2 \cdot 10^{-5}$  is the reference pressure in Pascals, i.e., the threshold of hearing.

The comparison of the numerical solution with the analytical solution is shown in the Figure 6.8 for the whole frequency range. The same conclusion from previous chapter can be drawn here. The numerical results become less accurate when the frequency increases (see Figure 6.10).

Figure 6.9 shows a good agreement of the results obtained with analytical equation and calculated in ACTRAN up to 500 Hz.

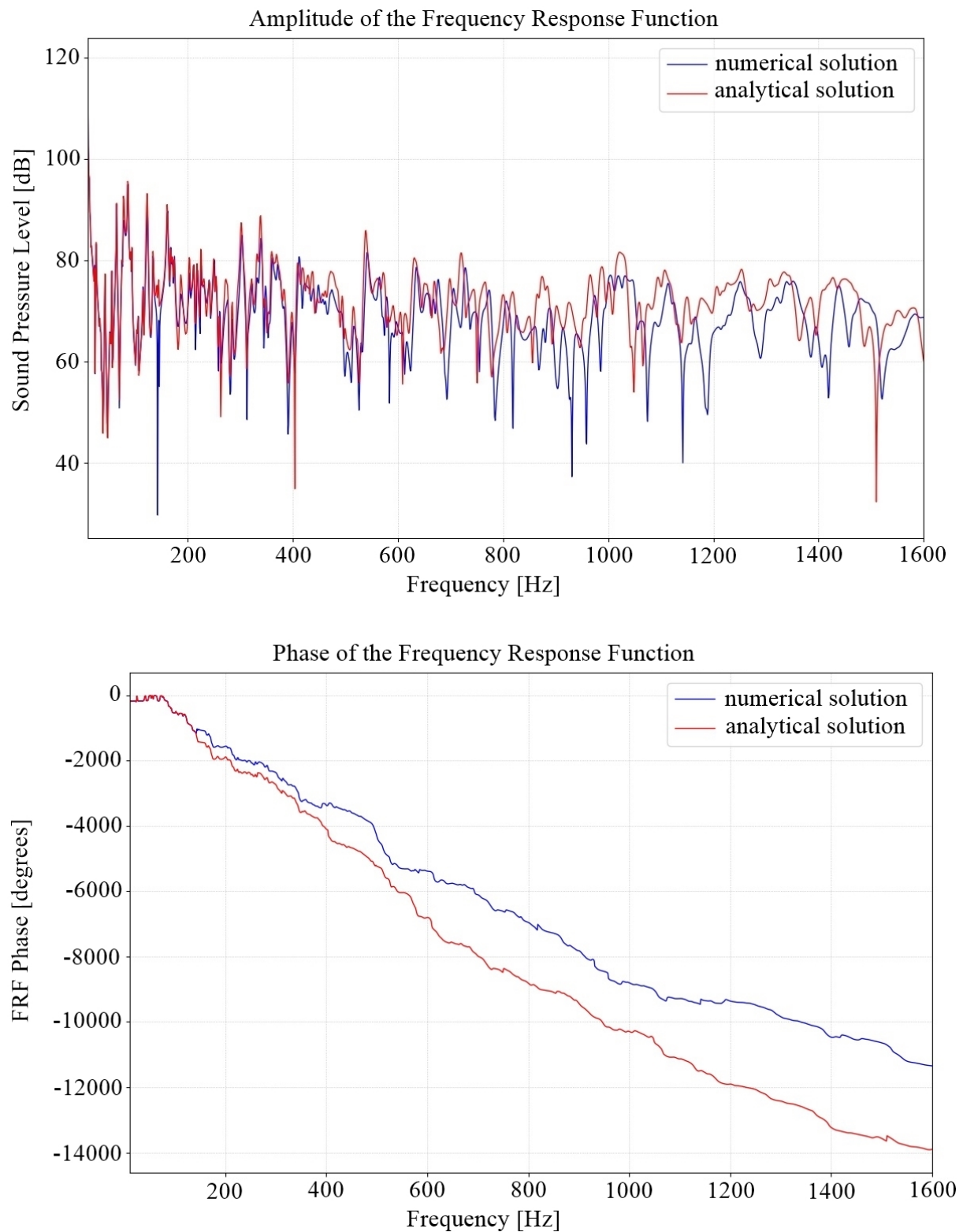


Figure 6.8: Sound pressure level at driver's ear for the whole frequency range

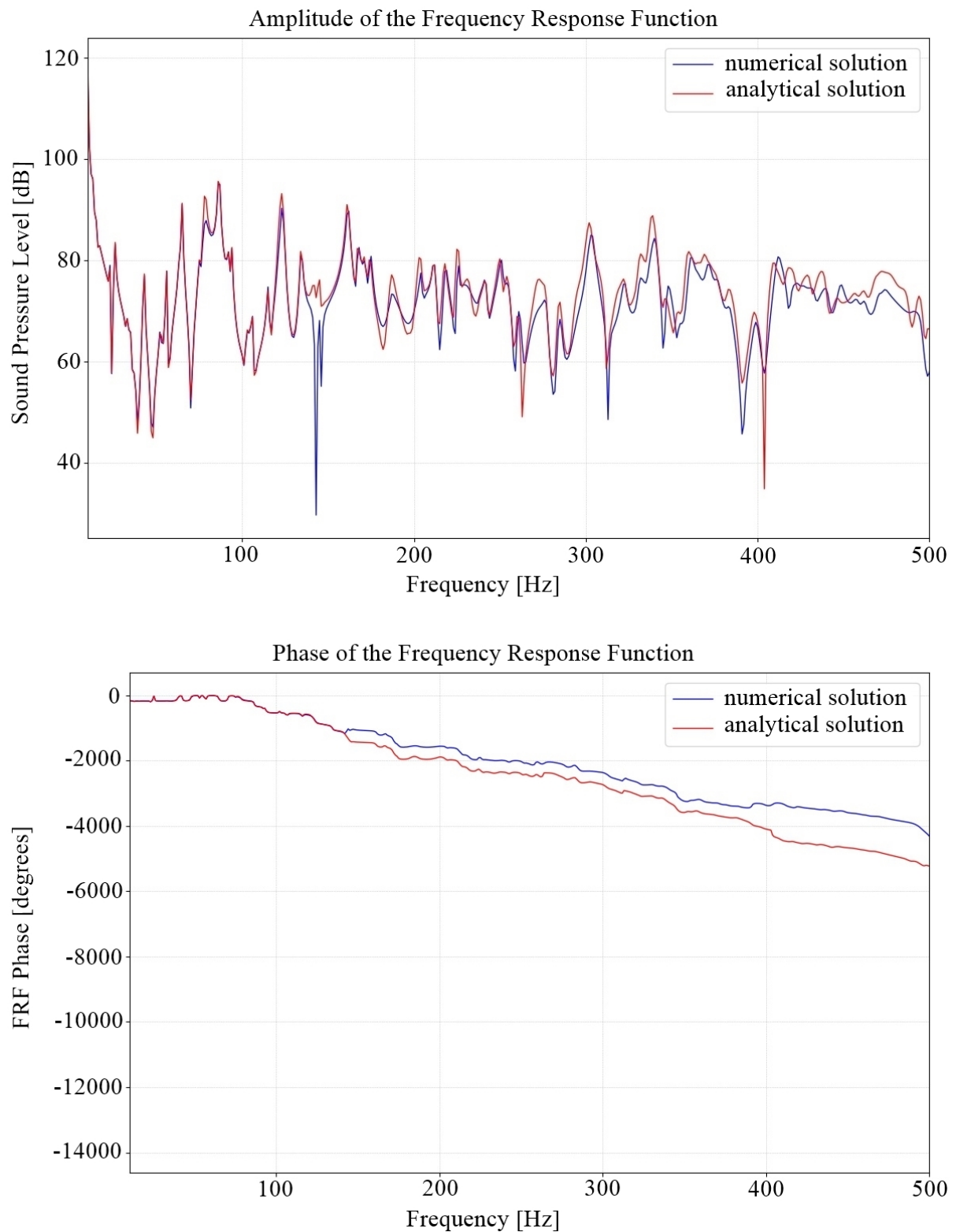


Figure 6.9: Sound pressure level at driver's ear up to 500 Hz

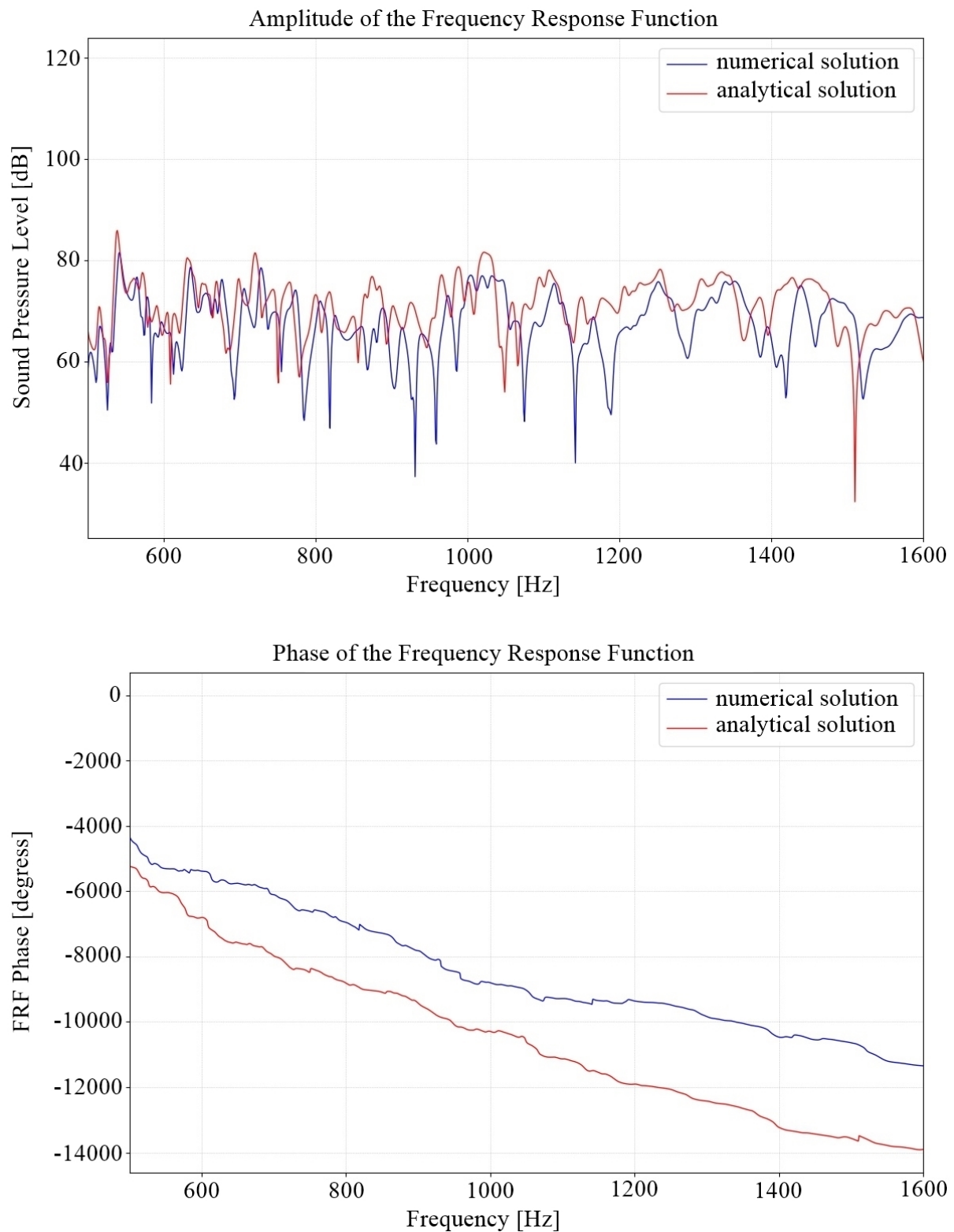


Figure 6.10: Sound pressure level at driver's ear from 500 Hz to 1600 Hz

Figure 6.11 shows the coupled resonances and antiresonances in the Frequency Response Function of the coupled vibro-acoustic model up to 300 Hz. Purple circles correspond to the peaks appearing due to plate modes and green circles correspond to

the peaks appearing due to cavity modes. Uncoupled plate and cavity modes have a little lower value than coupled peaks in FRF. The coupled eigenfrequencies shift toward higher frequencies. For example, the first uncoupled acoustic cavity mode appears at 77.28 Hz, while the coupled peak of the vibro-acoustic model corresponds to 78 Hz (the first green peak as seen from the left to right in the Figure 6.11). This is a relatively small shift in frequency indicating that the acoustic cavity is large enough not to impose a considerable stiffness onto the plate through its 0,0,0 breathing mode. Due to the relatively large acoustic cavity, the plate and cavity natural frequencies remain relatively uncoupled as shown in the following Figure 6.11.

Moreover, antiresonances, i.e. minimum sound pressure level at particular frequencies, appear due to several reasons. First, antiresonances appear when the position of the exciting force at a particular frequency is applied near a nodal line of the plate. Therefore, the force will not excite the plate mode at that particular frequency. Second, antiresonances occur when the location of the microphone in the cavity corresponds to the location of the nodal plane of a cavity mode at particular frequencies.

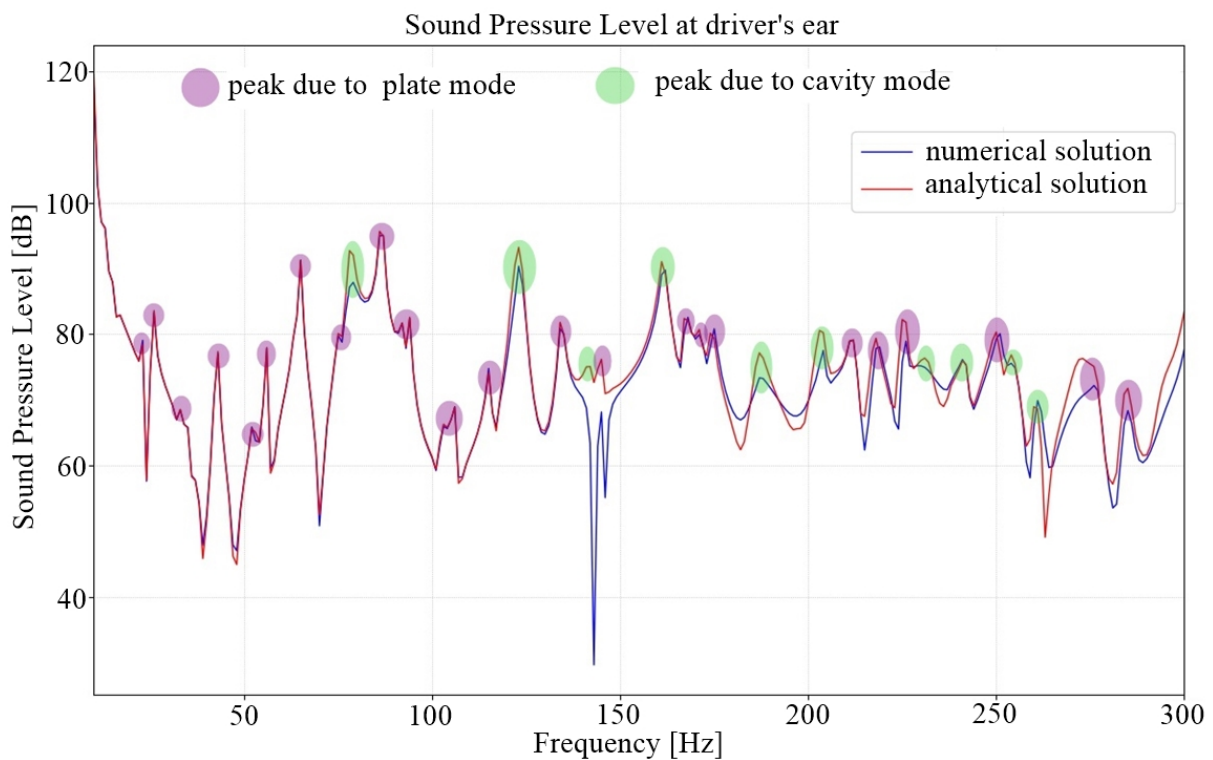


Figure 6.11: Sound pressure level at driver's ear up to 300 Hz

## 6.5 Conclusion

A comparison between the calculated eigenfrequencies and eigenmodes of a simply supported plate and rigid-wall acoustic cavity is made. Numerical models give results with excellent accuracy in comparison to analytical results. This implies that the numerical plate and cavity models are verified.

Furthermore, a comparison between the number of Frequency Response Function calculated analytically and numerically of the coupled vibro-acoustic model is done. It can be concluded that numerical model of the vibro-acoustic system gives very accurate results in the low frequency range (up to 500 Hz), while less result accuracy can be noted at high frequencies i.e. from 500 Hz to 1600 Hz. Discrepancies between the analytical and numerical results can be reduced by refining the mesh of the plate and cavity. Although this can be done, it will increase the computational time and memory consumption. Finally, a conclusion can be drawn that numerical vibro-acoustic model modeled with 10 elements per wavelength can give results with good accuracy up to 500 Hz (or a little bit higher), while in the high frequency range results calculated numerically qualitatively agree with the analytical ones in the sense that they exhibit the characteristic mass law. The mass law implies a reduction of the mean response as the frequency increases. This is typical for sound transmission through thin partitions such as panels [16]. The 10 elements rule corresponds to finite element size of shell element 10 mm and finite element size of the tetrahedral element 20 mm for the maximum frequency of 1600 Hz.

## Part II

Numerical simulation of the noise  
transmission from an exterior sound  
source into a vehicle interior



# Chapter 7

## Methodology to predict the exterior and interior sound field in ACTRAN

An objective of the thesis is to propose a methodology to predict the exterior and interior sound field due to the exterior sound source. The numerical simulation is performed on a *body-in-blue* vehicle model. Vehicle configuration *Body-in-blue* stands for a set of vehicle body parts consisting of the windows and the sheet metal components that are welded or glued together before other components such as e.g. the trim, the engine, etc. are joined to it. A *Body-in-blue* completely encloses the interior vehicle cavity.

The vehicle model was generously provided by AUDI AG. Besides the vehicle model, AUDI AG was courteous enough to share all the data needed to successfully perform this numerical simulation. This includes boundary conditions, materials, positions of the exterior sound sources, and locations of the microphones positioned around the vehicle and inside the passenger compartment. The vehicle model provided by AUDI AG is shown in Figure 7.1.

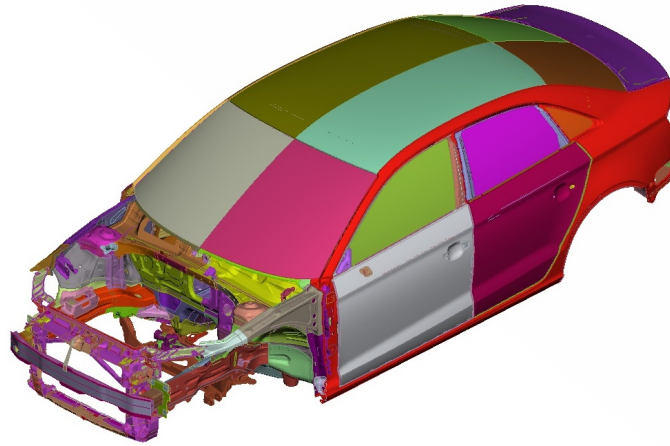


Figure 7.1: Body-in-blue finite element vehicle model

Figure 7.2 shows acoustic cavities of the mentioned vehicle. In total there are 11 acoustic cavities considered: passenger compartment cavity, A-, B- and CD-pillar cavities, small front and back cavities, bumper cavity, door cavities, trunk cavity, tailgate cavity and front feet cavity.

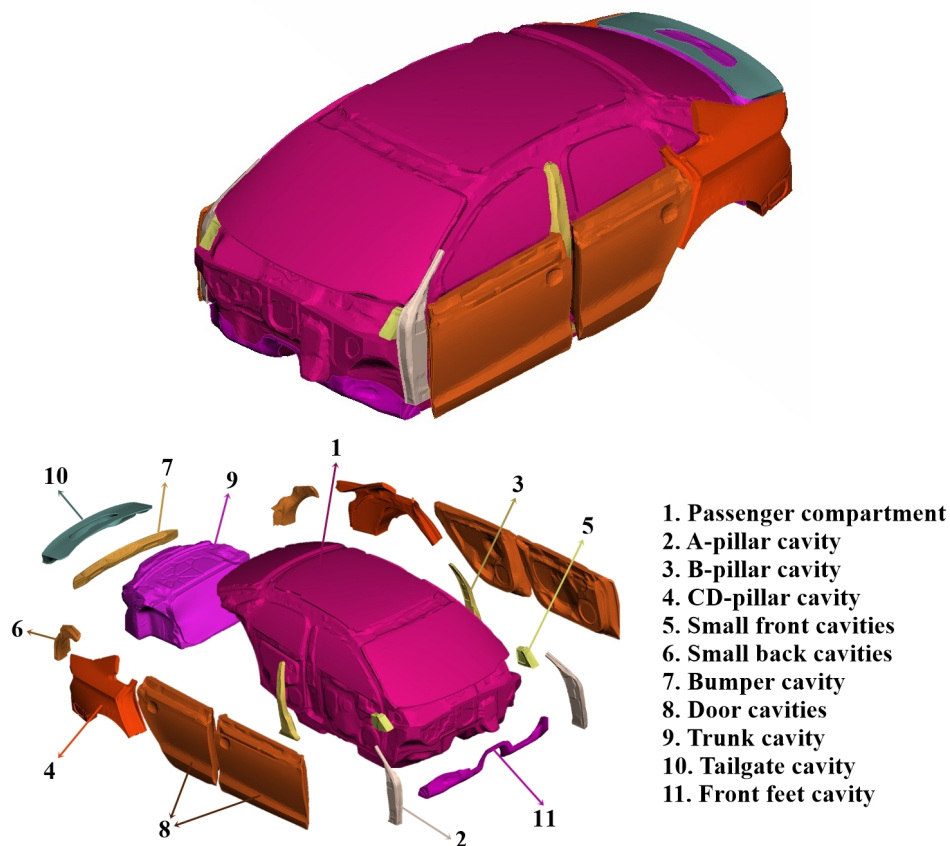


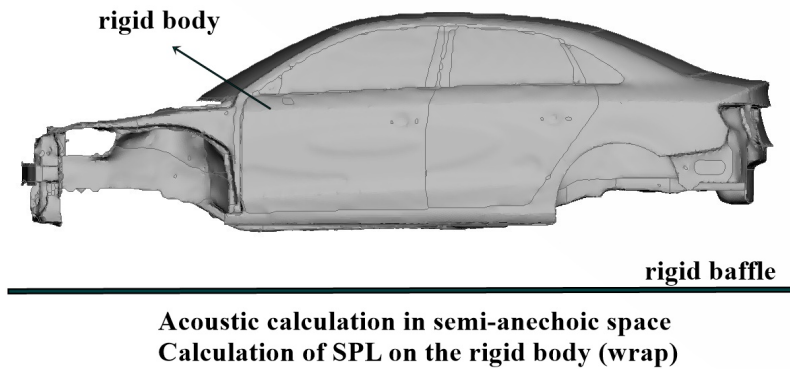
Figure 7.2: Acoustic cavities inside the body-in-blue vehicle

The methodology is divided into three steps:

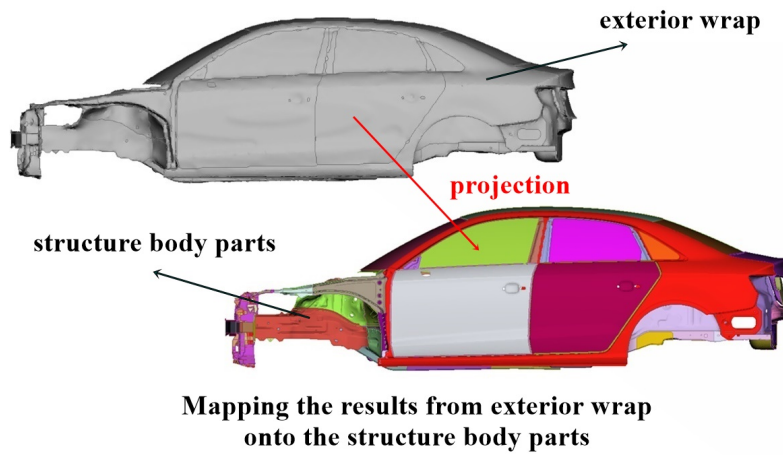
1. The first step involves a Finite Element (FE) model of the exterior wrap of the body-in-blue vehicle and a Finite Element/Infinite Element (FE/IE) model that represents unbounded exterior acoustic domain all around the vehicle. In future reference this model is called *exterior acoustic model*. The surface pressure on the rigid exterior wrap of the vehicle is computed.
2. The second step consists of the projection of the acoustic pressure calculated assuming the rigid surface of the vehicle wrap (results from step 1) onto the vehicle body parts. The projected pressure will be used to excite the flexible vehicle body in the following step 3. In order to achieve the best mapping quality, gap and plane tolerances have to be selected carefully.
3. The third step consists of the computation of the vibro-acoustic response by using the pressure field projected on the vehicle body from step 2 as excitation. In future reference, this model is called *vibro-acoustic model*.

Figure 7.3 shows the computational steps of the generated methodology.

## 1. Exterior acoustic model



## 2. Projection procedure



## 3. Vibro-acoustic model

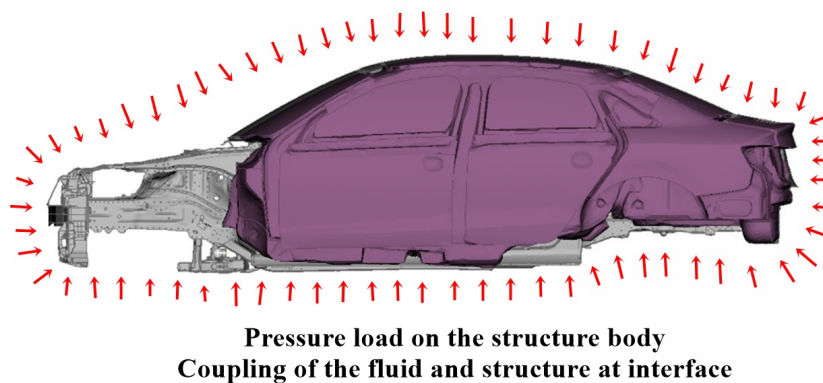


Figure 7.3: Computational steps in ACTRAN

## 7.1 Exterior acoustic model

An exterior acoustic model is created in order to compute the acoustic pressure on the exterior wrap of the vehicle due to the exterior sound source. The wrap of vehicle is modeled as a rigid surface. Unbounded acoustic domain is modeled with finite and infinite elements. The acoustic domain between the wrap of the vehicle and the boundary surface is modeled with the 3D acoustic finite elements. The boundary surface is modeled with infinite elements. With the use of infinite elements, the unbounded domain is truncated. The infinite elements impose a free-field condition, which means that no sound reflection occurs from the truncated boundary.

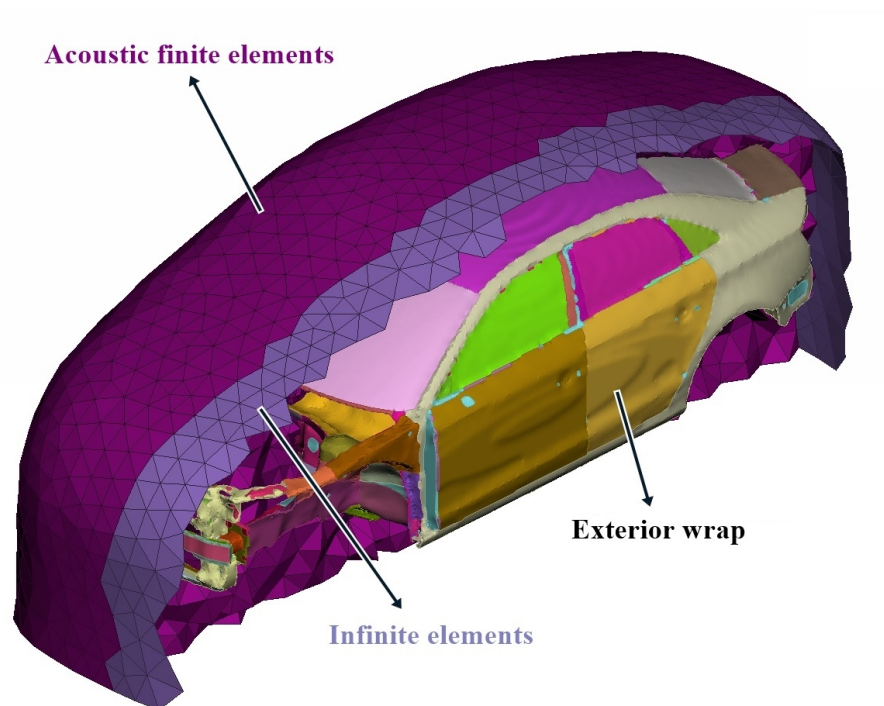


Figure 7.4: Exterior acoustic model

The exterior wrap of the body-in-blue vehicle is created in CAE pre-processing software ANSA. Before the creation of the exterior wrap of the vehicle, following actions, which are shown in Figure 7.6, are performed:

- Small structure body parts are removed from the vehicle model. Small structure body parts will have a very small impact on the vehicle interior response and these

can be easily neglected and removed from this part of the analysis. In the vibro-acoustic model in step 3, these parts will have zero-pressure boundary condition, which means no sound pressure will be applied.

- All openings of the vehicle are closed in order to successfully perform the process of wrapping.
- All interior parts are removed in order to reduce the time of the mapping procedure in step 2. The inside structure parts can be removed because the sound pressure is applied only to the exterior parts of the vehicle.

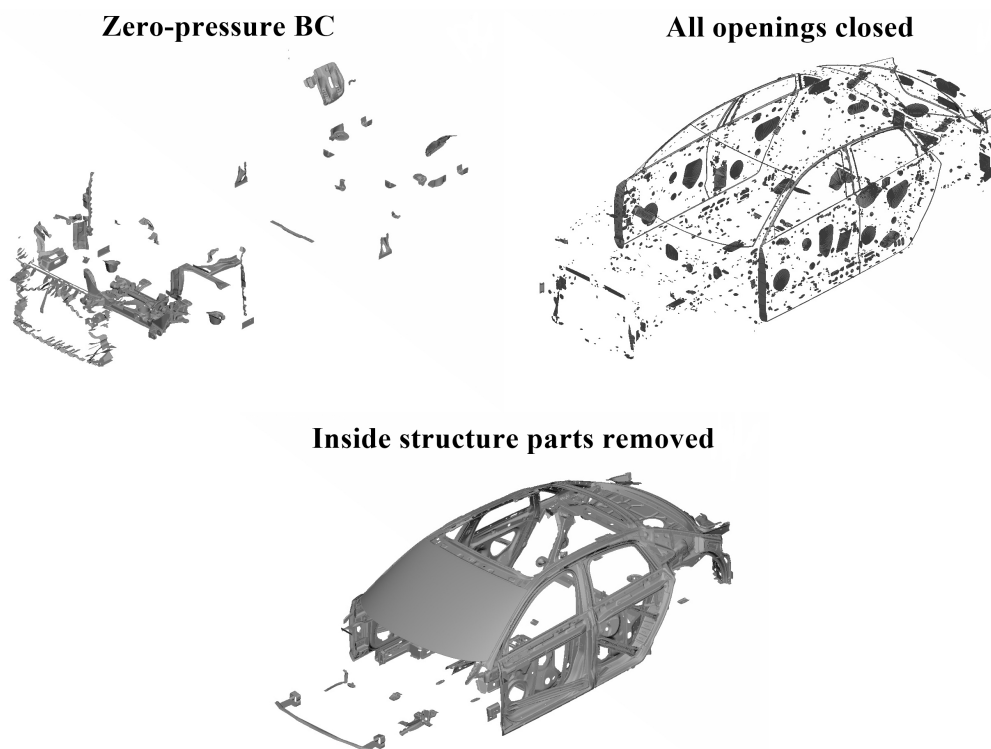
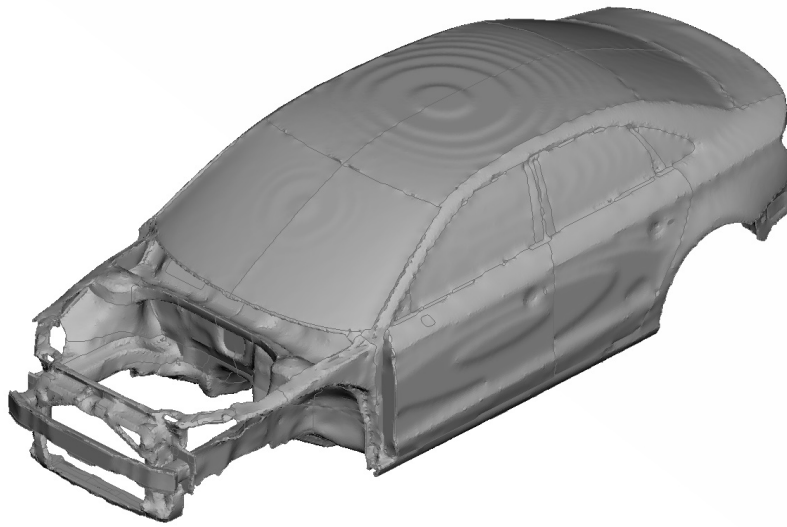


Figure 7.5: The workflow of the creation of the exterior wrap

The exterior wrap mesh contains 620668 shell elements and 310316 grid points. The surface of the wrap has to be clean and closed, i.e. watertight, in order to successfully create exterior acoustic component.



**Figure 7.6: Exterior wrap of the body-in-blue vehicle**

Furthermore, the unbounded exterior fluid domain is modeled using Finite Fluid and Infinite Fluid components. Finite fluid material is specified in both components. The sound speed is taken to be  $c = 344$  m/s. In exterior acoustic problems, damping of the air is neglected, because it has little effect on the calculated response.

Alternately, the unbounded exterior acoustic domain is modeled with the use of the Exterior Acoustic component that includes the automatic generation of the exterior fluid domain and boundary surfaces based on the wrap of the vehicle. The mesh generation consists in the creation of a convex hull, which is remeshed to the desired element length and used as boundary for the volume mesh. The newly formed convex hull is numerically resolved by means of infinite elements. The whole frequency range is divided into a finite number of frequency bands. Therefore, the size of the finite and infinite meshes depend on the maximum frequency of each frequency band. In other words, one mesh is created for each frequency band. This approach can save up to 77% of computational time, as shown in Figure 7.7.

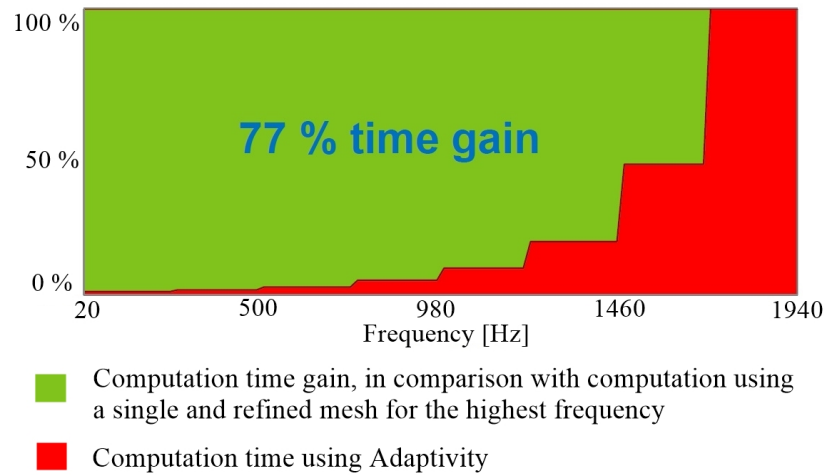


**Figure 7.7: Time comparison per frequency, [23]**

The frequency range of interest, which is from 80 to 1800 Hz, is divided into 12 frequency bands. There are also 12 corresponding meshes with increasing number of elements as the maximum frequency of the band increases. Their minimum and maximum frequencies are listed in Table 7.1.

**Table 7.1: Frequency bands for exterior acoustic component**

Frequency band	Minimum frequency [Hz]	Maximum frequency [Hz]
1	79.50	284.85
2	284.85	314.82
3	341.82	410.19
4	410.19	492.22
5	499.22	590.67
6	590.67	708.80
7	708.80	850.56
8	850.56	1020.67
9	1020.67	1224.81
10	1224.81	1469.77
11	1469.77	1763.73
12	1763.73	2116.47



Figure 7.8 shows the meshes generated by Actran for the frequency ranges from 79.5 to 284.85 Hz, 410.19 to 492.22 Hz, 850.56 to 1020.67 and 1763.73 to 2116.47 Hz. One can notice that indeed with the increase in frequency the element size decreases.

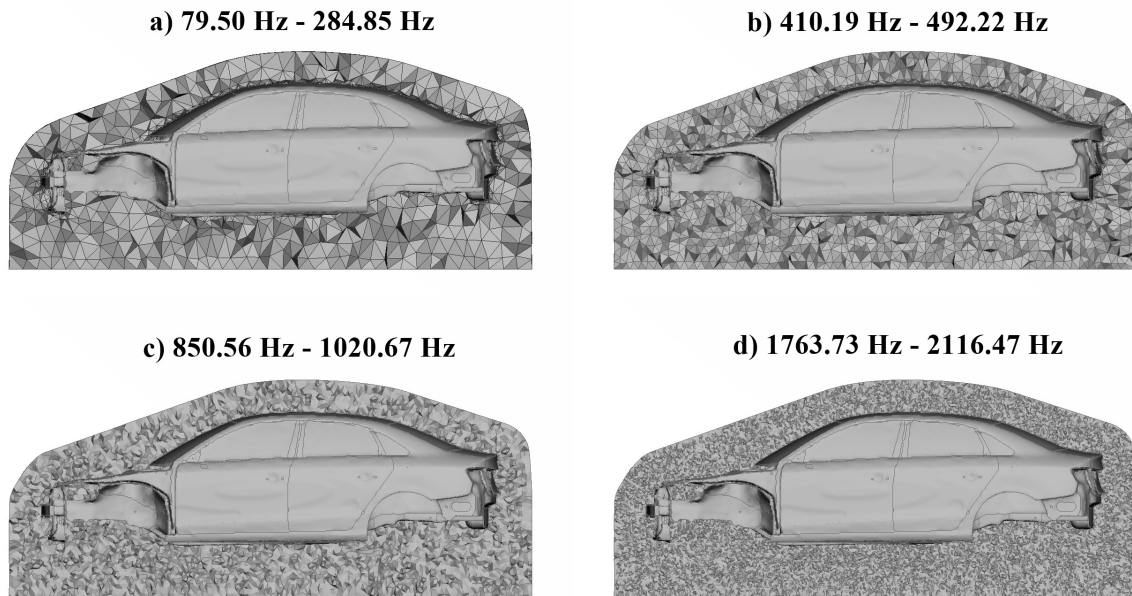


**Figure 7.8: Generated exterior acoustic mesh in relation to frequency range**

Advantages of the exterior acoustic component are:

- The exterior fluid domain surrounding the structure does not need to be meshed. This is done automatically by Actran.
- Acoustic finite and infinite elements are created and remeshed by Actran for different frequency bands.
- The automated generation of mesh related to the maximum frequency of interest will result in reduction of the computation time.

In order to model a semi-free field, e.g. a semi-anechoic chamber with rigid floor, the so-called symmetry data block is introduced within Actran. This data block is used to define the positions of rigid baffles. The position of the floor in the Cartesian coordinate system measured from the center of gravity is  $z = -595$  mm, as shown in the Figure 7.9.

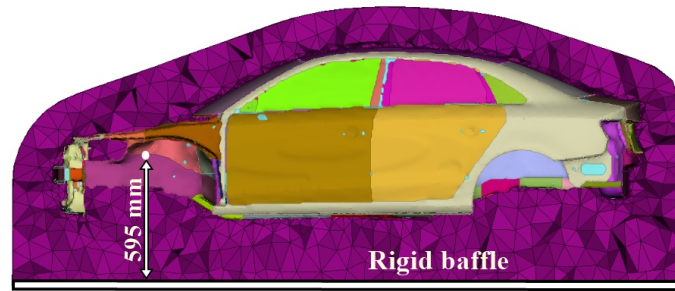


Figure 7.9: Rigid baffle in exterior acoustic model

Furthermore, acoustic monopole sources can be described in terms of pressure [Pa], mass flow [kg/s] and volume velocity [m<sup>3</sup>/s]. Volume velocity and mass flow of the monopole source are related through

$$V = \frac{Q}{\rho_0} \quad (7.1)$$

where  $Q$  is the mass flow and  $\rho_0$  is the density of the undisturbed air.

Mass flow of the monopole source can be related to the pressure amplitude  $A$  of the source through:

$$Q = \frac{4\pi A}{ick} \quad (7.2)$$

where  $i$  is the imaginary part,  $c$  is the speed of the sound and  $k$  is the wavenumber. [22]

A spherical monopole source, defined as a volume source, is introduced in ActranVI. The amplitude of the volume velocity monopole source is set to  $V = 0.001$  m<sup>3</sup>/s.

There are 4 locations for the monopole source that are separately considered in this analysis and they are located at:

- rear left wheelhouse,
- front left wheelhouse,
- engine compartment, and
- exhaust.

The position of each monopole sound source is shown in Figure 7.10. These locations are chosen because they correspond to the principal noise sources that contribute to the vehicle interior sound. In other words, the aim is to simulate the contributions to the interior noise due to

1. engine,

2. back tyre rolling,
3. front tyre rolling,
4. exhaust.

Due to the nearly symmetric shape of the car, it is enough to consider only a pair of tyres on one side of the vehicle.

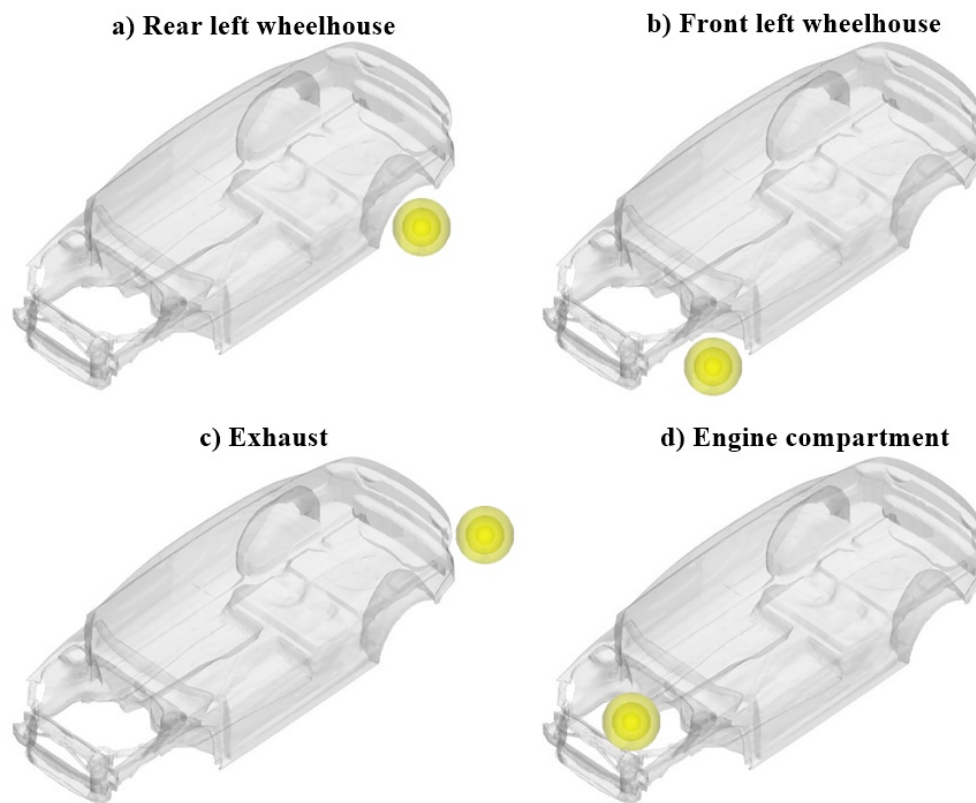


**Figure 7.10: Exterior sound source positions**

The main purpose of the exterior acoustic model is to calculate the acoustic pressure on the rigid exterior wrap. Acoustic pressure is also computed at the points located around the vehicle. These points represent locations of microphones which are located on the arrays (see Figure 7.11). Normally arrays of microphones are used in order to measure the sound pressure at a large number of points around a real vehicle in a semi-anechoic chamber. The results of such measurements can be used to assess the accuracy of numerically calculated sound pressure at the rigid vehicle wrap. Furthermore, the sound pressures at the microphone array locations are calculated numerically using ACTRAN

and shown and discussed in the forthcoming parts of the thesis. In other words, Frequency Response Functions are calculated between the exterior microphones and the volume velocity sound source. There is a total of 868 exterior microphone points.

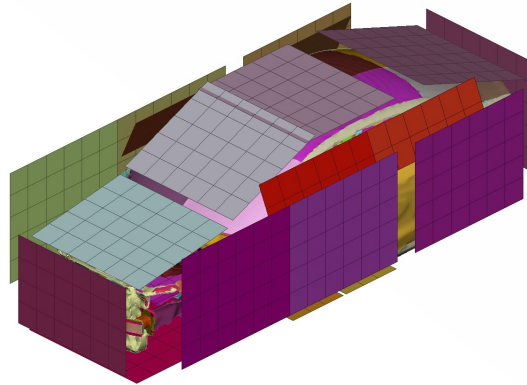


**Figure 7.11: Microphone arrays located around the vehicle**

## 7.2 Projection procedure

Projection procedure deals with the projection i.e. localization of nodes from the first coupling surface onto the second coupling surface and also mapping of the results from the first coupling surface onto the second coupling surface. As mentioned before, projection quality is controlled through gap and plane tolerance, see Figure 5.10. The projection procedure is done in Export load utility that is a part of ACTRAN software package. In this case, the first coupling surface is the exterior wrap of the vehicle and the second coupling surface is a set of the structural body parts of the vehicle on which the acoustic pressure is applied. Because of the variable distance between the wrap of the vehicle and vehicle itself, a list of gap and plane tolerances is given in Table 7.2. The gap tolerance is the absolute value of the extrusion of the pseudo-mesh along the normal direction to the surface, and plane tolerance is a relative value which extends the size of the extruded pseudo-mesh along its face plane.

**Table 7.2: Gap and plane tolerances specified for projecting the acoustic pressure saved on the wrap onto the structure body**

Gap tolerance [mm]	Plane tolerance [-]
2	0.05
4	0.05
6	0.05
8	0.05
10	0.05
15	0.05
20	0.05

With this combination of gap and plane tolerances, the Export Load utility starts with the first gap and plane tolerance, maps the values of the acoustic pressure from the first coupling surface onto the second coupling surface and then proceeds with the next gap and plane tolerance while keeping the values mapped from the previous set of gap and plane tolerance. In order to transfer information between different steps of the methodology, acoustic pressure is converted into forces acting on the vehicle's structure.

### 7.3 Vibro-acoustic model

The final computation is performed on a finite element vehicle body model that interacts with the finite element cavity model. The vehicle body mesh contains 827106 finite elements of which 627694 elements are shell elements. Acoustic cavity mesh contains 812600 tetrahedral finite elements. The finite element size of the vehicle model is approximately 10 mm, which is in accordance with the requirement concluded from the validation of the vibro-acoustic model. This finite element size is calculated for the maximum frequency 1600 Hz. Furthermore, the finite element size of the cavity model is ranging from 20 mm to 30 mm. This does not correspond to the requirement that the acoustic element size is under 20 mm. With this in mind, one can expect inaccurate interior response at higher frequencies. Moreover, these two models are coupled, i.e. the structural mesh is coupled to the acoustic mesh. At the interface, a boundary condition is satisfied

$$\frac{\partial p}{\partial n} = \rho_0 \omega^2 w \quad (7.3)$$

which means that the gradient of the pressure normal to the interface is equal to the product of the air density and acceleration of the vehicle body part.

A Direct Frequency Response Analysis is carried out next. The frequency range of interest is from 100 Hz to 1600 Hz. The topology, materials, components and Boundary Conditions (BC) are imported into Actran solver from an input file for the Nastran solver. The materials, components and boundary conditions are listed in Table 7.3.

**Table 7.3: Materials, components and BCs imported from NASTRAN input file**

Materials	Components	Boundary conditions
Beam Material	Beam	Displacement
Fluid Material	Discrete	Rotation
Isotropic Solid Material	Finite Fluid	
Sping Material	Mean constrain	
	Multiple Point Constraint	
	Point Mass	
	Rigid Body	
	Solid	
	Thin shell	

Beam, Discrete, Finite Fluid and, Solid and Thin shell components are modeled with Beam Material, Spring Material, Fluid Material and Isotropic Solid Material, respectively.

Moreover, an interface is introduced to couple the acoustic model with the structural model, i.e. the acoustic mesh with the structural mesh. The first coupling surface is a set of the selected meshes of the vehicle body parts that are interfacing the cavity, whereas the second coupling surface is the skin of the cavity. As previously mentioned, the projection procedure is controlled through gap and plane tolerances. Gap and plane tolerances are 5 mm and 0.05, respectively. Figures 7.12-7.22 show the projection quality with the specified gap and plane tolerances.

The process is a two step procedure:

- Projection of the nodes from first coupling surface to the second coupling surface. This is achieved with the help of a temporary mesh created based on the second coupling surface. The normals of the nodes of the second surface are computed. Elements of the second surface are extruded (gap tolerance) following the normals. The extruded elements are scaled by a factor to reach the target node (plane tolerance).
- Values are deduced on the projected nodes on the second coupling surface. These values are interpolated from the value of the closest nodes and the shape function of the elements. These values are then mapped on the first coupling surface.

In order to successfully perform a vibro-acoustic analysis and get the pleasing results, the projection quality needs to be as much higher as it can be. The values displayed in the color maps provide information on the quality of the projection:

- Nodes having a value spread from 0 to 1 are mapped during the procedure.
- Nodes having a value above 1 are not mapped during the projection.
- Nodes having a value close to 1 are the farthest from the projection surface, but the distance still remains within the tolerance. Nodes having a value close to 0 are located at shorter distance to the projection surface. [24]

The mapping process should not be confused with the projection/localisation process. The percentage of the localisation shows us the percentage of the projected nodes from

the first coupling surface to the second coupling surface, whereas mapping process is related to mapping of the results calculated in the nodes.

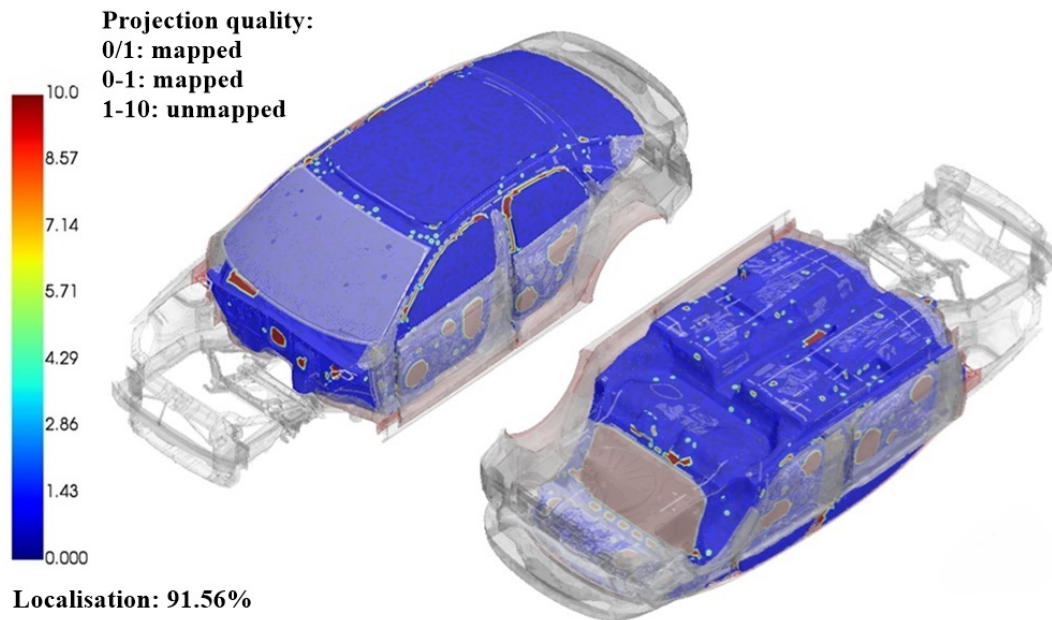


Figure 7.12: Projection quality of the interface for the vehicle structure and the passenger compartment cavity with gap and plane tolerance specified as 5 mm and 0.05, respectively

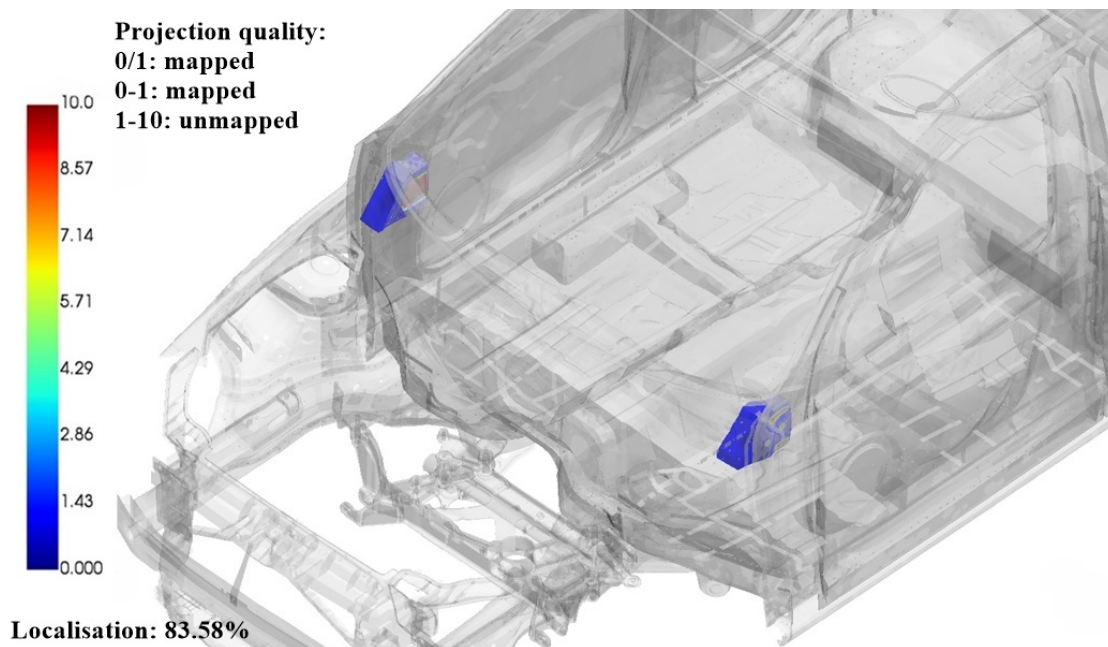


Figure 7.13: Projection quality of the interface for the vehicle structure and small front cavity with gap and plane tolerance specified as 5 mm and 0.05, respectively



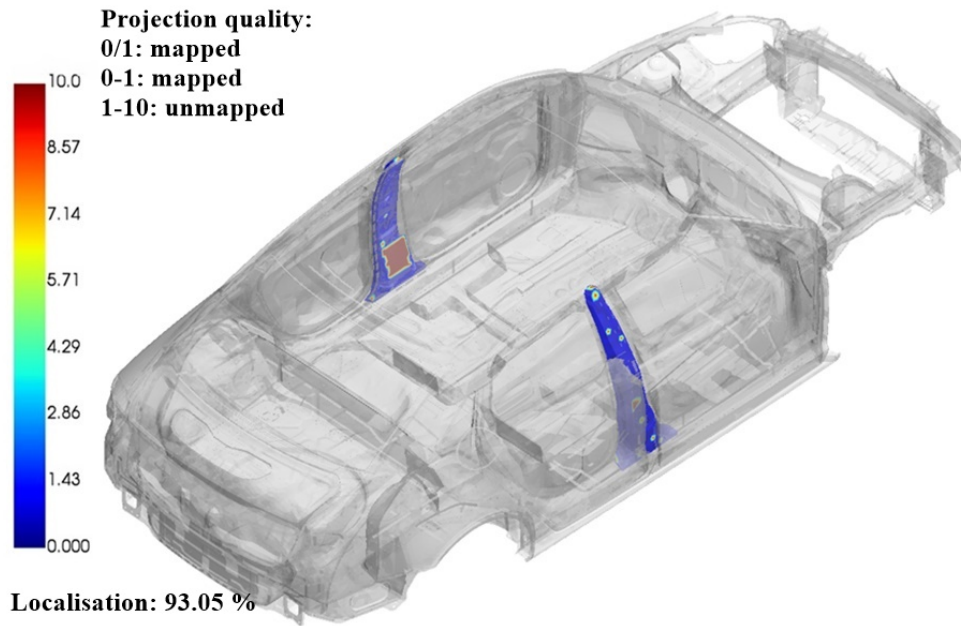


Figure 7.14: Projection quality of the interface for the vehicle structure and B-pillar cavity with gap and plane tolerance specified as 5 mm and 0.05, respectively

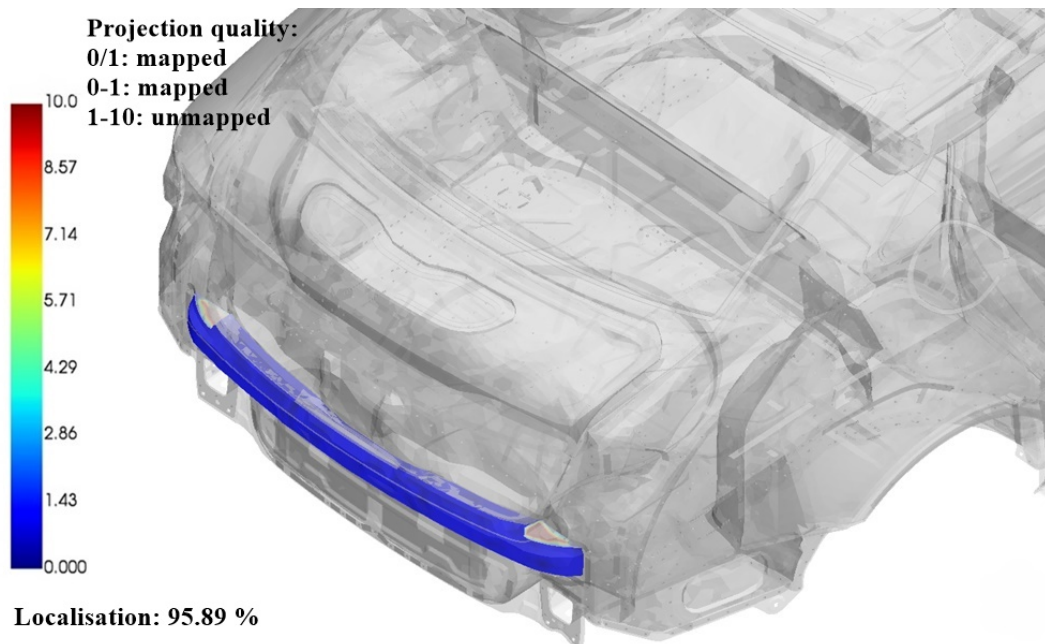


Figure 7.15: Projection quality of the interface for the vehicle structure and bumper cavity with gap and plane tolerance specified as 5 mm and 0.05, respectively

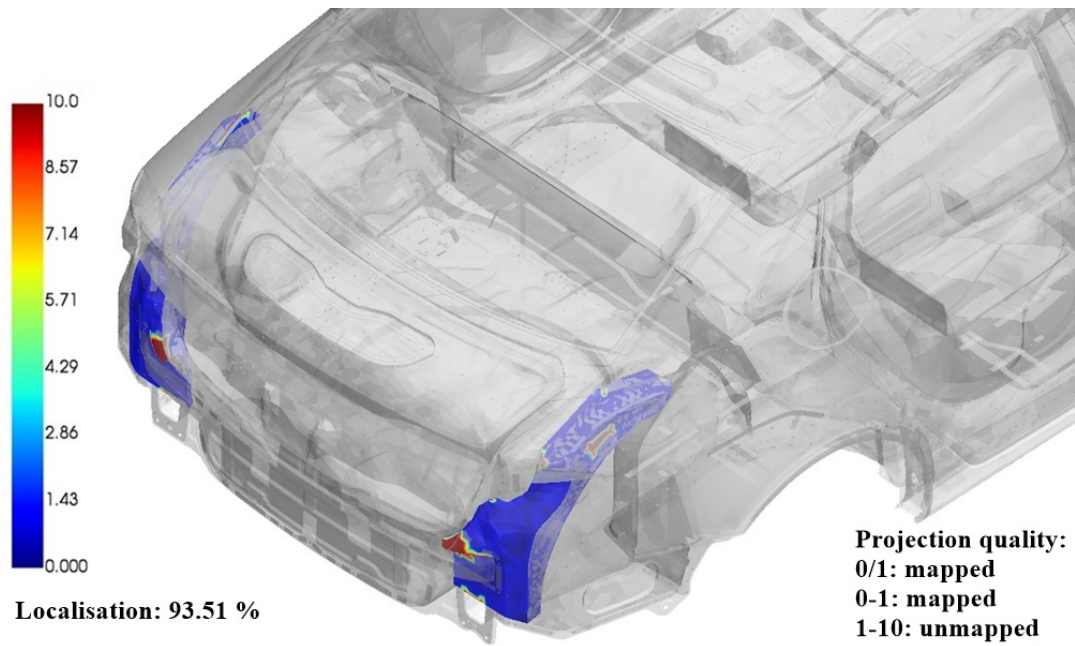


Figure 7.16: Projection quality of the interface for the vehicle structure and small back cavity with gap and plane tolerance specified as 5 mm and 0.05, respectively

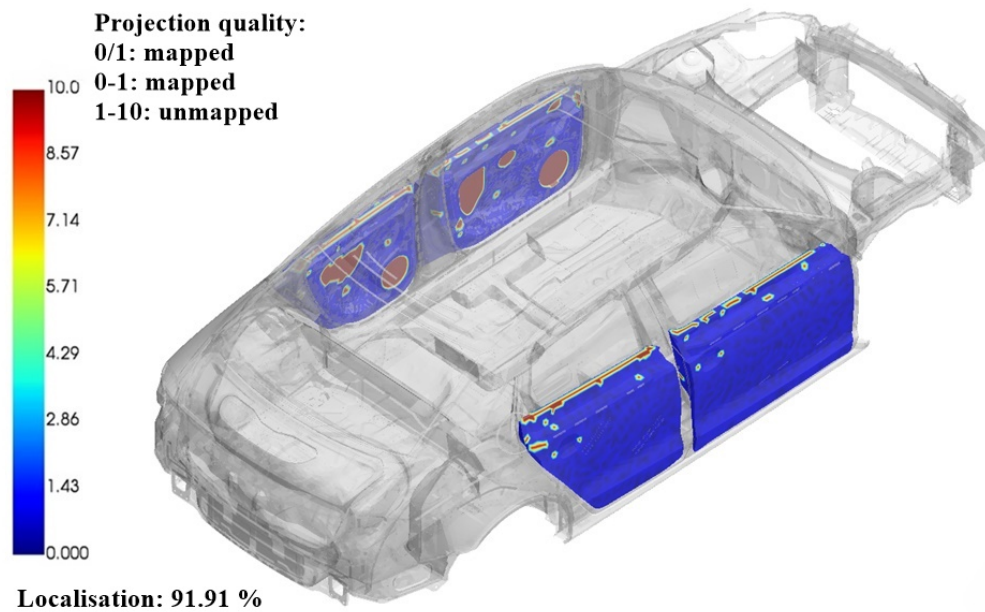


Figure 7.17: Projection quality of the interface for the vehicle structure and door cavities with gap and plane tolerance specified as 5 mm and 0.05, respectively

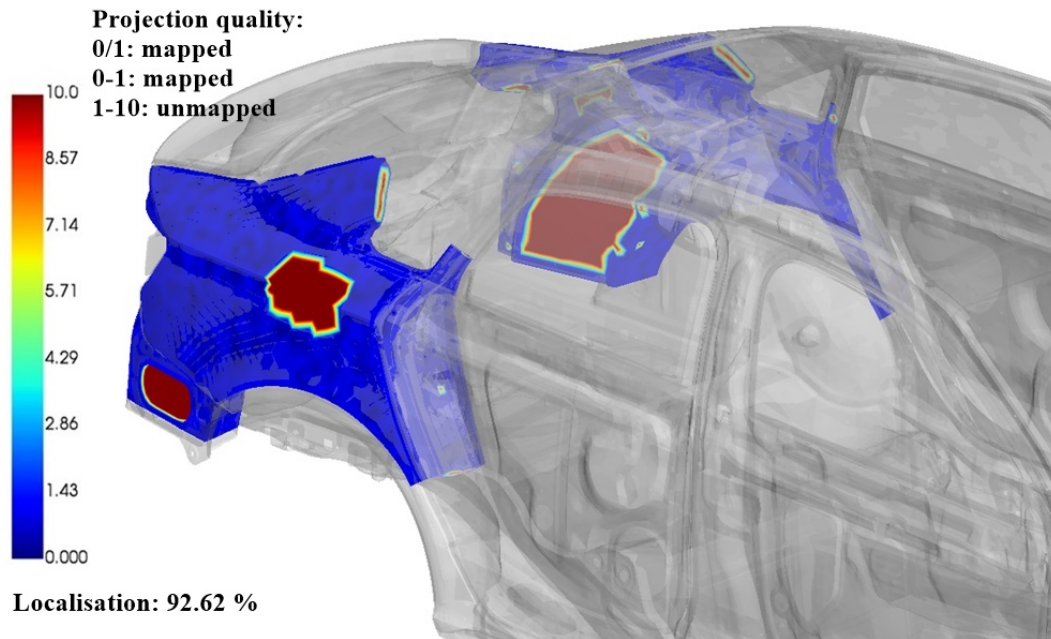


Figure 7.18: Projection quality of the interface for the vehicle structure and CD-pillar cavities with gap and plane tolerance specified as 5 mm and 0.05, respectively

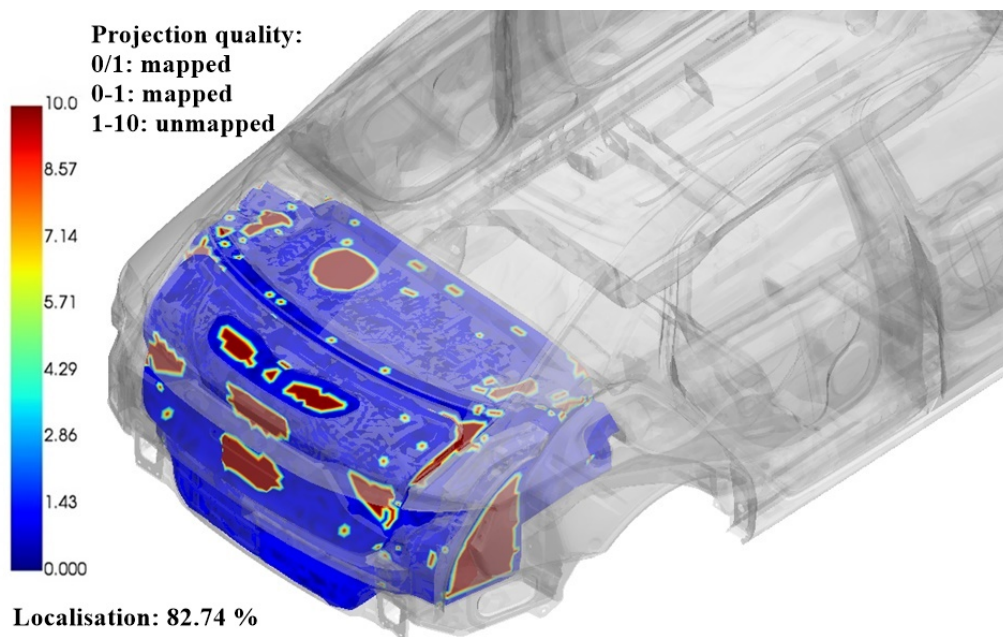


Figure 7.19: Projection quality of the interface for the vehicle structure and trunk cavity with gap and plane tolerance specified as 5 mm and 0.05, respectively

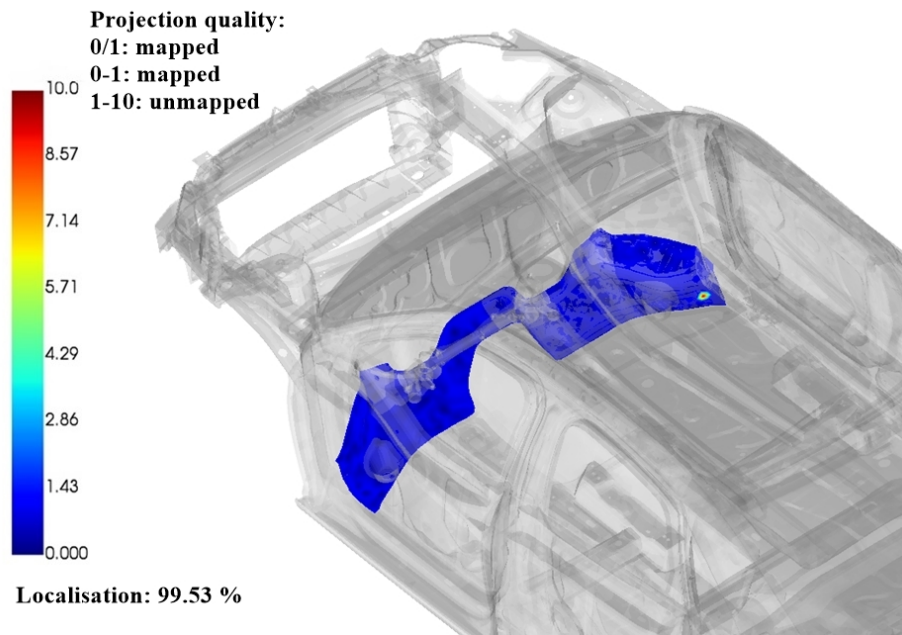


Figure 7.20: Projection quality of the interface for the vehicle structure and front feet cavity with gap and plane tolerance specified as 5 mm and 0.05, respectively

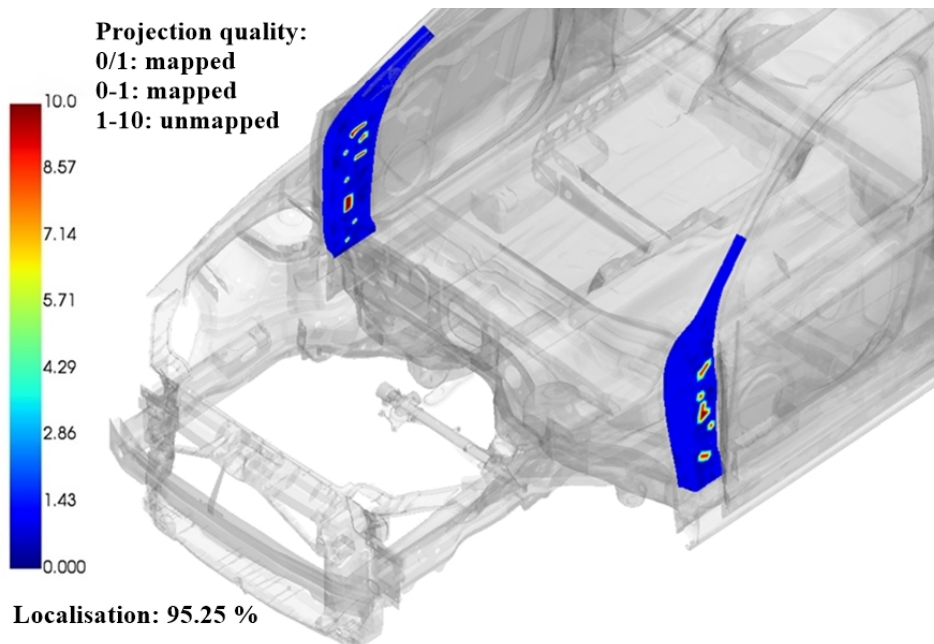
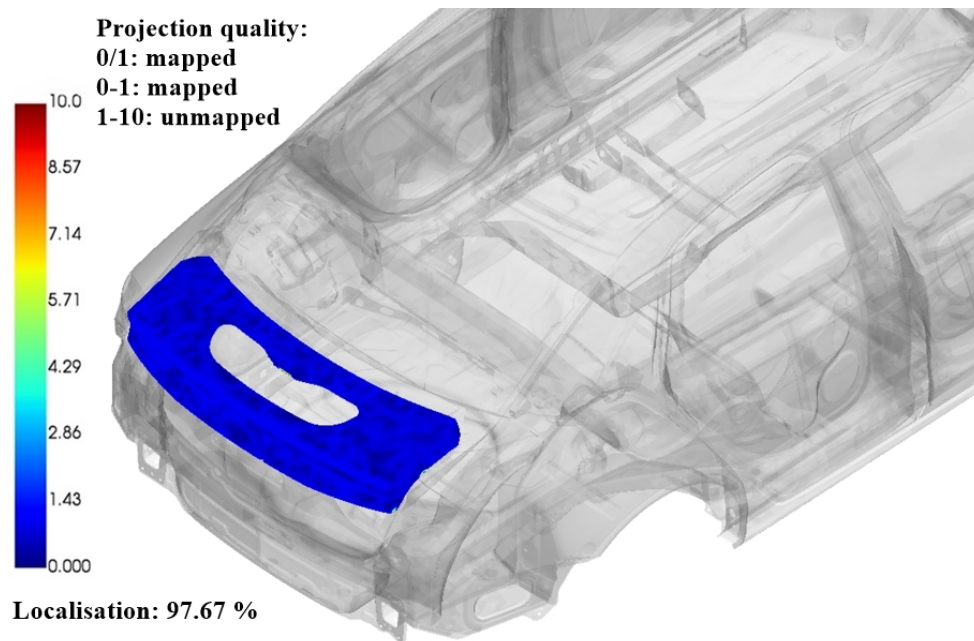
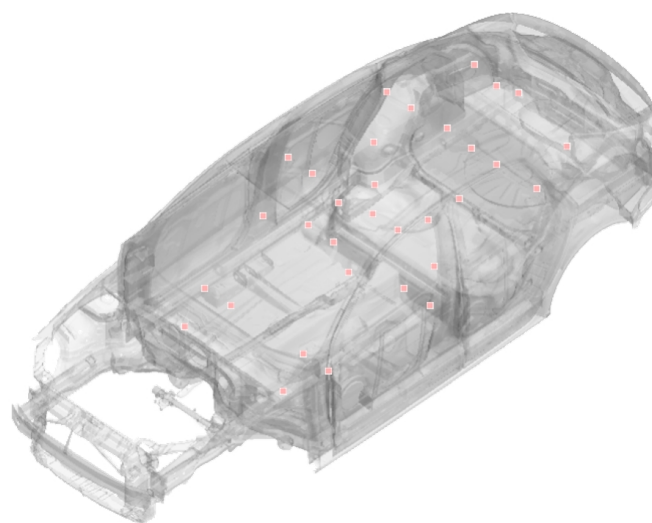


Figure 7.21: Projection quality of the interface for the vehicle structure and A-pillar cavity with gap and plane tolerance specified as 5 mm and 0.05, respectively



**Figure 7.22:** Projection quality of the interface for the vehicle structure and tailgate cavity with gap and plane tolerance specified as 5 mm and 0.05, respectively

Finally, the results from the second step are introduced as the excitation to the vibro-acoustic model. A boundary condition, linking the imported acoustic pressure from second step and the vibro-acoustic analysis, is specified. Acoustic pressure is computed and output maps are created for the acoustic cavities. Also, FRFs between 32 interior microphones (see Figure 7.23) and the four volume velocity sound sources are computed and presented.



**Figure 7.23:** Position of the interior microphones

# Chapter 8

## Results

Results of the numerical simulation which predicts the vehicle exterior and interior sound field, as described in previous chapter, are shown and discussed in this chapter.

Firstly, numerical results are divided into two parts: results obtained from the exterior acoustic model and the results obtained from vibro-acoustic model. Secondly, numerical results are shown for four studied cases, i.e., for the four different positions of exterior sound source (see Figure 7.10).

Starting with the exterior acoustic model, acoustic pressure calculated on the rigid exterior wrap and the acoustic pressures captured on the exterior microphone arrays are visualized. Next, FRFs between the six exterior microphones and exterior volume sound source are shown. The microphone positions are selected in order to present the impact of the distance between the microphone and the exterior sound source on the Frequency Response Function. Moreover, the first two positions of the microphones correspond to the microphones near the volume sound source. The last two positions of the microphones stand for the microphones that are located far from the exterior sound source, whereas third and fourth microphone are located somewhere between the first and the last set of the microphones. The coordinates of the position of the exterior microphones for each considered position of the sound source are listed in Table 8.1.

**Table 8.1: Coordinates of the microphone positions located outside of the vehicle on the microphone arrays**

	Left Rear Wheelhouse			Left Front Wheelhouse		
	x	y	z	x	y	z
Mic 1	2658.273	-957.908	202.7509	-141.727	-957.908	202.7509
Mic 2	2658.273	-957.908	802.7509	-141.727	-957.908	802.7509
Mic 3	1058.273	-957.908	202.7509	1258.273	-957.908	202.7509
Mic 4	1058.273	-957.908	802.7509	1258.273	-957.908	802.7509
Mic 5	548.762	-1.908	996.4799	1593.998	-1.908	1208.729
Mic 6	-466.652	-1.908	693.3247	2874.393	-1.908	994.1204
	Engine compartment			Exhaust		
	x	y	z	x	y	z
Mic 1	-466.652	-1.908	693.3247	3536.273	-401.908	100.7509
Mic 2	723.174	-1.908	1076.23	3536.273	-401.908	700.7509
Mic 3	1593.998	-1.908	1208.729	2858.273	-957.908	202.7509
Mic 4	2874.393	-1.908	994.1204	2686.455	-401.908	1062.524
Mic 5	-141.727	957.908	602.7509	1058.273	-957.908	202.7509
Mic 6	-141.727	-957.908	602.7509	1193.998	-201.908	1208.729

Proceeding with the vibro-acoustic model, acoustic pressure field in the vehicle interior is visualized. Next, FRFs between the six interior microphones and volume velocity sound source is shown. The position of six interior microphones represent the characteristic positions where the sound pressure Level is measured. Therefore, interior microphones marked as 1, 2, 3, 4, 5 and 6 represent positions of the left driver's ear, right driver's ear, left co-driver's ear, right co-driver's ear, right passenger's ear and left passenger's ear, respectively. The coordinates of the interior microphones are listed in Table 8.2.

**Table 8.2: Coordinates of the microphone positions located in the vehicle interior**

	x	y	z
Mic 1	1346.33	445.144	900
Mic 2	1346.33	245.144	900
Mic 3	1346.33	-245.144	900
Mic 4	1346.33	-445.144	900
Mic 5	2146.33	245.144	900
Mic 6	2146.33	-245.144	900

## 8.1 Numerical results of the exterior acoustic analysis

This section deals with the results obtained from the exterior acoustic model.

The first set of the results is presented which considers results of the acoustic pressure computed on the rigid exterior wrap of the body-in-blue vehicle due to the exterior sound source. Figures 8.1, 8.2, 8.3 and 8.4 show the distribution of the acoustic pressure field calculated on the exterior wrap due to exterior sound source located at the left rear wheelhouse, at the left front wheelhouse, in the engine compartment and at the exhaust, respectively.

Furthermore, the second set of the results is presented and shows the distribution of the acoustic pressure computed on the exterior microphone arrays due to the exterior sound source. Figures 8.5, 8.6, 8.7 and 8.8 visualize the acoustic pressure captured on the exterior microphone arrays due to exterior sound source located at the left rear wheelhouse, at the left front wheelhouse, in the engine compartment and at the exhaust, respectively.

First and second set of results are expressed in decibels and presented in 1/3 octave frequency bands.

It is intuitive to expect higher sound levels closer to the sound source, and this is evident from the Figure 8.1 - 8.8. One can also notice that with the increase of frequency, the acoustic wavelength also increases. Consequently, the distribution of the acoustic pressure becomes more complex at high frequencies than that at low frequencies. This is a typical manifestation of the acoustic scattering effect.

Finally, the third set of the results is presented where FRFs between the exterior microphones and exterior volume sound source are calculated and shown. FRF between the exterior microphone and exterior sound source is given by

$$H_{p,V} = \frac{p_{ext}(\omega)}{V(\omega)} \quad (8.1)$$

where  $p_{ext}(\omega)$  is the acoustic sound pressure in [Pa] and  $V(\omega)$  is the volume velocity of the monopole source in [m<sup>3</sup>/s]. The FRF between the exterior microphone and volume



velocity source is expressed in decibels and is computed as

$$H_{p,V}(dB) = 20 \cdot \log_{10} \frac{H_{p,V}}{1} \quad (8.2)$$

where 1 is the reference value for decibel scale in [Pa/(m<sup>3</sup>/s)].

Each of the Figures 8.9, 8.10, 8.11 and 8.12 show six FRFs calculated between the six exterior microphones and a volume sound source which is located at the left rear wheelhouse, at the left front wheelhouse, in the engine compartment and at the exhaust, respectively.

The maximum peaks represent coupled structural-acoustic resonances, whereas antiresonances are minimum peaks. Antiresonances appear when the position of the exterior microphone matches the position of a nodal surface at a particular frequency. In resonance the response has a high finite value due to the structural and acoustic damping. Resonances correspond to the natural frequencies of the coupled structural-acoustic system.

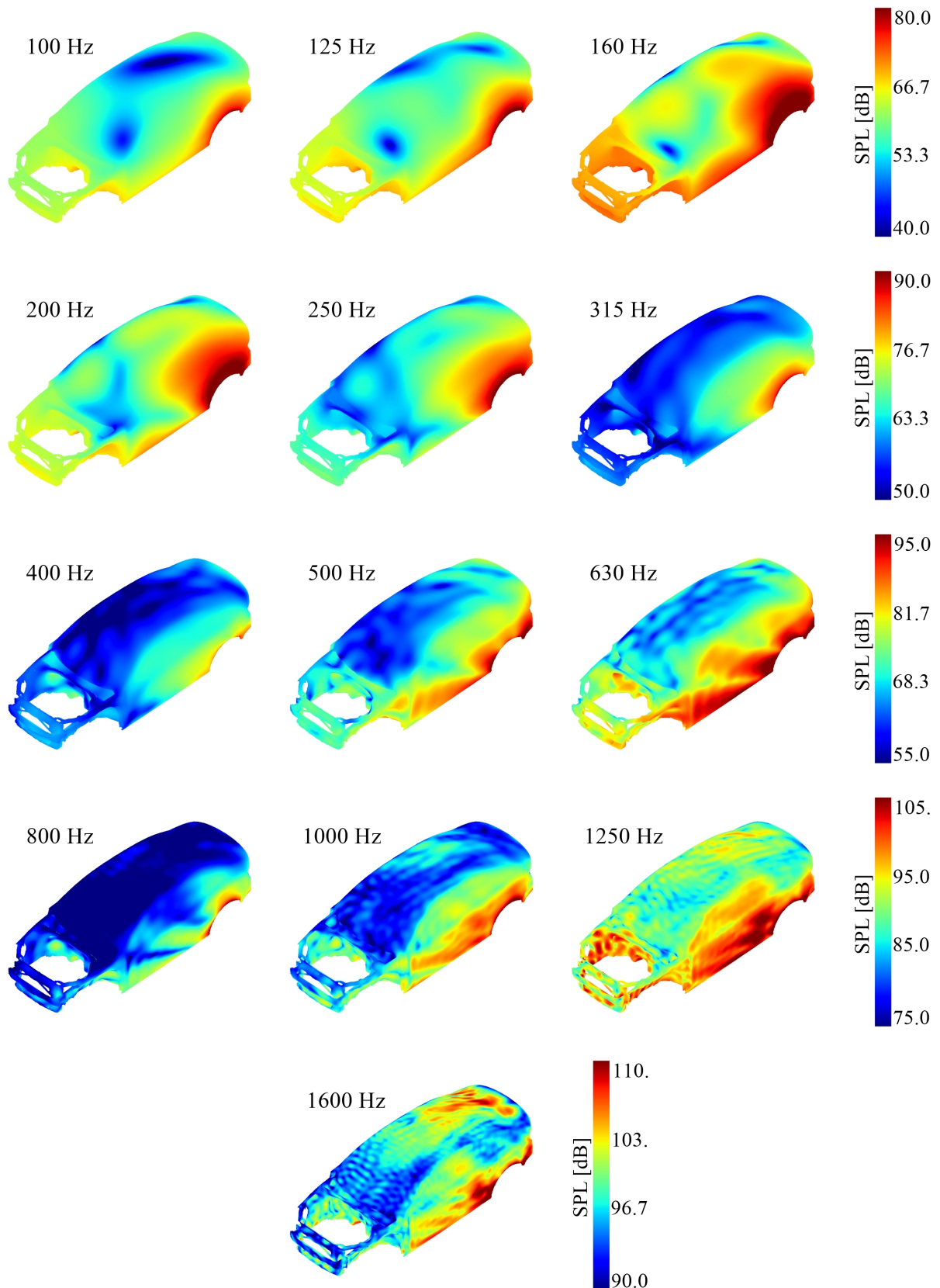


Figure 8.1: Sound Pressure Level computed on the rigid exterior wrap of the body-in-blue vehicle due to a volume monopole source located at the left rear wheelhouse

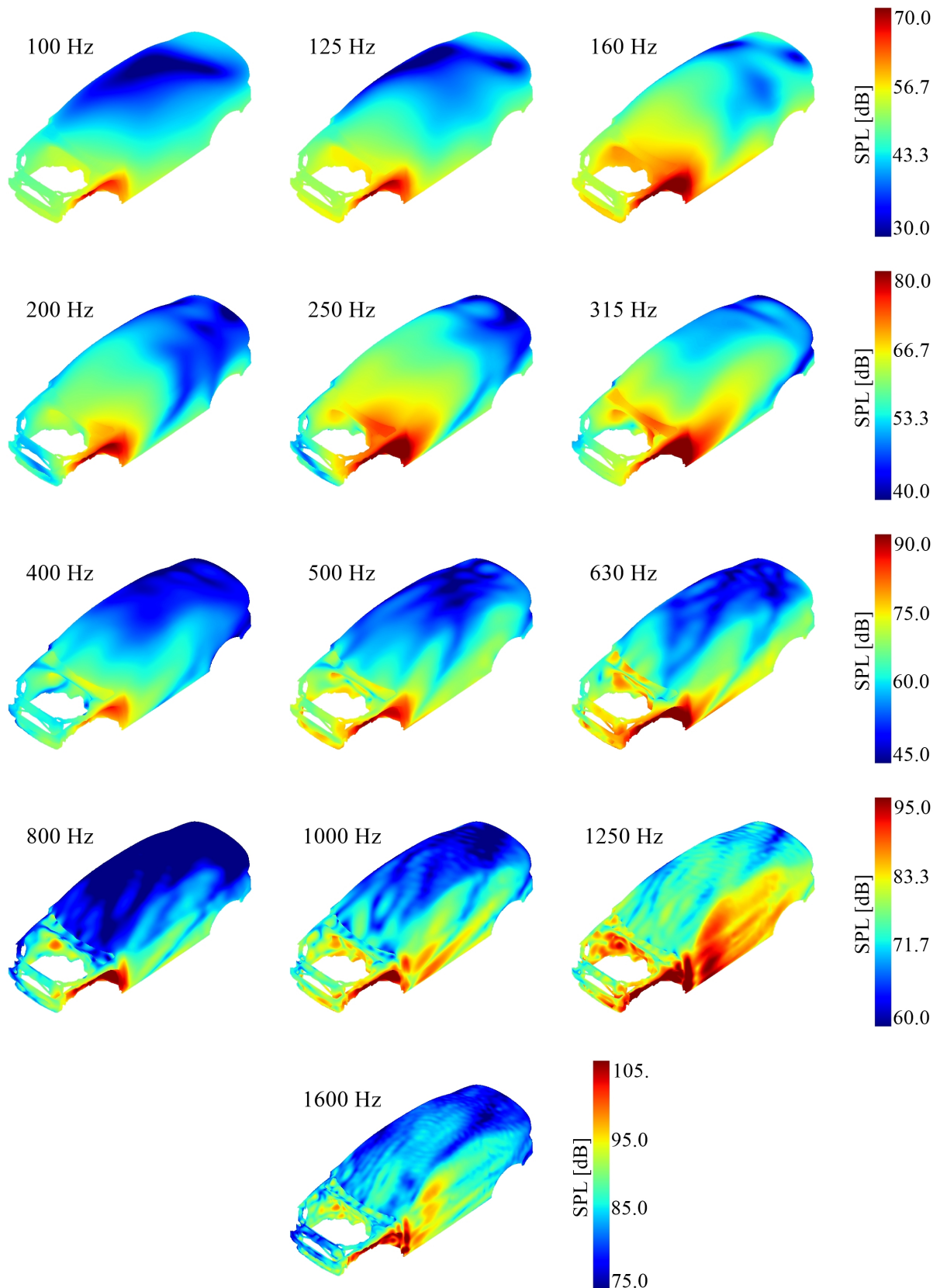


Figure 8.2: Sound Pressure Level on the rigid exterior wrap of the body-in-blue vehicle due to a volume velocity source located at the left front wheelhouse

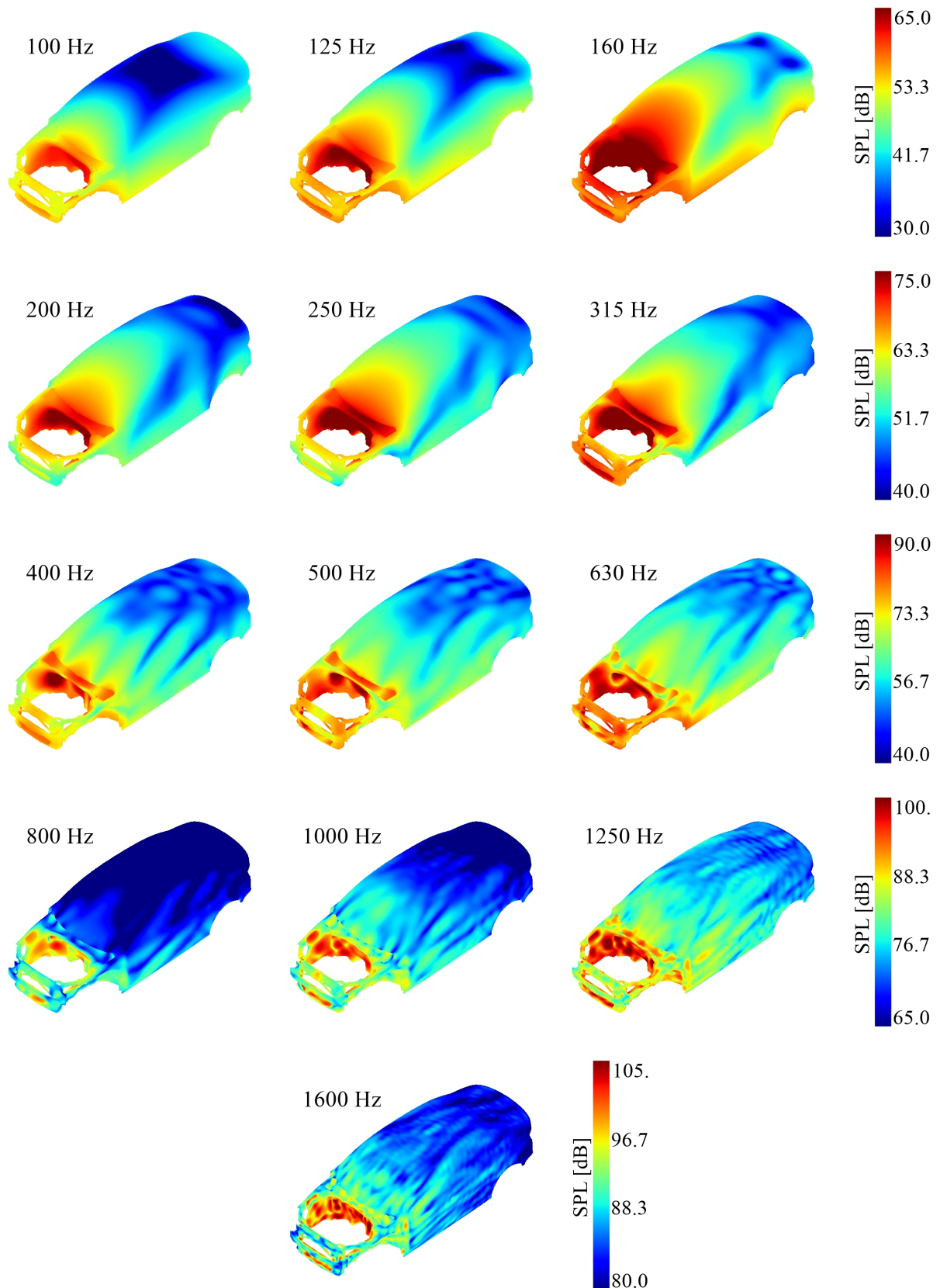


Figure 8.3: Sound Pressure Level computed on the rigid exterior wrap of the body-in-blue vehicle due to a volume velocity sound source located in the engine compartment

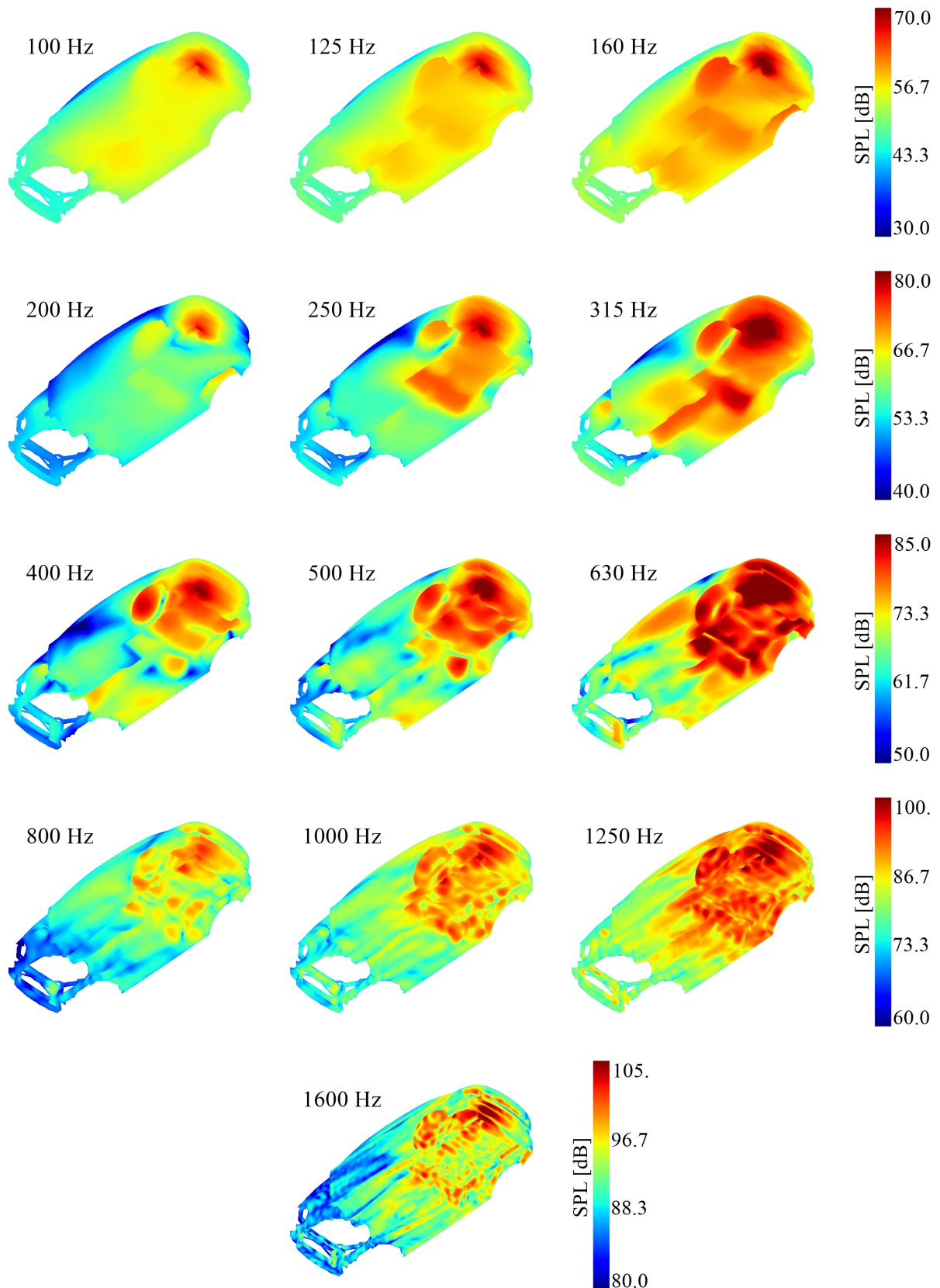


Figure 8.4: Sound Pressure Level computed on the rigid exterior wrap of the body-in-blue vehicle due to a volume velocity sound source located at the exhaust

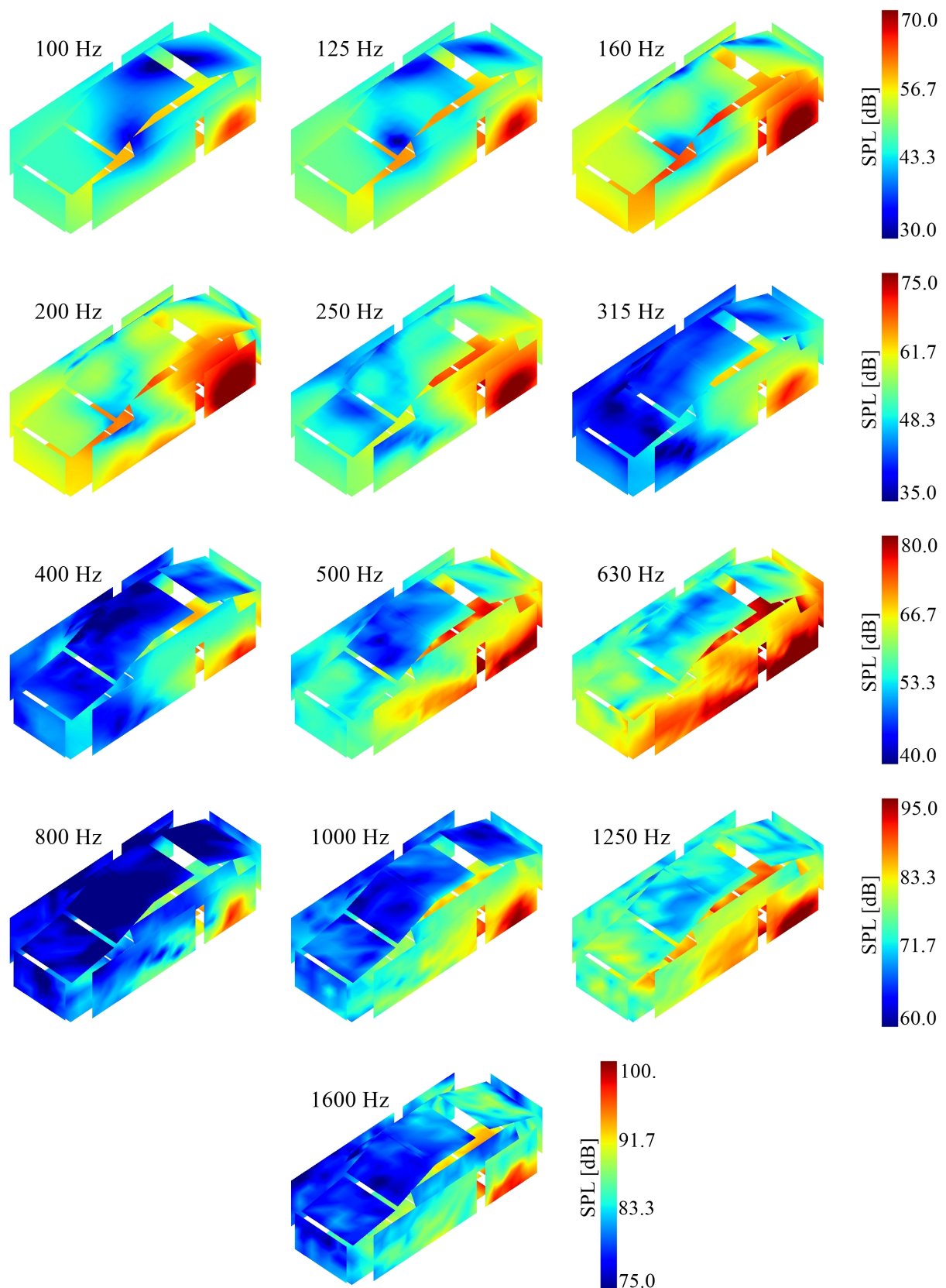


Figure 8.5: Sound Pressure Level computed on microphone arrays positioned around the vehicle due to a volume velocity sound source located at the left rear wheelhouse

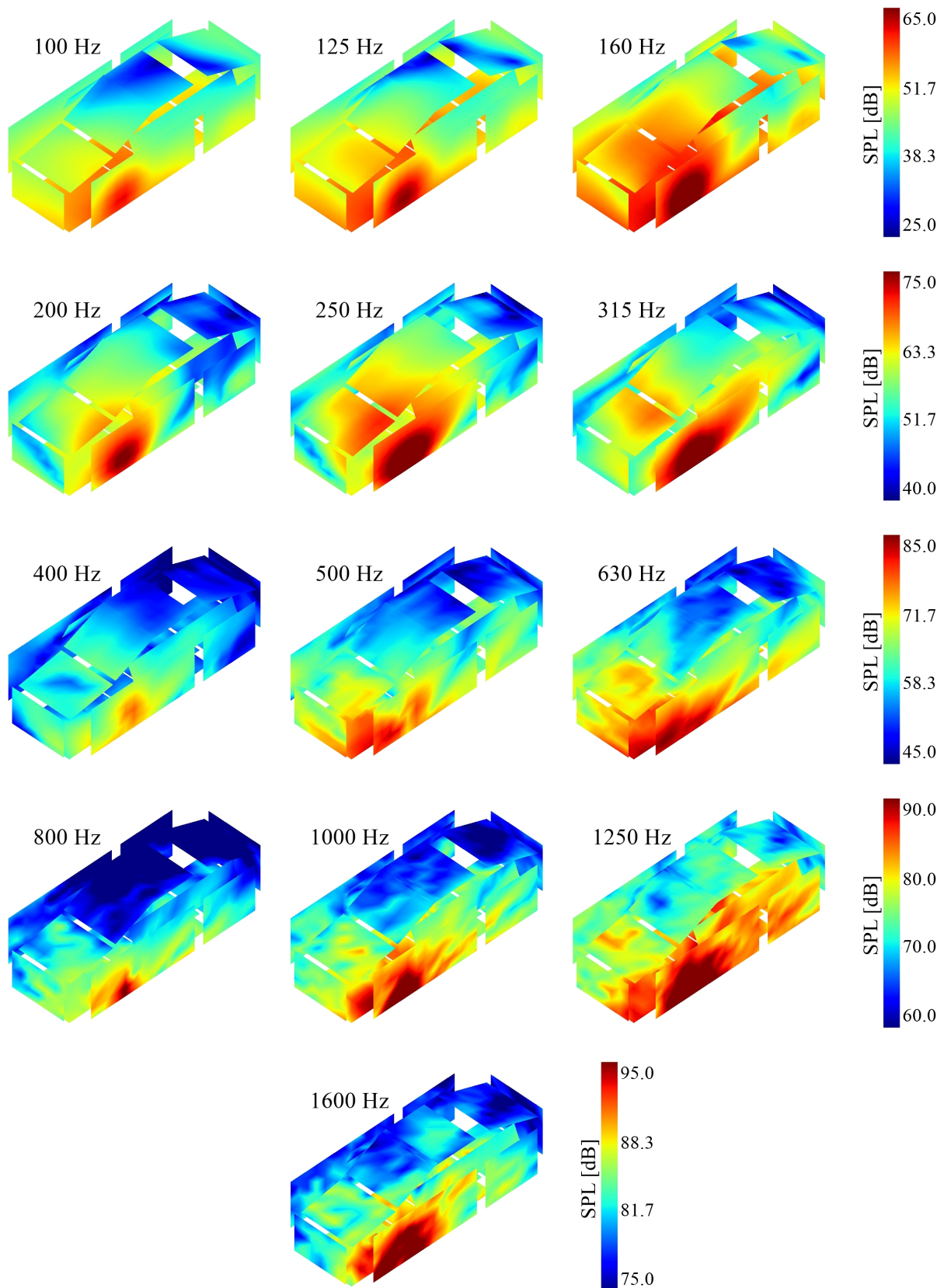


Figure 8.6: Sound Pressure Level computed on microphone arrays positioned around the vehicle due to a volume velocity sound source located at the left front wheelhouse

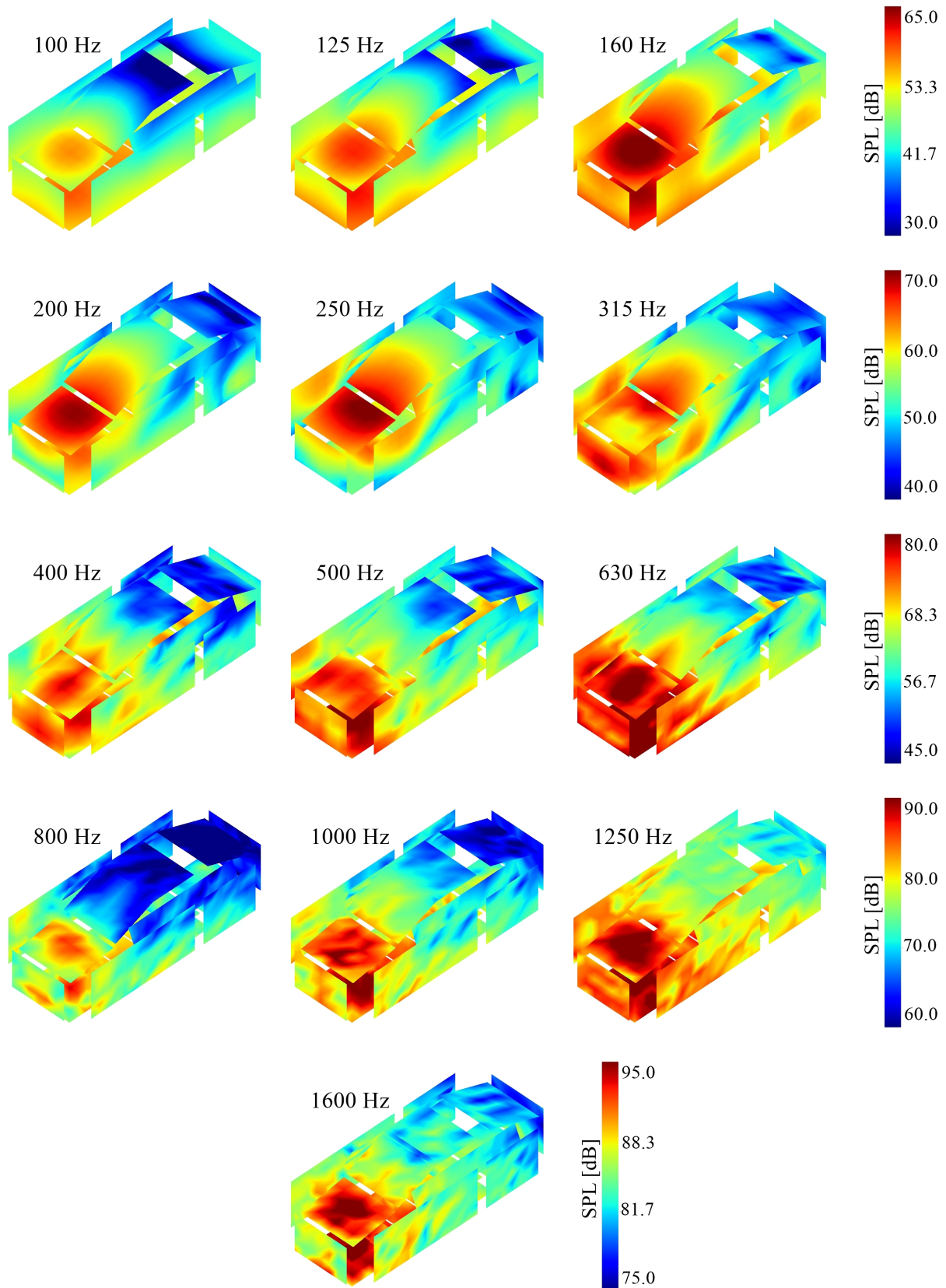


Figure 8.7: Sound Pressure Level computed on microphone arrays positioned around the vehicle due to a volume velocity sound source located in the engine compartment



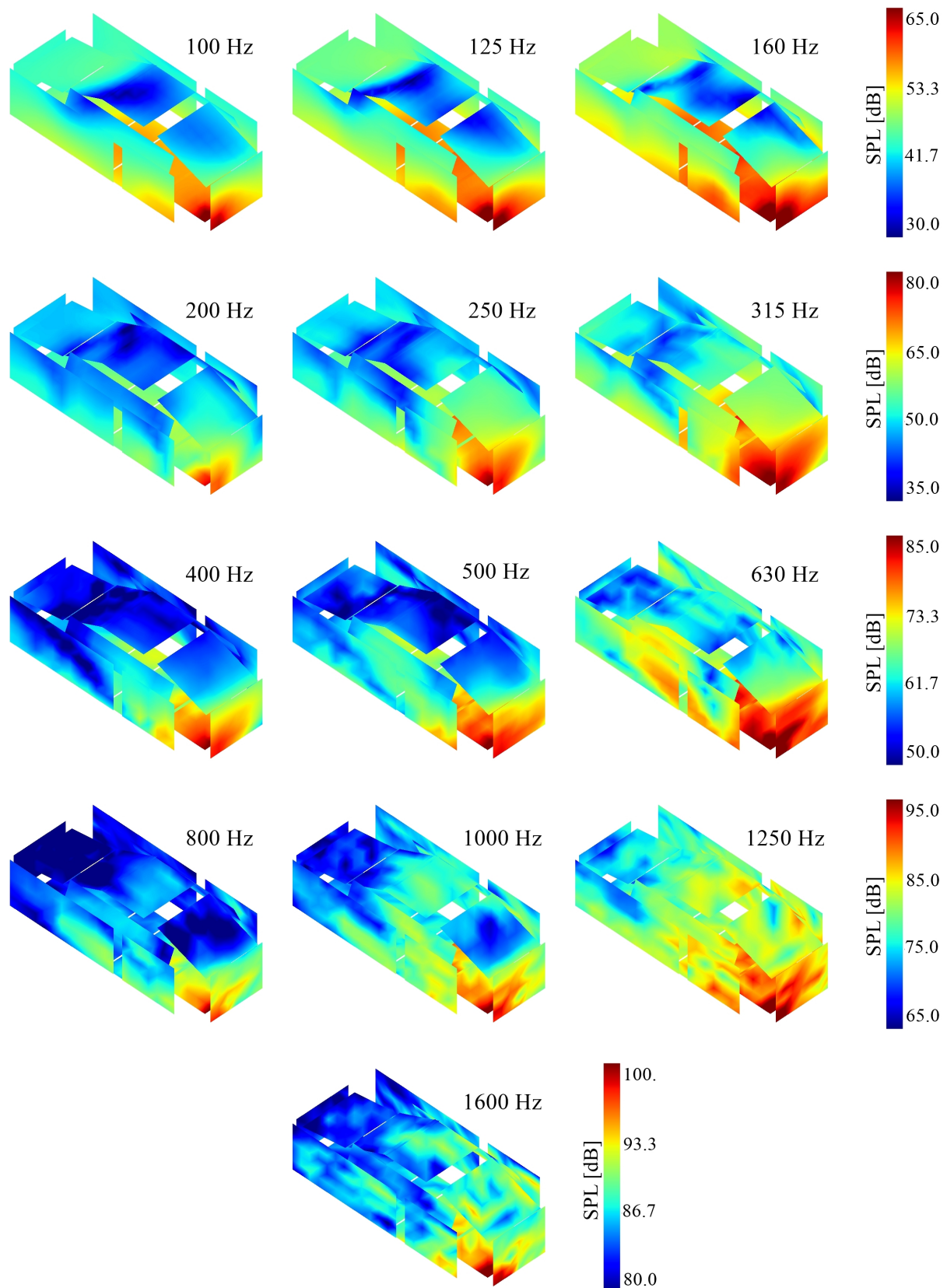
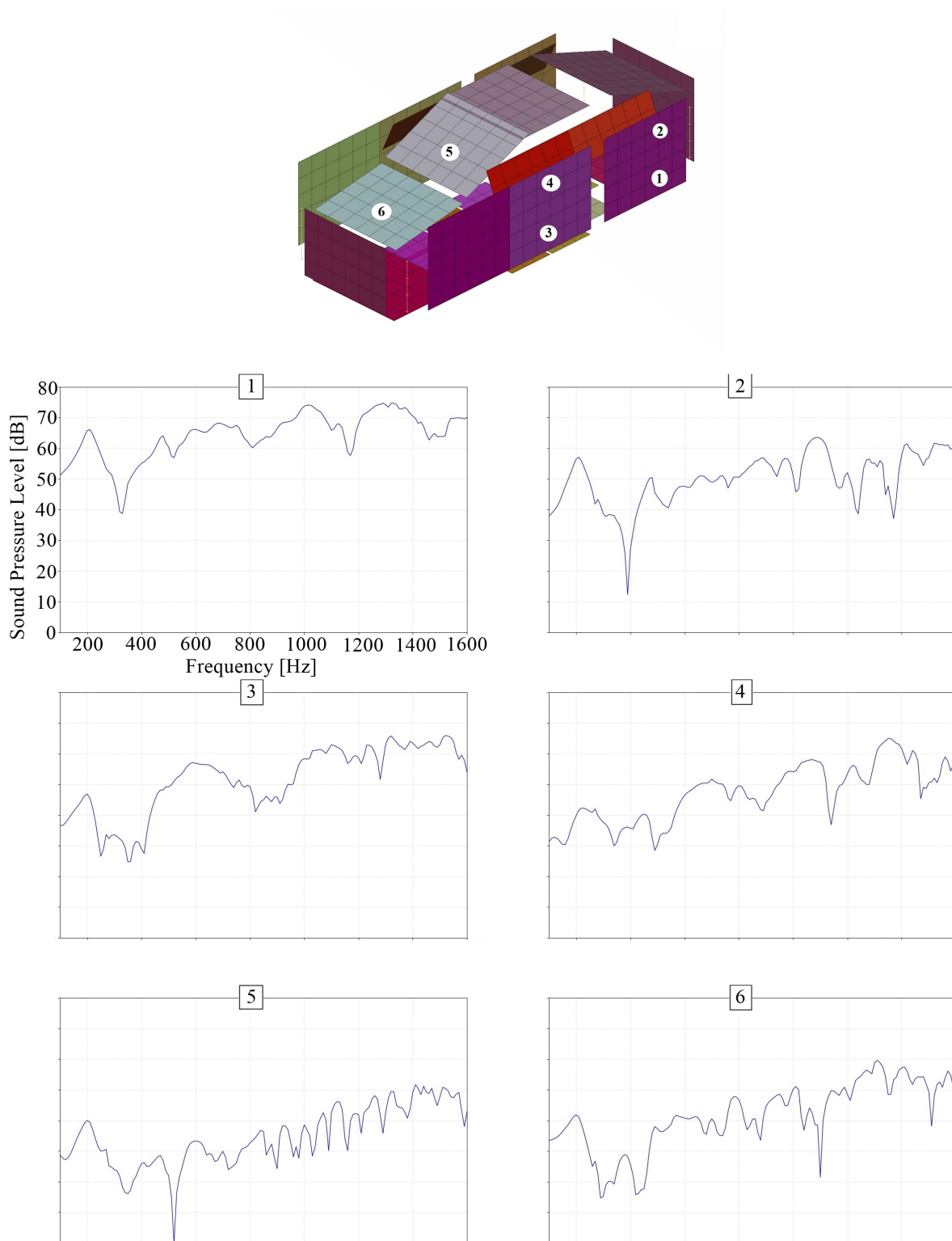
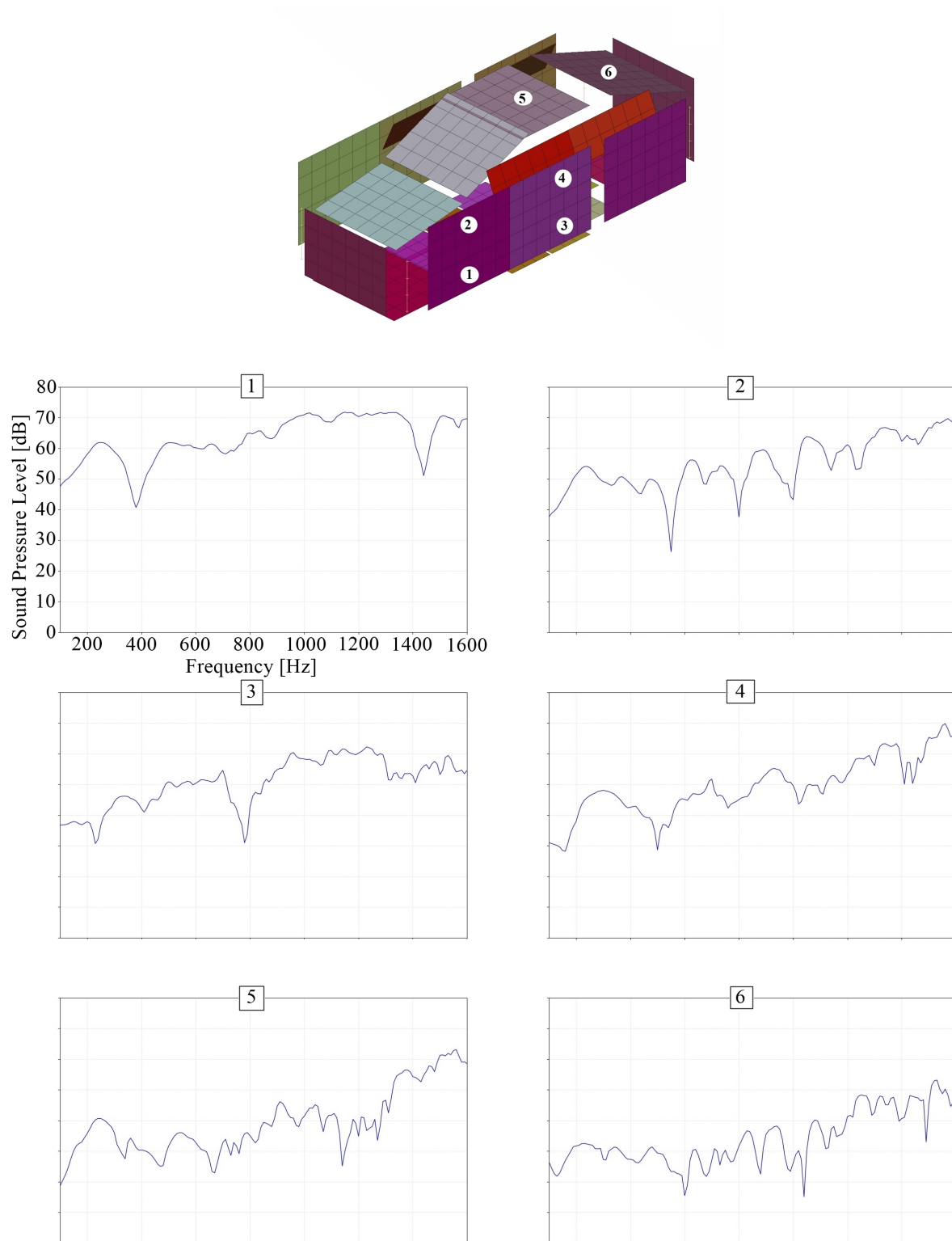


Figure 8.8: Sound Pressure Level computed on microphone arrays positioned around the vehicle due to a volume velocity sound source located at the exhaust



**Figure 8.9: Frequency Response Function (FRF) calculated between the exterior microphones and volume velocity sound source located at the left rear wheelhouse**



**Figure 8.10: Frequency Response Function (FRF) calculated between the exterior microphones and volume velocity sound source located at the left front wheelhouse**

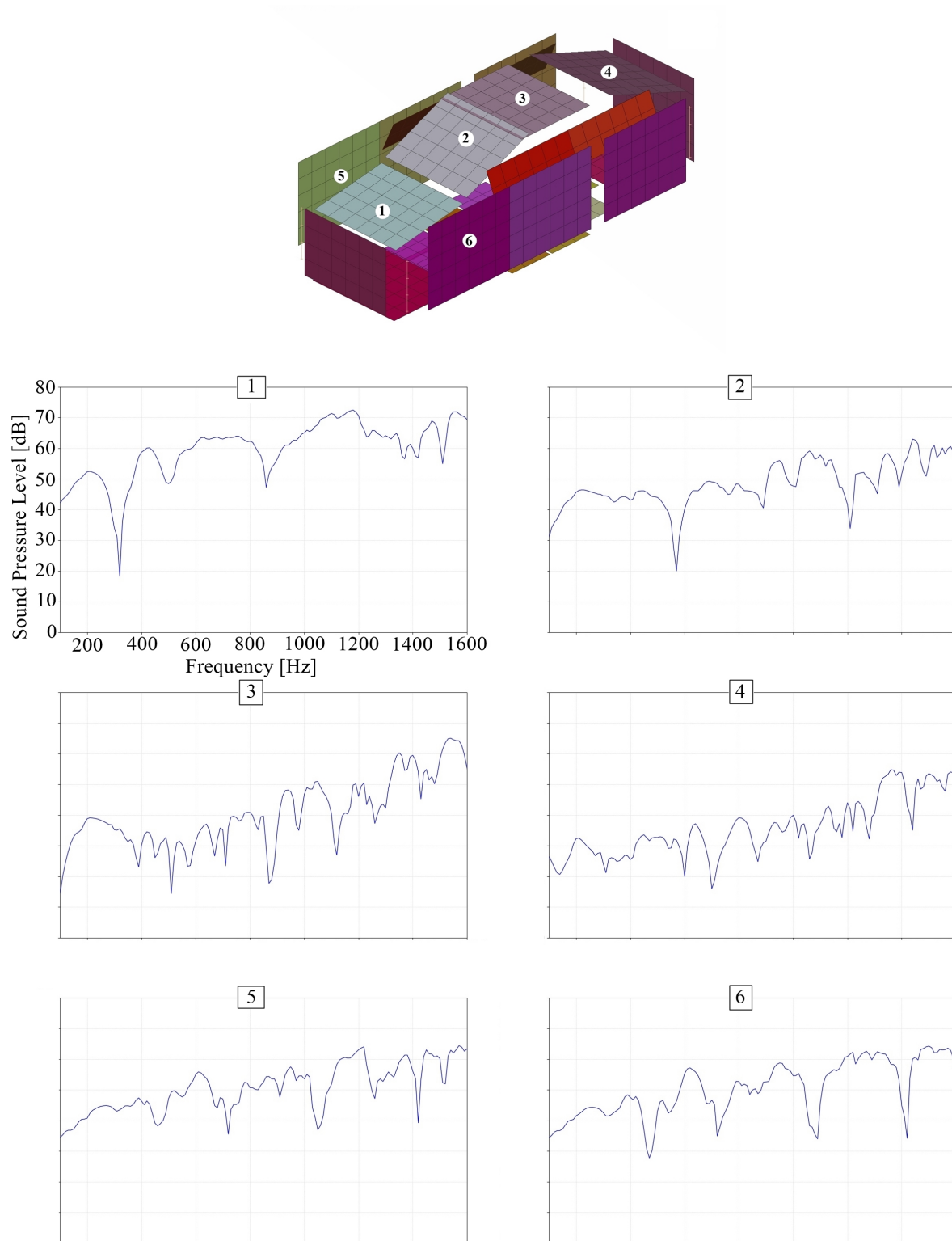


**Figure 8.11: Frequency Response Function (FRF) calculated between the exterior microphones and volume velocity sound source located in the engine compartment**

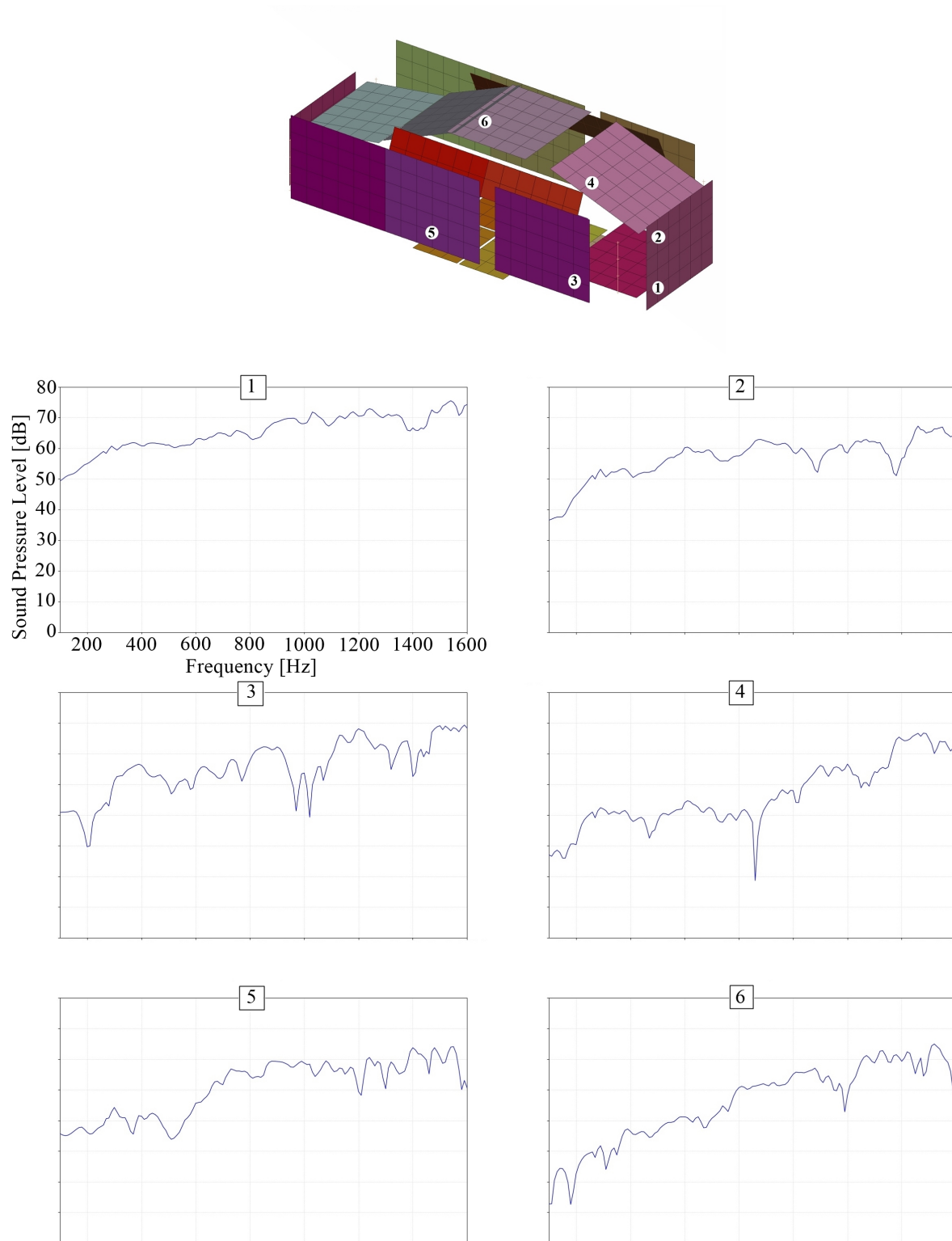


**Figure 8.12: Frequency Response Function (FRF) calculated between the exterior microphones and volume velocity sound source located at the exhaust**

## 8.2 Numerical results of vibro-acoustic analysis

This section deals with the numerical results obtained from the vibro-acoustic model. First, acoustic pressure is computed in the cavities of the vehicle. The distribution of the Sound Pressure Level in cavities of the vehicle is visualized in Figures 8.13, 8.14, 8.15 and 8.16 for the volume velocity sound source located at the left rear wheelhouse, at the left front wheelhouse, in the engine compartment and at the exhaust, respectively. The results are expressed in decibel and presented in 1/3 octave frequency bands.

Second, FRFs calculated between the interior microphones and volume velocity sound source are shown. FRF is given by

$$H_{p,V} = \frac{p_{int}(\omega)}{V(\omega)} \quad (8.3)$$

where  $p_{int}(\omega)$  is the acoustic sound pressure in [Pa] and  $V(\omega)$  is the volume velocity of the monopole source in [m<sup>3</sup>/s]. The FRF between the interior microphone and volume velocity source is expressed in decibel and is computed as

$$H_{p,V}(dB) = 20 \cdot \log_{10} \frac{H_{p,V}}{1} \quad (8.4)$$

where 1 is the reference value for dB in [Pa/(m<sup>3</sup>/s)].

Each of the Figures 8.17, 8.18, 8.19 and 8.20 show six FRFs calculated between the six interior microphones and a volume velocity sound source which is located at the left rear wheelhouse, left front wheelhouse, engine compartment and exhaust, respectively. Interior microphones marked as 1, 2, 3, 4, 5 and 6 represent left driver's side, right driver's side, left co-driver's side, right co-driver's side, right passenger's side and left passenger's side, respectively.

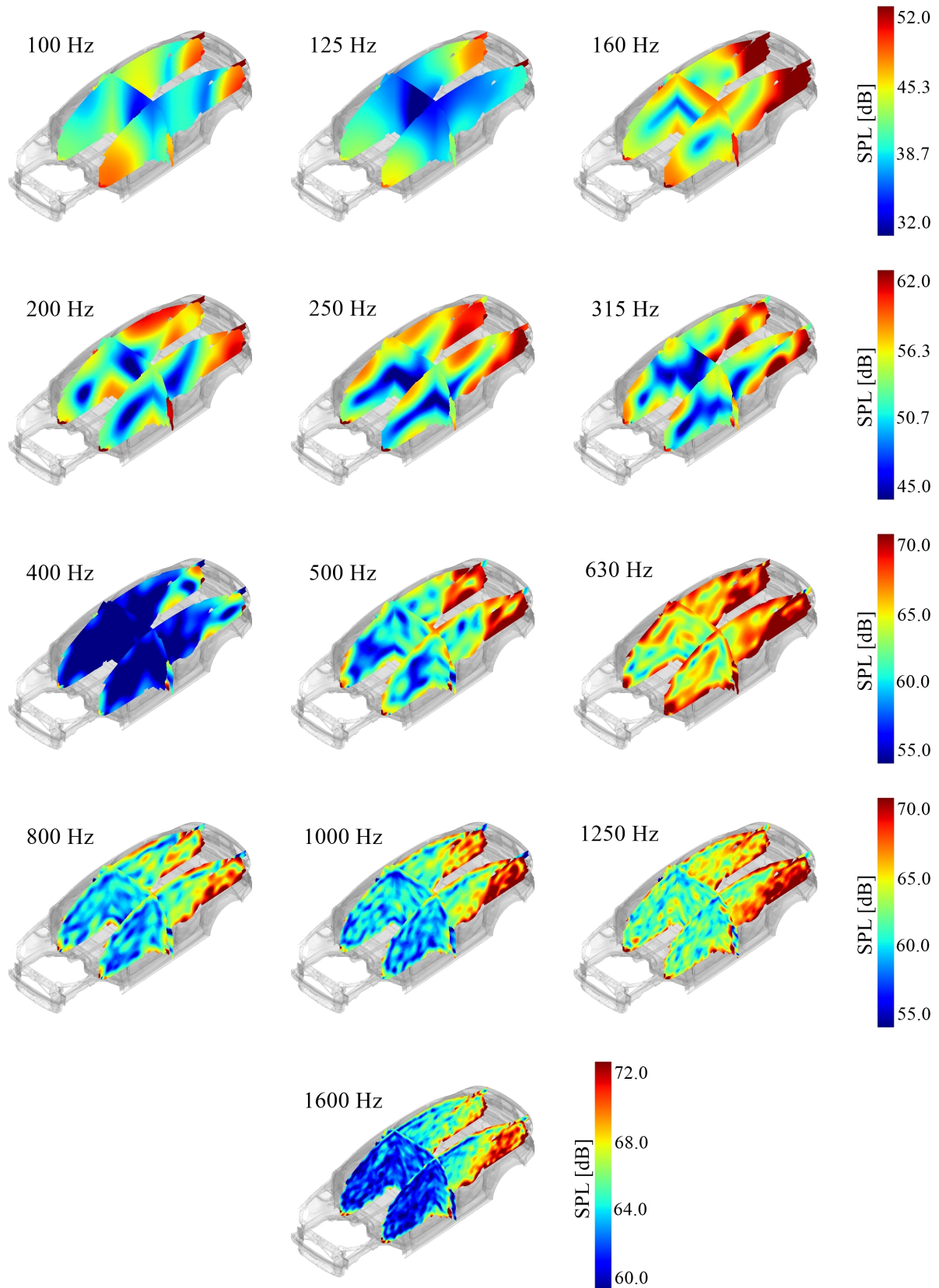


Figure 8.13: Sound Pressure Level computed in the vehicle cavities due to the volume velocity sound source located at the left rear wheelhouse

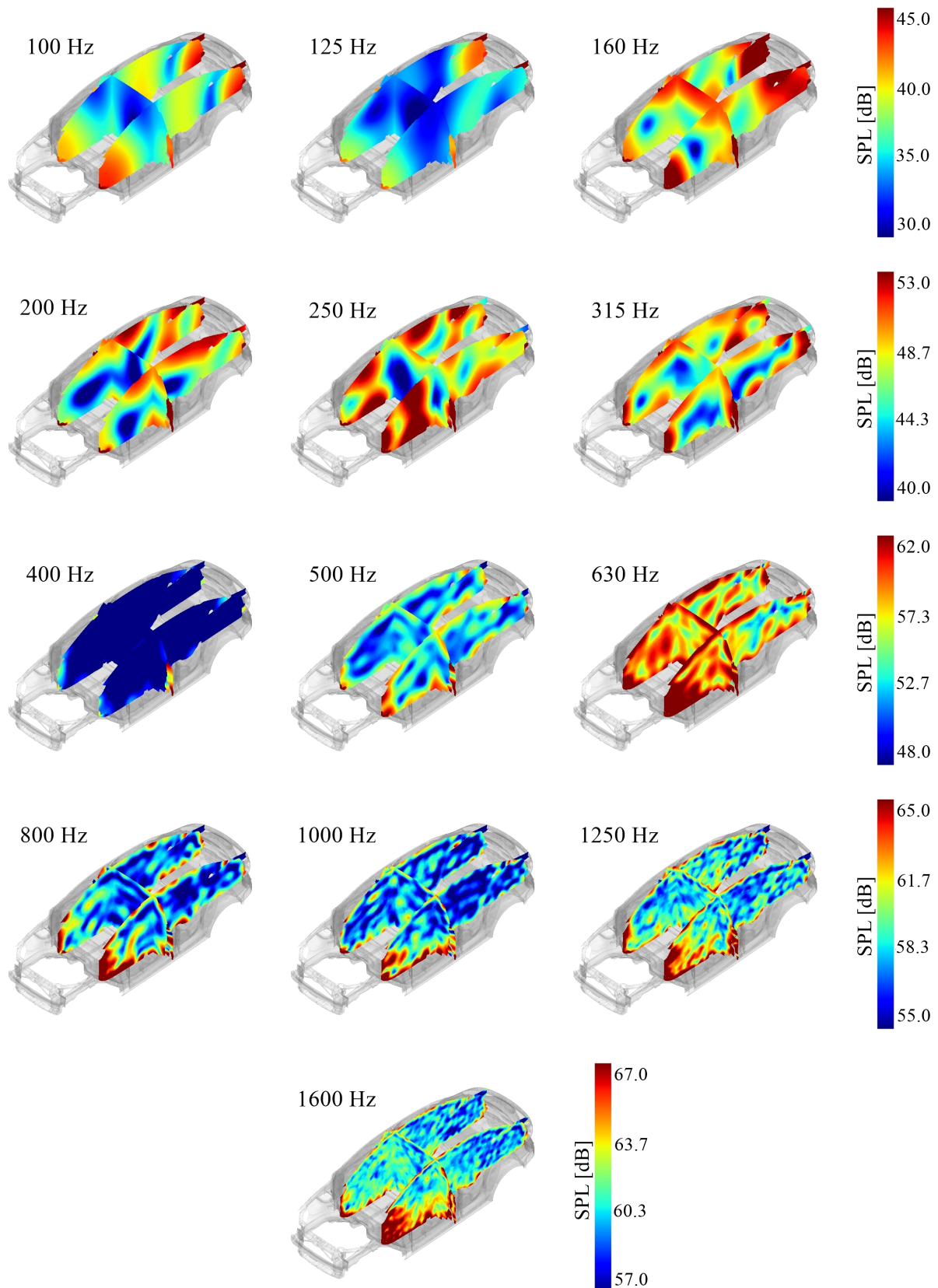


Figure 8.14: Sound Pressure Level computed in the vehicle cavities due to the volume velocity sound source located at the left front wheelhouse



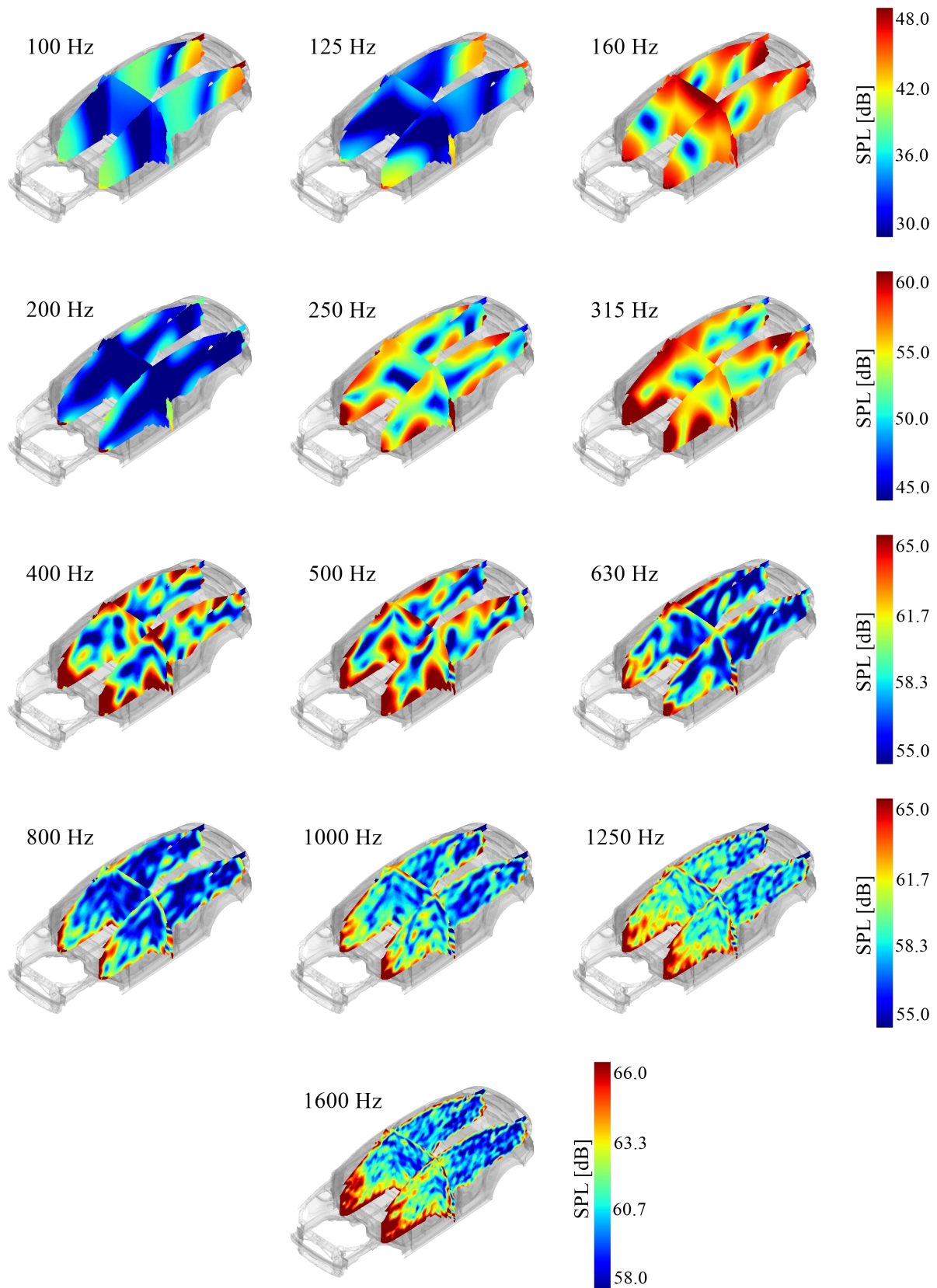


Figure 8.15: Sound Pressure Level computed in the vehicle cavities due to the volume velocity sound source located in the engine compartment

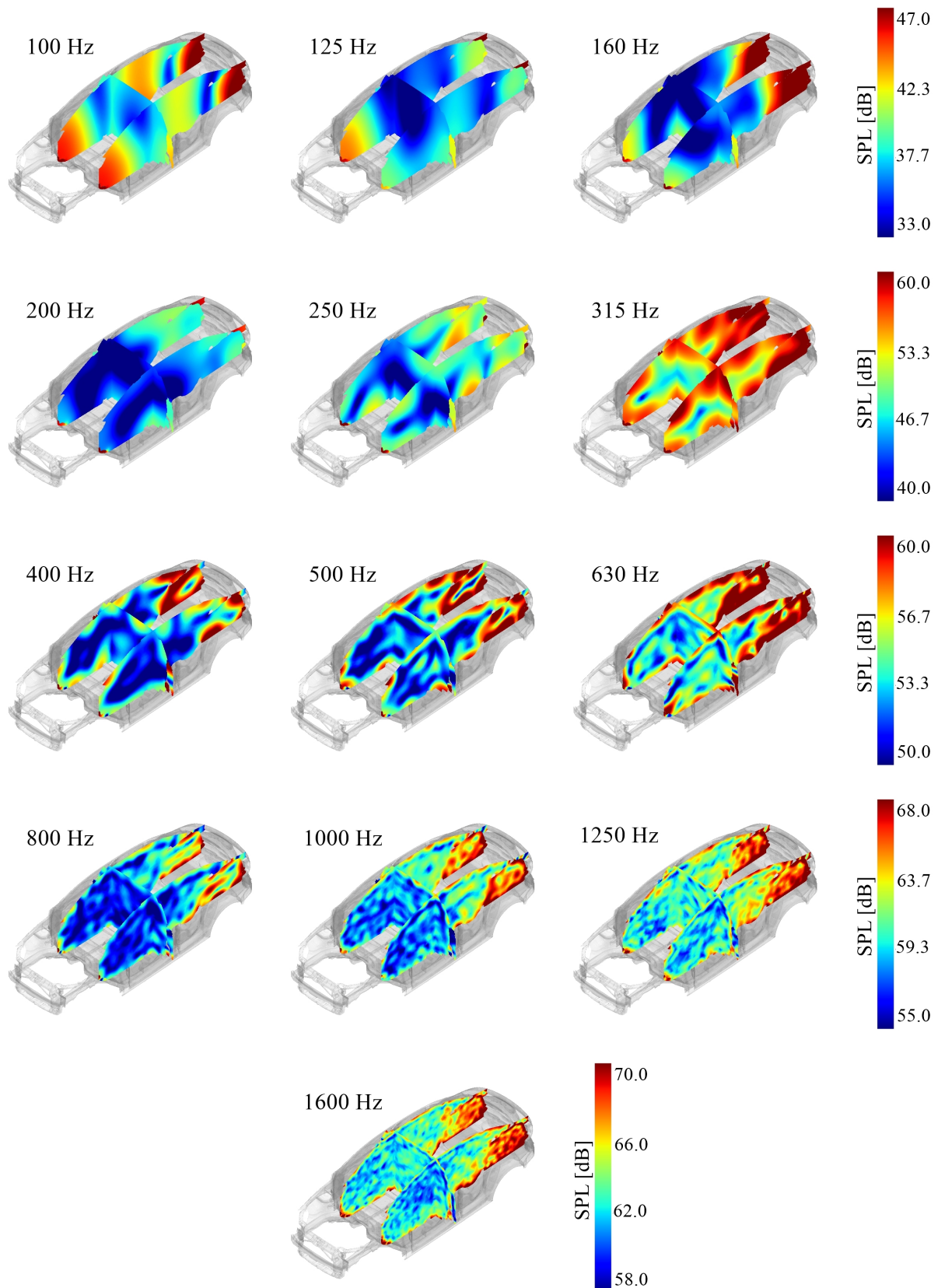
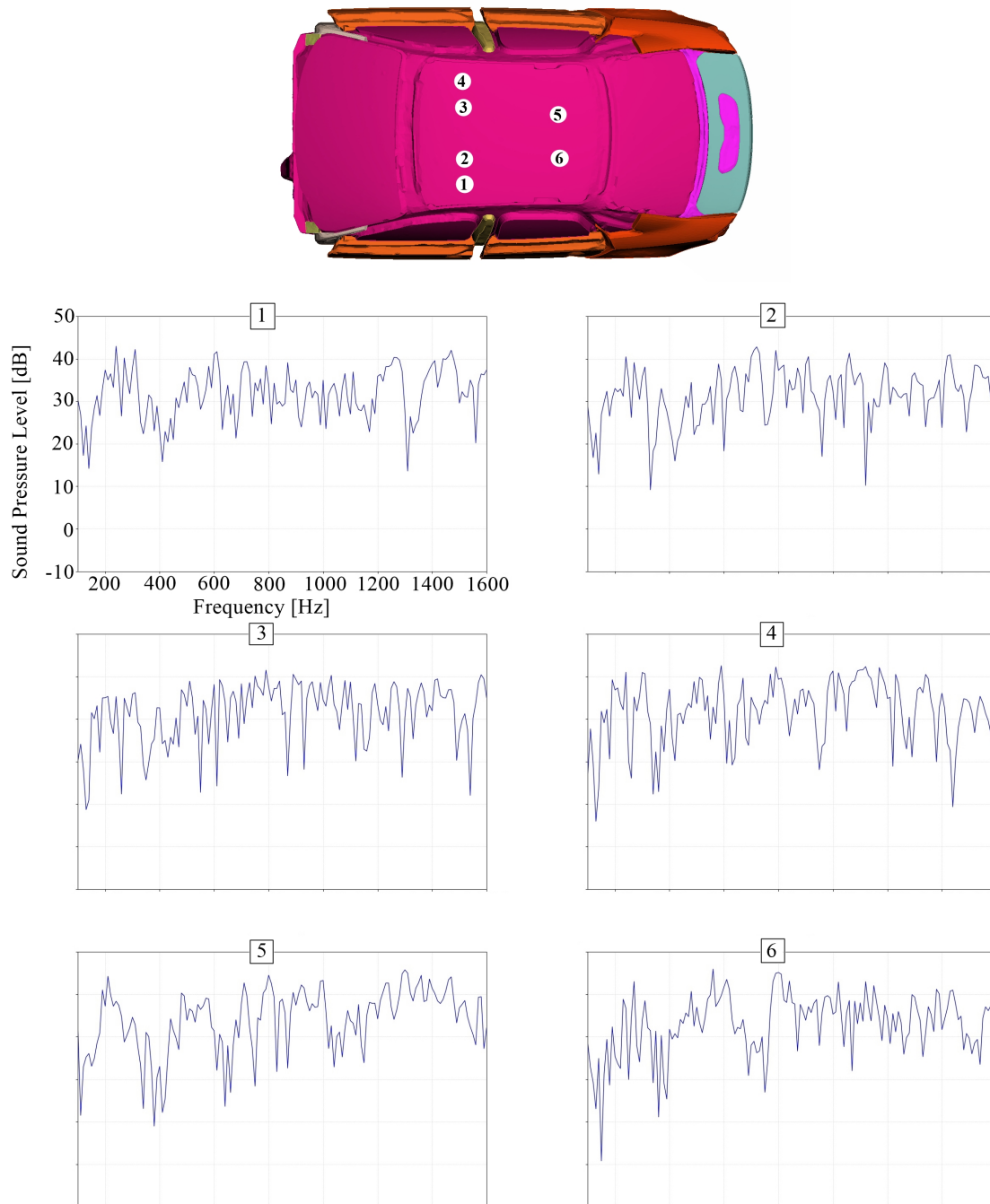
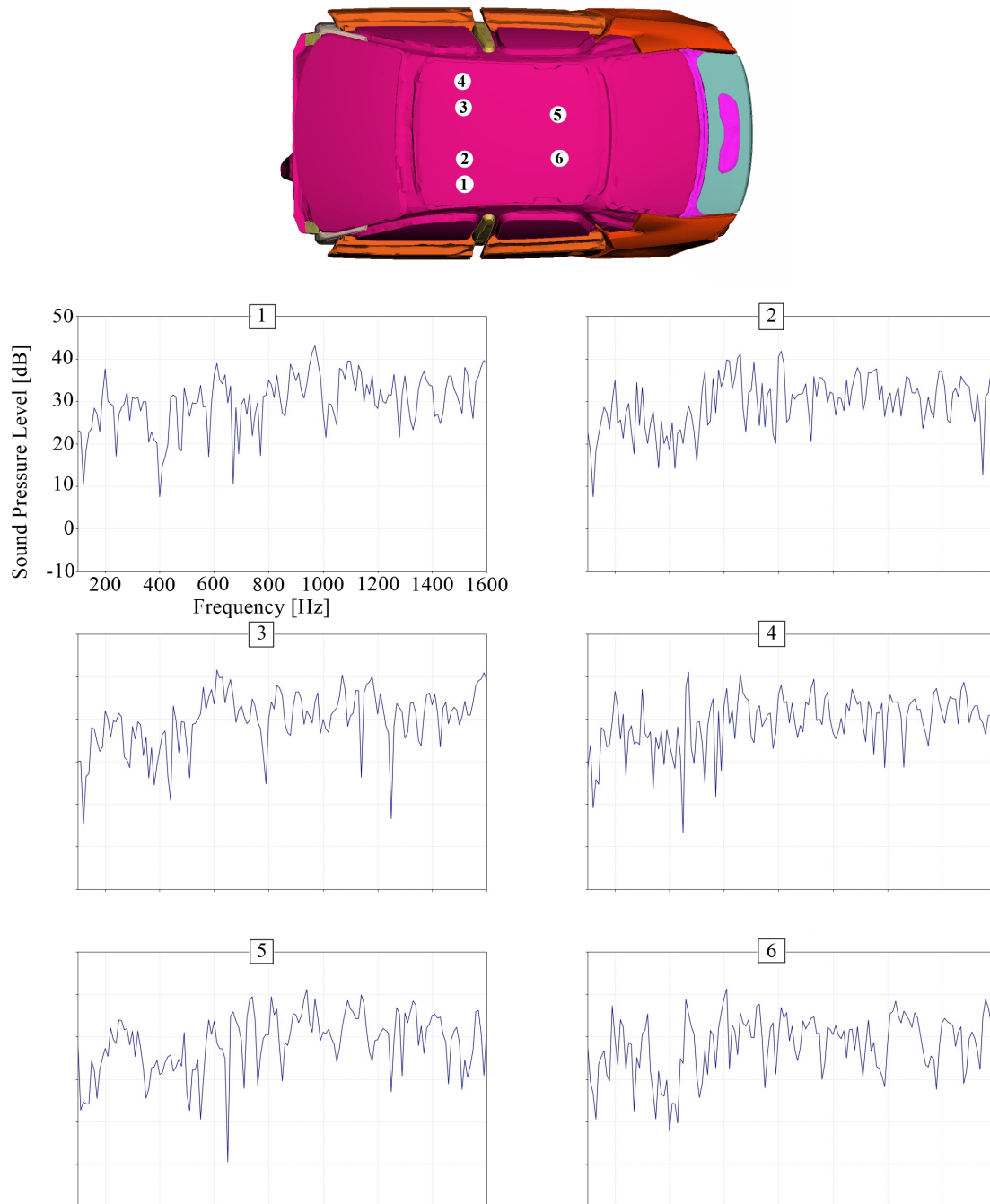


Figure 8.16: Sound Pressure Level computed in the vehicle cavities due to the volume velocity sound source located at the exhaust



**Figure 8.17: Frequency Response Function (FRF) calculated between the interior microphones and volume velocity sound source located at the left rear wheelhouse**



**Figure 8.18: Frequency Response Function (FRF) calculated between the interior microphones and volume velocity sound source located at the left front wheelhouse**

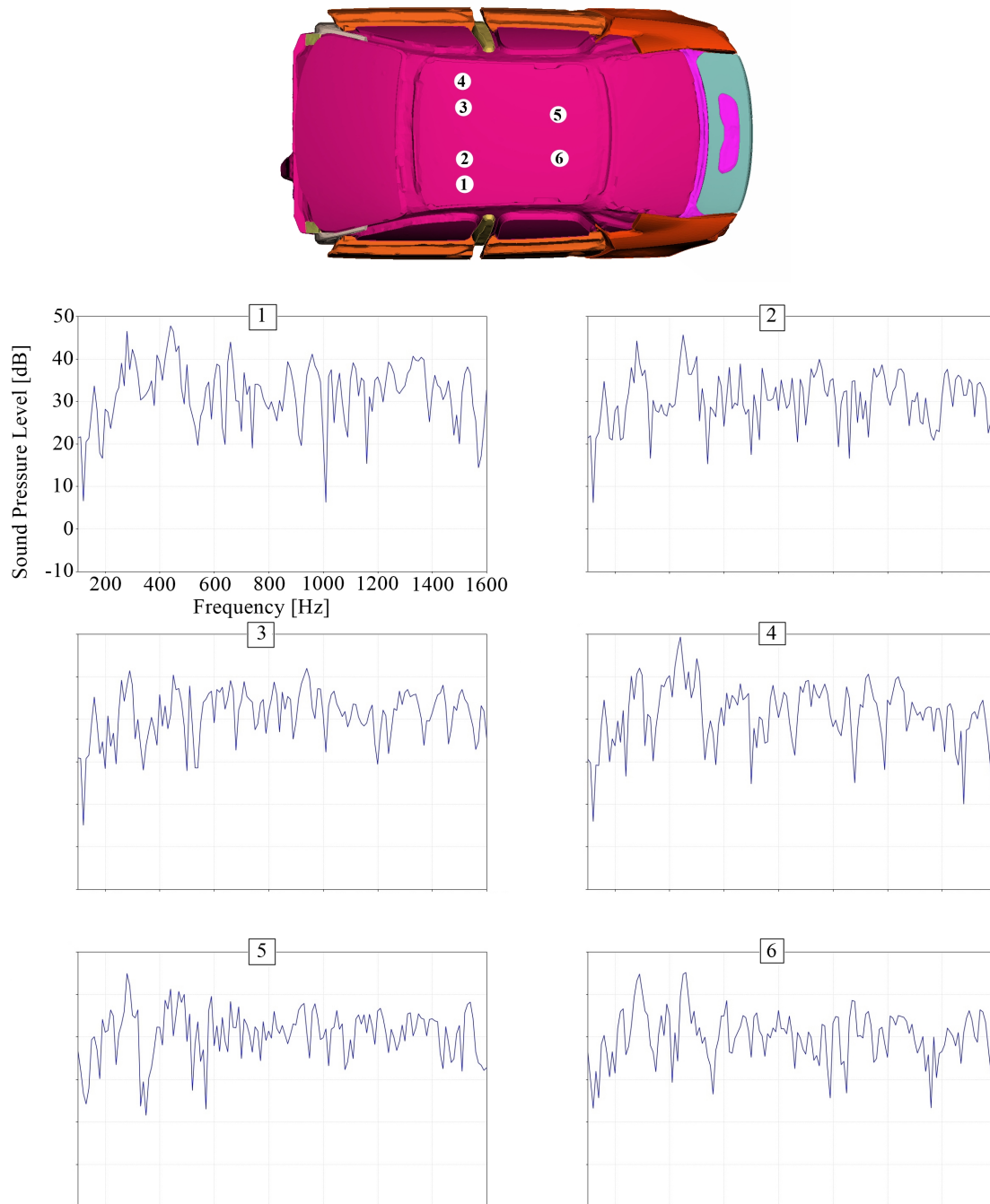


**Figure 8.19: Frequency Response Function (FRF) calculated between the interior microphones and volume velocity sound source located in the engine compartment**

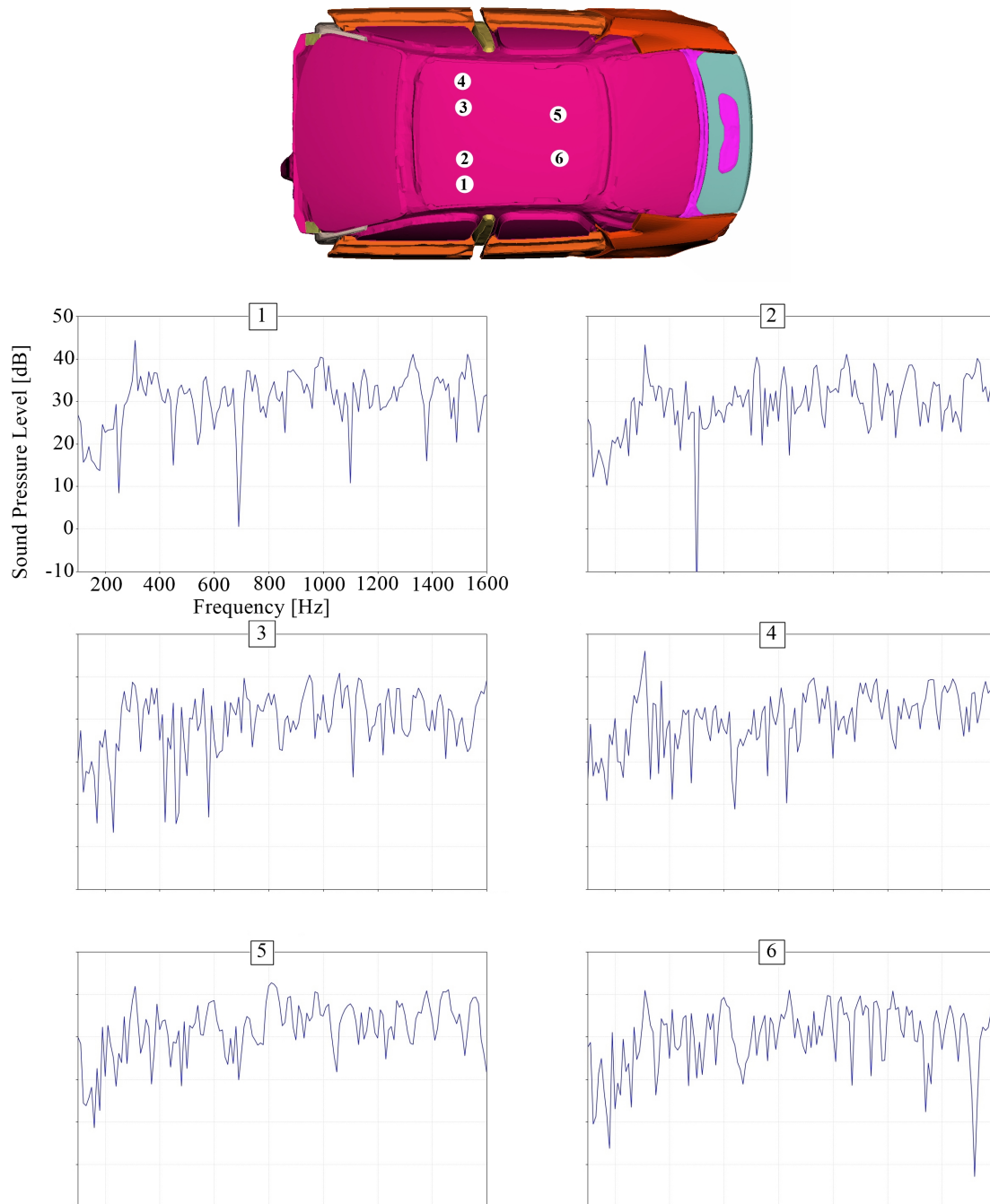


**Figure 8.20: Frequency Response Function (FRF) calculated between the interior microphones and volume velocity sound source located at the exhaust**

# Chapter 9

## Conclusions and recommendations for future work

In this thesis, a methodology to predict vehicle exterior and interior sound fields due to three characteristic automotive sound sources: engine noise, tyre rolling noise, and exhaust noise, has been developed and discussed in detail. The work has been carried out using two models of different complexity.

1. **The simplified model** consists of a simply supported rectangular plate fully coupled to a box-shaped acoustic cavity. The study using this model has been performed in two ways: analytically using the developed closed-form mathematical formulation, and numerically using the commercial FE software package ACTRAN. The purpose of the analysis performed using the simplified model is threefold. First, it serves to gain a physical insight into how sound transmits through thin partitions into acoustic enclosures. Second, the results obtained with the simplified analytical model are used to validate the accuracy of the simplified numerical model in terms of the FE size and the maximum frequency where the numerical results are still accurate. Third, the critical contrasting of the analytical and numerical results has been valuable to efficiently setup the complex model of the real vehicle and to understand and interpret the complex sound fields that stem from the intricate vehicle geometry. The main conclusions of the analysis using the simplified model can be summarized as follows.

- It is sufficient to model the plate and cavity model with 10 finite elements per

wavelength. Thus, the plate model is discretized with shell elements of 10 mm size for the maximum frequency of 1600 Hz. The same is applied to the cavity model which is discretized with acoustic tetrahedral elements whose element size is 20 mm.

- The numerical vibro-acoustic model can predict the interior sound pressure very accurately up to 500 Hz. The results also qualitatively agree in the frequency range between 500 and 1600 Hz, however, without an exact match between natural frequencies or resonant/antiresonant amplitudes. Nevertheless, either the analytical or the numerical results clearly agree in terms of the average responses in terms of acoustic pressures or plate vibrations. Both the numerical and analytical results clearly demonstrate the characteristic mass law which implies a reduction of the plate vibrations and the interior acoustic pressure with the increase in frequency.

2. **The complex model of a real vehicle.** The study using this model has been carried out numerically using ACTRAN. A three-step methodology has been developed. The first step includes the computation of the surface pressure on the rigid exterior wrap of the vehicle due to the acoustic waves radiated by the exterior sound source at the characteristic locations: wheels, engine compartment, and the exhaust pipe. The second step includes the projection of the surface pressure from the exterior wrap of the vehicle to structural parts of the vehicle. The third step includes the calculation of the noise transmitted into the vehicle interior, where results from the previous step are introduced as the excitation imposed on the flexible structural parts of the car. The main conclusions of the analysis using the complex model can be summarized as follows.

- The three-step methodology is validated on a simplified one-step methodology which is a very time and memory consuming computation. One-step methodology includes a Direct Frequency Response where all the vehicle interior noise computation due to the exterior sound source is done simultaneously in one step. The three-step methodology is almost 5x faster than the one-step methodology, which is the reason why this three-step methodology is developed. This validation is not shown in this thesis.



- Another benefit of the three-step methodology is the following. If the geometry of the vehicle in the early design stage is not satisfactory in terms of NVH, then the geometry, as well as e.g. the materials, the thickness of the structure, the foam materials, etc. are to be changed. In this event, the first step of the developed methodology does not need to be computed again because the sound pressure field is computed on the rigid exterior wrap and then projected on the real structure. This reduces the computation time of the NVH analysis of the vehicle interior in general.
- The computation time and memory consumption in the first step of the methodology are greatly affected by two parameters: interpolation order of the infinite exterior elements, and the size of the modelled exterior acoustic domain. Therefore, a good balance between the accuracy of the results and the computation cost must be found through the careful selection of these modelling parameters.
- By using the adaptive exterior acoustic meshing in the first step, the computation time has been greatly reduced.
- Choosing the right set of projection parameters is a key to achieve a good projection quality. The appropriate values of the plane and gap tolerance have to be selected in order to achieve a good mapping quality.
- The vehicle is modelled using shell elements with the element size of 10 mm which corresponds to the requirement of ten elements per wavelength. However, the vehicle cavity is modelled with acoustic elements with the element size ranging from 20 mm to 30 mm, which is not in accordance with the requirement that the maximum finite element is 20 mm. Therefore, the calculated interior sound field is probably not accurate in the higher frequency range above approximately 500 Hz.

Recommendations for future work are summarized below.

- In order to further reduce computational time and memory consumption of the process, an adaptive interior meshing technique could be used, combined with the already implemented adaptive exterior meshing technique. Adaptive interior meshing technique would consider the process of re-meshing the interior cavity

volume for a number of predefined frequency bands. In other words, each frequency band should have one mesh with the appropriate acoustic finite element size. Consequently, the accuracy of calculated interior pressure at higher frequencies would improve due to the correct acoustic finite element size with respect to the wavelength, without significantly increasing the computation time.

- In order to reduce the time needed for the pre-processing (preparation) of the vibro-acoustic model, an automatic coupling feature could be used. This feature automatically recognizes incompatible meshes, i.e. structural and acoustic, and does the coupling automatically based on the defined tolerances.
- Future work will be aimed at comparing and validating the numerical results obtained from the three-step methodology with the measurement results.
- After performing the simulation on the body-in-blue vehicle, future efforts should be aimed at applying the established methodology on the trimmed vehicle body. The main focus of the vibro-acoustic analysis of a trimmed body vehicle would be on including models of trim materials which may greatly increase the damping and thus reduce the resonant sound transmission into the vehicle interior.

# Bibliography

- [1] Migeot, J. L., Coyette, J. P., Lielens, G. (2016). *Acoustics - Essential concepts, theory and models of linear acoustics for engineers*. Belgium, IJK Numerics.
- [2] Shorter, P. (2008). "Recent Advances in Automotive Interior Noise Prediction", SAE Technical paper 2008-36-0592, doi: 10.4271/2008-36-0592.
- [3] Fahy, F. (1994). "Statistical energy analysis: a critical overview", *Philosophical Transactions of the Royal Society of London*, A346, 431-447, doi: <https://doi.org/10.1098/rsta.1994.0027>.
- [4] DeJong, R., "A Study of Vehicle Interior Noise Using Statistical Energy Analysis," SAE Technical Paper 850960, 1985, <https://doi.org/10.4271/850960>.
- [5] DeJong, R., (1985). "A Study of Vehicle Interior Noise Using Statistical Energy Analysis," SAE Technical Paper 850960, <https://doi.org/10.4271/850960>.
- [6] d'Udekem, D., Saitoh, M., Van den Nieuwenhof, B., Yamamoto, T. (2011). "Numerical Prediction of the Exhaust Noise Transmission to the Interior of a Trimmed Vehicle by Using the Finite/Infinite Element Method", SAE Technical paper 2011-01-17-10, doi: 10.4271/2011-01-1710.
- [7] Cotoni, V., Shorter, P. (2007). "Numerical and experimental validation of a hybrid finite element-statistical energy analysis method", *The Journal of the Acoustical Society of America* 122, 259-270, <https://doi.org/10.1121/1.2739420>.
- [8] Chen, S. M., Wang, D. F., Zan, J. M. (2011). "Interior Noise Prediction of the Automobile Based on Hybrid FE-SEA Method", *Mathematical Problems in Engineering*, vol. 2011, Article ID 327170, 20 pages, <https://doi.org/10.1155/2011/327170>.

- [9] Zhang, Y., Lee, M., Stanecki, P., Brown, G. et al., "Vehicle Noise and Weight Reduction Using Panel Acoustic Contribution Analysis," SAE Technical Paper 951338, 1995, <https://doi.org/10.4271/951338>.
- [10] Han, X., Guo, Y.J., Yu, H.D. (2009). "Interior sound field refinement of a passenger car using modified panel acoustic contribution analysis", *International Journal of Automotive Technology* 10(1): 79-85. <https://doi.org/10.1007/s12239-009-0010-8>.
- [11] Nilsson, A. C. (2000). *Vibroacoustics Part I*. Stockholm, KTH, Royal Institute of Technology, Department of Vehicle Engineering.
- [12] Nilsson, A. C. (2000). *Vibroacoustics Part II*. Stockholm, KTH, Royal Institute of Technology, Department of Vehicle Engineering.
- [13] Wallin, H. P., Carlsson, U., Abom, M., Boden, H. (2010). *Sound and Vibration*. Stockholm: KTH, Institutionen för farkostteknik, Tekniska högskolan.
- [14] Kinsler, L. E., Frey, A. R., Coppens, A. B., Sanders, J. V. (1962). *Fundamentals of Acoustics*. New York: Wiley.
- [15] Sung, S.H., Nefske, D.J. (1984). "A Coupled Structural-Acoustic Finite Element Model for vehicle Interior Noise Analysis", *Journal of Vibration and Acoustics*, 106(2), 314-318. doi: 10.1115/1.3269187
- [16] Fahy, F., Gardonio, P. (2007). *Sound and structural vibration*, second ed., Elsevier.
- [17] Caiazzo, A., Alujevic, N., Pluymers, B., Desmet, W. (2018). "Active control of turbulent boundary layer-induced sound transmission through the cavity-backed double panels", *Journal of Sound and Vibration*, Volume 422, 161-188. doi:<https://doi.org/10.1016/j.jsv.2018.02.027>.
- [18] Jensen, F.B., Kuperman, W. A., Porter, M. B., Schmidt, H. (1993). *Computational ocean acoustics*. Retrieved from <https://books.google.hr>
- [19] <https://en.wikipedia.org/wiki/Actran>
- [20] [www.mscsoftware.com/product/actran-acoustics](http://www.mscsoftware.com/product/actran-acoustics)

- 
- [21] FFT & MSC Software, General Program Organization, Actran Training-ACOUSTICS
- [22] Free Field Technologies, ACTRAN 19 User's Guide - Volume 1: Installation, Operations, Theory and Utilities, 2018.
- [23] FFT & MSC Software, Adaptivity-Introduction, Actran Training
- [24] Free Field Technologies, ACTRAN 19 User's Guide, 2018.
- [25] Free Field Technologies, ACTRAN 19 User's Guide - Volume 2: Extended DAT (EDAT) Input File Syntax, 2018.
- [26] Ganty, B., Jacqmot, J., Zhou, Z. and Jeong, C., "Numerical Simulation of Noise Transmission from A-pillar Induced Turbulence into a Simplified Car Cabin", SEA Technical Paper 2015-01-2322, 2015, doi:10.4271/2015-01-2322.
- [27] Caillet, A., Guellec, A., Dejaeger, L., Henry, A., "Prediction of exterior sound field of an automotive for airborne excitation and transmission to the interior of the vehicle", INTER-NOISE and NOISE-CON Congress and Conference Proceedings, InterNoise16, Hamburg GERMANY, pages 3858-4854, pp. 4502-4511(10).
- [28] Nefske, D.J., Sung, S.H., "Vehicle Interior Acoustic Design Using Finite Element Methods", International Journal of Vehicle Design, Vol 6(1), pages 24-39, doi:10.1504/IJVD.1985.061343.

# Appendix

## I. CD-R disc